TECHNICAL MEMORANDUM

X-317

WIND-TUNNEL INVESTIGATION AT MACH NUMBERS FROM 0.40 TO 1.20 OF THE STATIC AERODYNAMIC AND CONTROL CHARACTERISTICS OF A MODEL OF A NONLIFTING REENTRY CAPSULE IN COMBINATION WITH A ROCKET BOOSTER

By Albin O. Pearson

Langley Research Center
Langley Field, Va.

NATIONAL AERONAUTICS AND SPACE ADMINISTRATION
WASHINGTON
September 1960

Boell

copy #1

NATIONAL AERONAUTICS AND SPACE ADMINISTRATION

TECHNICAL MEMORANDUM X-317

WIND-TUNNEL INVESTIGATION AT MACH NUMBERS FROM 0.40 TO 1.20 OF THE STATIC AERODYNAMIC AND CONTROL CHARACTERISTICS OF A MODEL OF A NONLIFTING REENTRY CAPSULE IN COMBINATION WITH A ROCKET BOOSTER*

By Albin O. Pearson

SUMMARY

An investigation was conducted in the Langley 8-foot transonic pressure tunnel to determine the static aerodynamic characteristics of a model of a capsule—rocket-booster configuration. In addition, the pitching- and rolling-moment effectiveness and the hinge-moment and normal-force characteristics of six different control surfaces mounted on the tips of the horizontal stabilizing fins were determined. The tests were conducted over an angle-of-attack range which at its maximum extended from -9° to 9°. The Reynolds number varied from 0.86×10^6 to 1.56×10^6.

The results of the investigation show that the basic model was statically stable in pitch throughout the Mach number range and that the center-of-pressure location had a maximum variation from about 0.74 to 0.57 body diameter from the model base. Positive pitching-moment and rolling-moment effectiveness were obtained by the six control surfaces for angles of attack of 0° and 4° at all Mach numbers. The hinge-moment variations with angle of attack and also with control deflection were nonlinear, and in most instances reversals in the slopes of the curves occurred. The longitudinal center of pressure of the control surfaces tended to move rearward with increase in Mach number, except for the rectangular control surfaces at an angle of attack of 0° and a deflection angle of 0° at the higher Mach numbers.

INTRODUCTION

To project a vehicle out of the earth's atmosphere and successfully return it to the earth's surface requires a knowledge of the aerodynamic

*Title, Unclassified.

characteristics of the vehicle and rocket-booster combination during the period following launch and of the vehicle alone after its separation from the rocket booster. In order to obtain this knowledge the National Aeronautics and Space Administration has initiated a wind-tunnel research program to investigate the aerodynamic characteristics of vehicles (capsules) having varied shapes and of several capsule—rocket-booster combinations. The results of some tests of capsules alone are presented in references 1 and 2.

The present investigation was performed in the Langley 8-foot transonic pressure tunnel and provides information at subsonic and transonic speeds concerning the static aerodynamic characteristics of a model of a capsule—rocket-booster combination. The capsule model used for this investigation was similar in shape to one reported in references 1 and 2, whereas the rocket booster was simulated by a cylindrical afterbody with stabilizing fins mounted at the base. In addition, the effects on the aerodynamic characteristics of the model due to all-movable control surfaces mounted on the tips of the stabilizing fins were investigated. A total of six different control surfaces were tested. The normal-force and hinge-moment characteristics of each control surface were determined.

The investigation was conducted at Mach numbers from 0.40 to 1.20 over an angle-of-attack range which at its maximum extended from -9° to 9°. The control surfaces were tested at nominal deflection angles of 0°, 5°, and 10° and at a differential deflection of $\pm 10^\circ$. The Reynolds number, based on maximum body diameter, varied from 0.86×10^6 to 1.56×10^6.

SYMBOLS

The data presented herein are referred to the body system of axes with the origin located at approximately the 70.5-percent-length station. The hinge moments were taken about the hinge line, which was at the 40-percent-root-chord station for the rectangular shaped controls and at the 63-percent-root-chord station for the triangular shaped controls. The positive directions of forces, moments, and displacements are shown in figure 1. The coefficients and symbols are defined as follows:

A maximum body cross-sectional area, sq ft

C_A axial-force coefficient, $\dfrac{\text{Axial force}}{qA}$

$C_{A,b}$ base axial-force coefficient,

$$\frac{\text{Base pressure - Free-stream static pressure}}{q}$$

$C_{A,\alpha\approx0}$ axial-force coefficient at $\alpha \approx 0^{\circ}$

C_h hinge-moment coefficient, $\frac{\text{Hinge moment}}{qS\bar{c}}$

C_l rolling-moment coefficient, $\frac{\text{Rolling moment}}{qAd}$

ΔC_l incremental rolling-moment coefficient due to control-surface deflection

C_m pitching-moment coefficient, $\frac{\text{Pitching moment}}{qAd}$

C_{m_α} slope of pitching-moment coefficient per degree at $C_m \approx 0$, $\frac{\partial C_m}{\partial \alpha}$

C_{m_δ} slope of pitching-moment coefficient per degree at $\delta \approx 0^{\circ}$ to 5°, $\frac{\partial C_m}{\partial \delta}$

C_N normal-force coefficient, $\frac{\text{Normal force}}{qA}$

$C_{N,c}$ control-surface normal-force coefficient, $\frac{\text{Normal force of control surface}}{qS}$

C_{N_α} slope of normal-force coefficient per degree at $\alpha \approx 0^{\circ}$, $\frac{\partial C_N}{\partial \alpha}$

$\bar{c}$ mean aerodynamic chord of control surface, in.

d maximum body diameter, in.

M free-stream Mach number

q free-stream dynamic pressure, lb/sq ft

R Reynolds number based on maximum body diameter and free-stream conditions

S area of control surface, sq ft

x longitudinal distance from model base or from control-surface hinge line to center of pressure of model or control surface, respectively, positive direction measured upstream, in.

α angle of attack of model center line, deg

δ nominal control-surface deflection angle in plane normal to hinge line, positive when trailing edge is down, deg

MODELS

Details of the basic model are shown in figure 2 and photographs are presented in figure 3. The basic model consisted of a capsule identical in shape to a reentry vehicle of references 1 and 2, a cylindrical afterbody simulating a rocket booster, and four stabilizing fins spaced 90° apart and located near the model base. The capsule was attached to the rocket booster with the conical portion facing the relative wind as opposed to the reentry attitude of reference 1 where the base of the capsule (after separation from a booster) faced the relative wind. Both the capsule and cylindrical afterbody were made of aluminum alloy, whereas the stabilizing fins, which had 45° sweptback leading edges and wedge-shaped airfoil sections, were made of steel.

Details of the control surfaces are shown in figure 4. A total of six different control surfaces, located at the tips of the horizontal stabilizing fins, were tested in combination with the basic model. These control surfaces had wedge-shaped airfoil sections and were made of steel. The planform shapes of three control surfaces were rectangular, and the other three were triangular. The planform area for all control surfaces was constant, but the aspect ratio was varied.

End plates, made of steel, were mounted at the tips of the horizontal stabilizing fins during the investigation of all control surfaces. Details of these end plates are shown in figure 2.

The model was mounted on a four-component strain-gage balance and was sting supported in the wind tunnel. The control surfaces were mounted on a two-component strain-gage balance located within the right stabilizing fin near the fin tip.

TESTS

The investigation was conducted in the Langley 8-foot transonic pressure tunnel at Mach numbers from 0.40 to 1.20. The tests were performed at a stagnation pressure of 0.75 atmosphere and at a dewpoint such that the airflow was free of condensation shocks. All data presented from this investigation are essentially free of wall-reflected disturbances. The model angle of attack was varied from about -9° to 9° and was determined by means of a fixed-pendulum strain-gage unit mounted in the forward portion of the model. The control surfaces were tested at deflections of 0°, 5°, and 10° and at a differential deflection of $\pm 10^\circ$. The nominal control deflection angles presented herein are uncorrected for the deflection due to control loading. The variation of Reynolds number, based on maximum body diameter and free-stream conditions, with Mach number is shown in figure 5.

Normal force, axial force, pitching moment, and rolling moment for the model were determined by means of the internal strain-gage balance with the pitching moments taken about the 70.5-percent-length station. The axial-force results have been corrected to a condition of free-stream static pressure at the model base. Normal force and hinge moment for the control surfaces were determined by means of the balance located within the right stabilizing fin.

ACCURACY

Based upon balance accuracy and repeatability of data, it is estimated that the coefficients at two representative Mach numbers are accurate within the following limits:

Coefficient	Accuracy at -	
	M = 0.40	M = 1.20
Model:		
C_N	±0.20	±0.05
C_A	±0.04	±0.01
C_m	±0.04	±0.01
C_l	±0.02	±0.005
Control surface:		
$C_{N,c}$	±0.06	±0.014
C_h	±0.02	±0.004

The angle of attack is estimated to be accurate to within $\pm 0.20^{\circ}$. The maximum variation of the actual test Mach numbers from the presented nominal values is less than ± 0.005.

RESULTS AND DISCUSSION

An index of the figures presenting the aerodynamic results is given in table I. The longitudinal aerodynamic characteristics of the basic model with and without end plates and control surfaces are presented in figures 6 to 12. The rolling-moment characteristics of the basic model with and without end plates and control surfaces are presented in figure 13. The hinge-moment and normal-force characteristics of the control surfaces are presented in figures 14 and 15, respectively. Figures 16 to 21 are summary plots. The addition of end plates and control surfaces to the basic model had no effect on the variation of $C_{A,b}$ with α shown in figure 6(d); hence, the data of this figure are applicable to all configurations tested.

Aerodynamic Characteristics of Basic Model

The basic data of figure 6 and the summary data of figure 16 show that the addition of end plates to the basic model has no effect on the static longitudinal aerodynamic characteristics of the basic model. The basic model is statically stable (for the center-of-gravity location of this investigation) throughout the Mach number range (fig. 16) with the center of pressure varying from about 0.74 to 0.57 body diameter from the model base (fig. 17). The slope C_{N_α} varies a maximum of about 12 percent through the Mach number range (fig. 16). The variation of $C_{A,\alpha \approx 0}$ with Mach number (fig. 16) follows the usual trend for the Mach number range of this investigation with a maximum value occurring near a Mach number of about 1.05.

Control Characteristics

Pitching-moment effectiveness.- The values of C_{m_δ} presented in figure 18 are based on control deflections from 0° to 5° and assume a linear variation of C_m over this range. Positive control effectiveness in pitch (fig. 18) is maintained for all six control surfaces at angles of attack of 0° and 4° throughout the Mach number range of the investigation. In general, the control effectiveness for all six control surfaces tended to decrease with increase of angle of attack.

Rolling-moment effectiveness.- Positive rolling-moment effectiveness, as indicated by ΔC_l (fig. 19), is maintained by all six control surfaces at angles of attack of 0° and 4° at all test Mach numbers. For these angles of attack, rolling-moment effectiveness increased with aspect ratio. The data of figure 13, however, indicate that at angles of attack greater than about 4° the opposite occurred; the rolling-moment effectiveness decreased with increase in aspect ratio.

Hinge moment.- The hinge-moment coefficients for the six control surfaces are shown in figure 14 to be nonlinear, with reversals in slope occurring with change in angle of attack. Near angles of attack of 0° for $\delta = 0^\circ$ the hinge-moment coefficients have positive slopes for all control surfaces except control surface 6 at supersonic speeds. The hinge-moment-coefficient variations with control-surface deflection (fig. 20) are also generally nonlinear for the six control surfaces and in many instances (for example, fig. 20(a)) reversals in the slope of the curve occur.

Center of pressure.- The control-surface longitudinal center-of-pressure locations shown in figure 21 were computed directly from the hinge-moment data of figure 14 and the normal-force data of figure 15. For all control surfaces at angles of attack of 0° and 4° and at deflection angles of 0°, 5°, and 10° the center of pressure tends to move rearward with increase in Mach number except for the rectangular controls at an angle of attack of 0° and a deflection angle of 0°. For this condition, the center of pressure shifts forward at the higher Mach numbers.

CONCLUSIONS

The static aerodynamic characteristics of a model of a capsule—rocket-booster configuration with and without control surfaces mounted on the tips of the horizontal stabilizing fins were investigated. In addition, the hinge-moment and normal-force characteristics of the control surfaces were determined. The results warranted the following conclusions:

1. The basic capsule—rocket-booster model was statically stable in pitch throughout the Mach number range of the investigation, and the center-of-pressure location had a maximum variation from about 0.74 to 0.57 body diameter from the model base.

2. Positive pitching-moment effectiveness and rolling-moment effectiveness were obtained by the six control surfaces investigated at angles of attack of 0° and 4° at all Mach numbers.

3. The hinge-moment variations with angle of attack and also with control-surface deflection angle were generally nonlinear and in most instances reversals in the slopes of the curves occurred.

4. The longitudinal control-surface center-of-pressure location tended to move rearward with increase in Mach number except for the rectangular control surfaces near an angle of attack of 0° and a deflection of 0°.

Langley Research Center,
National Aeronautics and Space Administration,
Langley Field, Va., June 3, 1960.

REFERENCES

1. Pearson, Albin O.: Wind-Tunnel Investigation at Mach Numbers From 0.40 to 1.14 of the Static Aerodynamic Characteristics of a Nonlifting Vehicle Suitable for Reentry. NASA MEMO 4-13-59L, 1959.

2. Turner, Kenneth L., and Shaw, David S.: Wind-Tunnel Investigation at Mach Numbers From 1.60 to 4.50 of the Static Stability Characteristics of Two Nonlifting Vehicles Suitable for Reentry. NASA MEMO 3-2-59L, 1959.

TABLE I.- INDEX OF FIGURES PRESENTING AERODYNAMIC RESULTS

Figure	Type of plot	Configuration	Remarks
6	C_m, C_N, C_A, $C_{A,b}$ against α	Basic model with and without end plates	Effects of end plates on static longitudinal aerodynamic characteristics of basic model
7	C_m, C_N, and C_A against α	Basic model with and without end plates and control surface 1	Effects of control surface 1 on longitudinal aerodynamic characteristics of basic model
8	C_m, C_N, and C_A against α	Basic model with and without end plates and control surface 2	Effects of control surface 2 on longitudinal aerodynamic characteristics of basic model
9	C_m, C_N, and C_A against α	Basic model with and without end plates and control surface 3	Effects of control surface 3 on longitudinal aerodynamic characteristics of basic model
10	C_m, C_N, and C_A against α	Basic model with and without end plates and control surface 4	Effects of control surface 4 on longitudinal aerodynamic characteristics of basic model
11	C_m, C_N, and C_A against α	Basic model with and without and plates and control surface 5	Effects of control surface 5 on longitudinal aerodynamic characteristics of basic model
12	C_m, C_N, and C_A against α	Basic model with and without end plates and control surface 6	Effects of control surface 6 on longitudinal aerodynamic characteristics of basic model
13	C_l against α	Basic model with and without end plates and control surfaces, $\delta = \pm 10^\circ$	Effects of control surfaces on rolling-moment characteristics of basic model
14	C_h against α	Basic model with end plates and control surfaces 1 to 6	Hinge-moment characteristics of control surfaces
15	$C_{N,c}$ against α	Basic model with end plates and control surfaces 1 to 6	Normal-force characteristics of control surfaces
16	C_{m_α}, C_{N_α}, and $C_{A,\alpha=0}$ against M	Basic model with and without end plates	Summary
17	$\frac{x}{d}$ against M	Basic model with and without end plates	Summary
18	C_{m_δ} against M	Basic model with end plates and control surfaces 1 to 6	Summary
19	ΔC_l against M	Basic model with end plates and control surfaces, $\delta = \pm 10^\circ$	Summary
20	C_h against δ	Basic model with end plates and control surfaces 1 to 6	Summary
21	$\frac{x}{\bar{d}}$ against M	Basic model with end plates and control surfaces 1 to 6	Summary

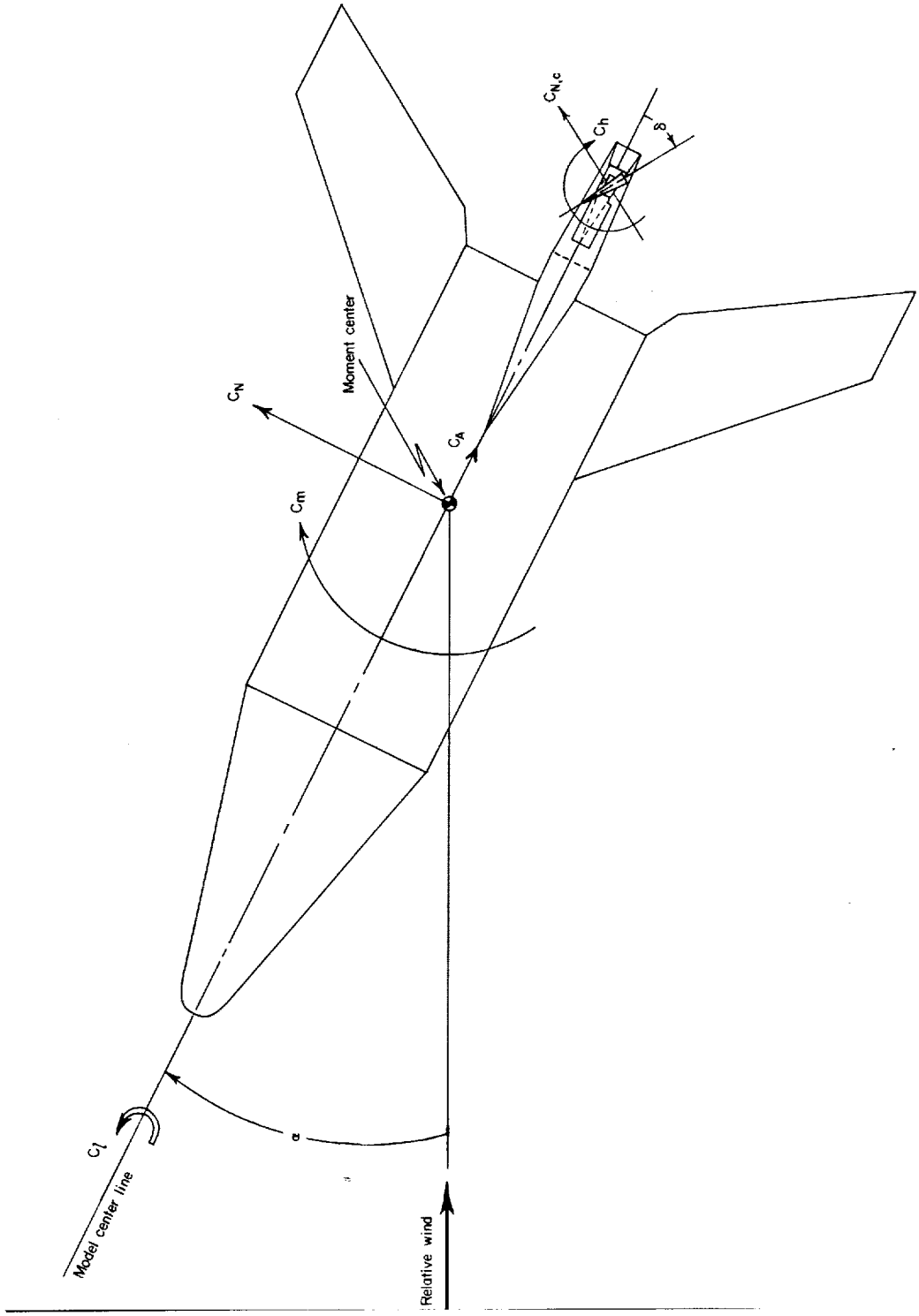

Figure 1.- Body axis system. Arrows indicate positive directions.

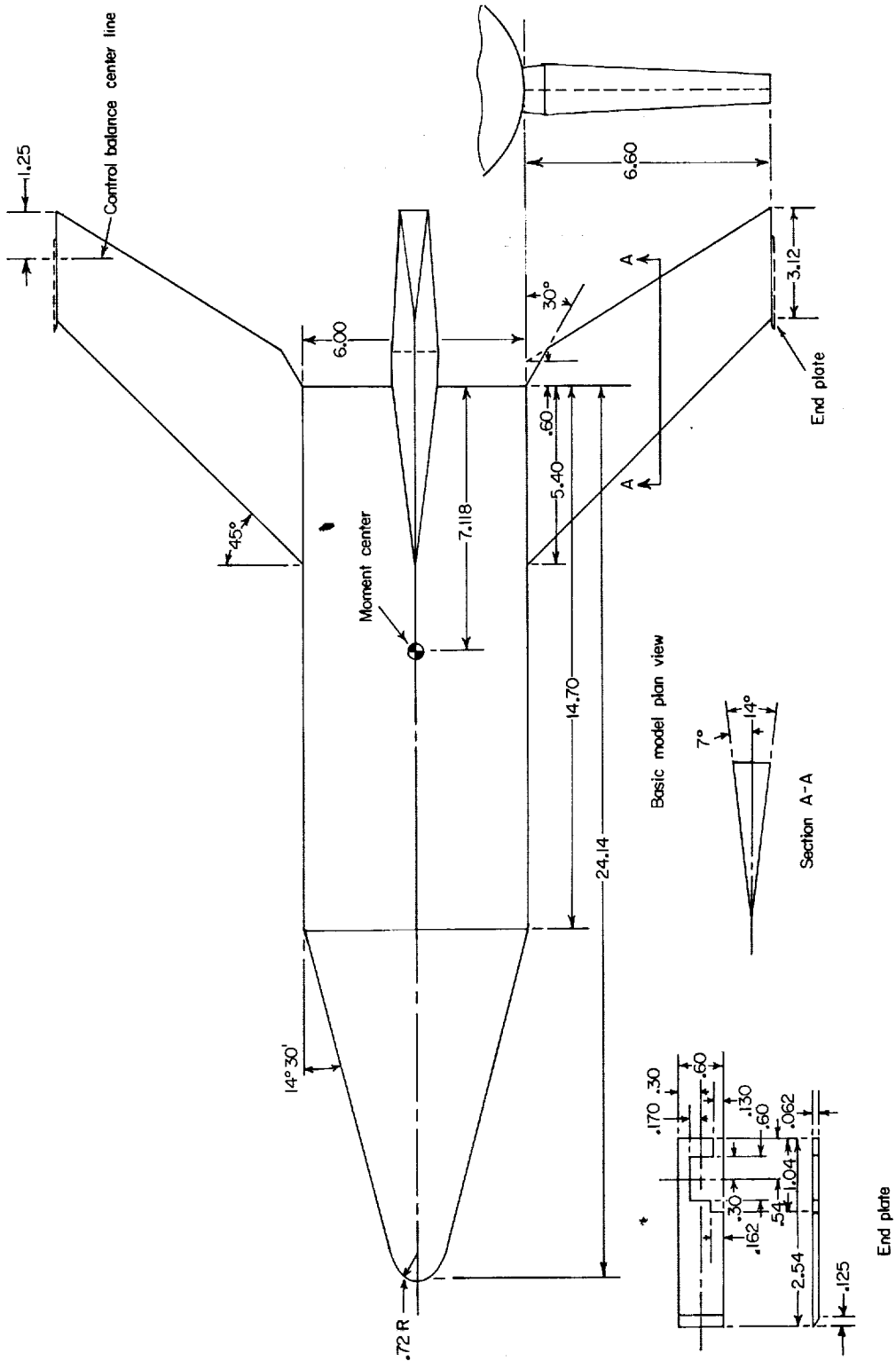

Figure 2.- Details of basic model and of end plates. All dimensions are in inches unless otherwise noted.

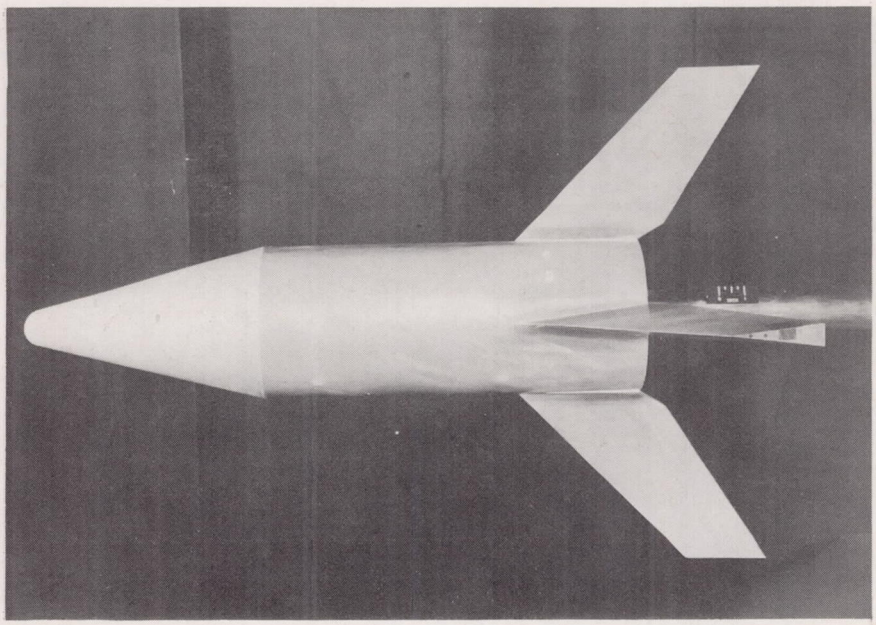

(a) Side view. L-58-4183

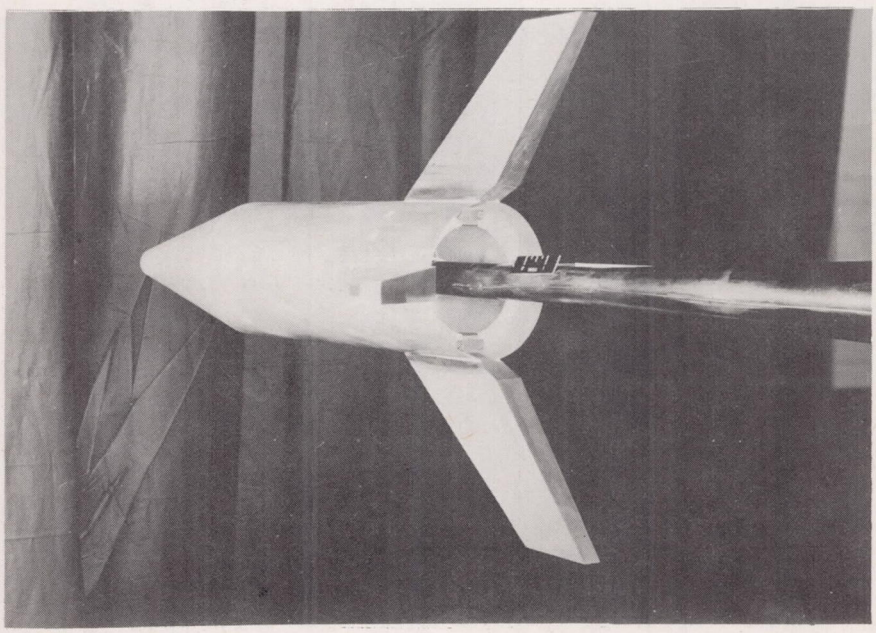

(b) Three-quarter view. L-58-4182

Figure 3.- Basic model.

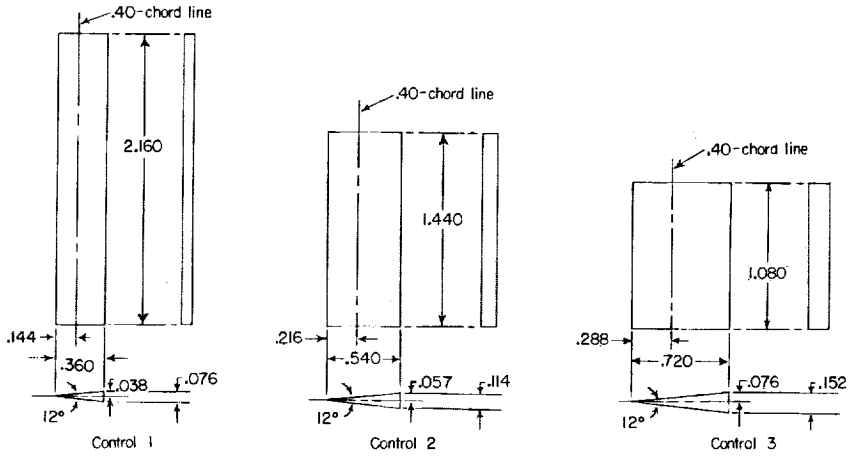

Control	Area, sq. in.	Aspect ratio	$\bar{c}$
1	0.7776	6.00	0.360
2	.7776	2.67	.540
3	.7776	1.50	.720
4	.7776	6.00	.480
5	.7776	2.67	.720
6	.7776	1.50	.960

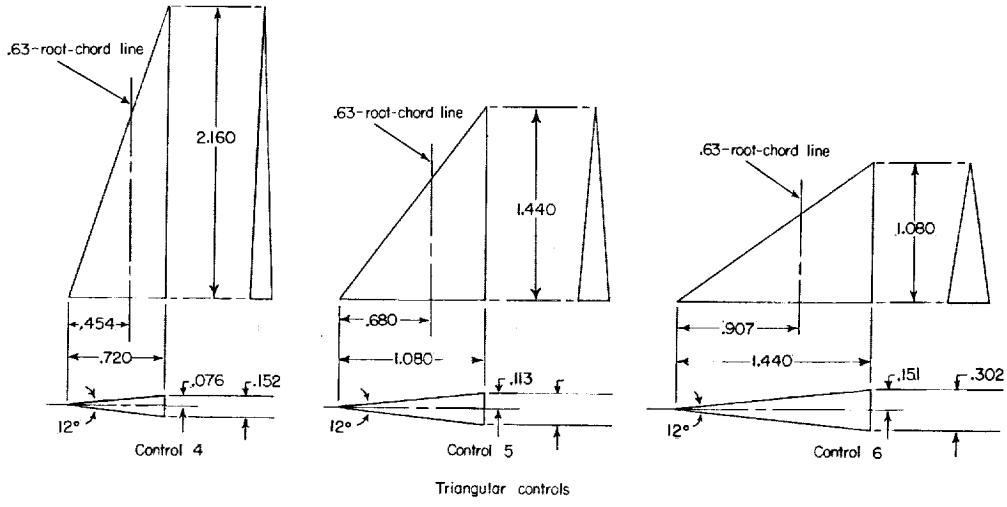

Figure 4.- Details of control surfaces. All dimensions are in inches unless otherwise noted.

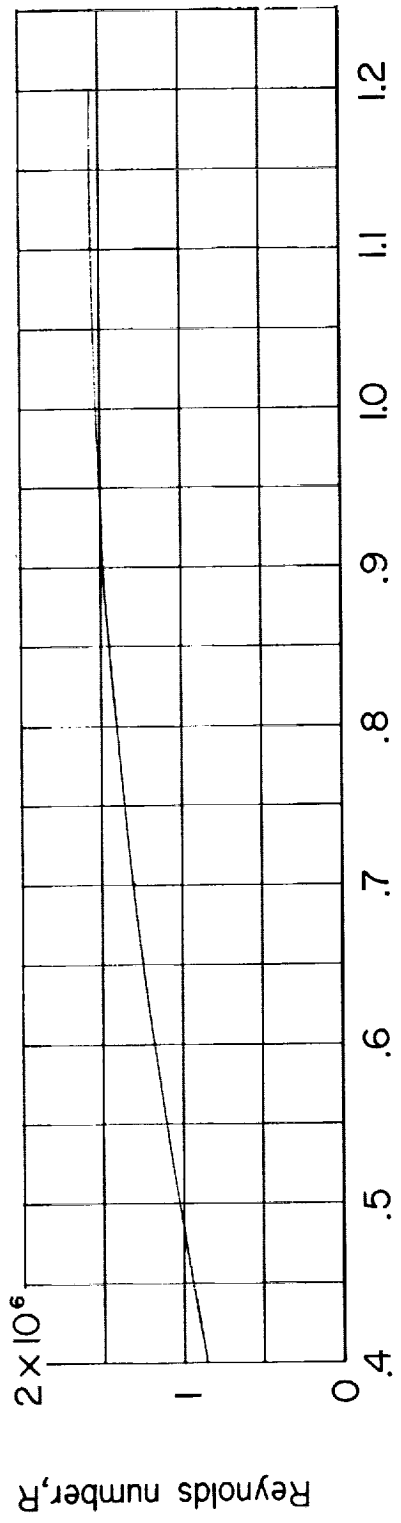

Figure 5.- Variation of Reynolds number, based on maximum body diameter and free-stream conditions, with Mach number.

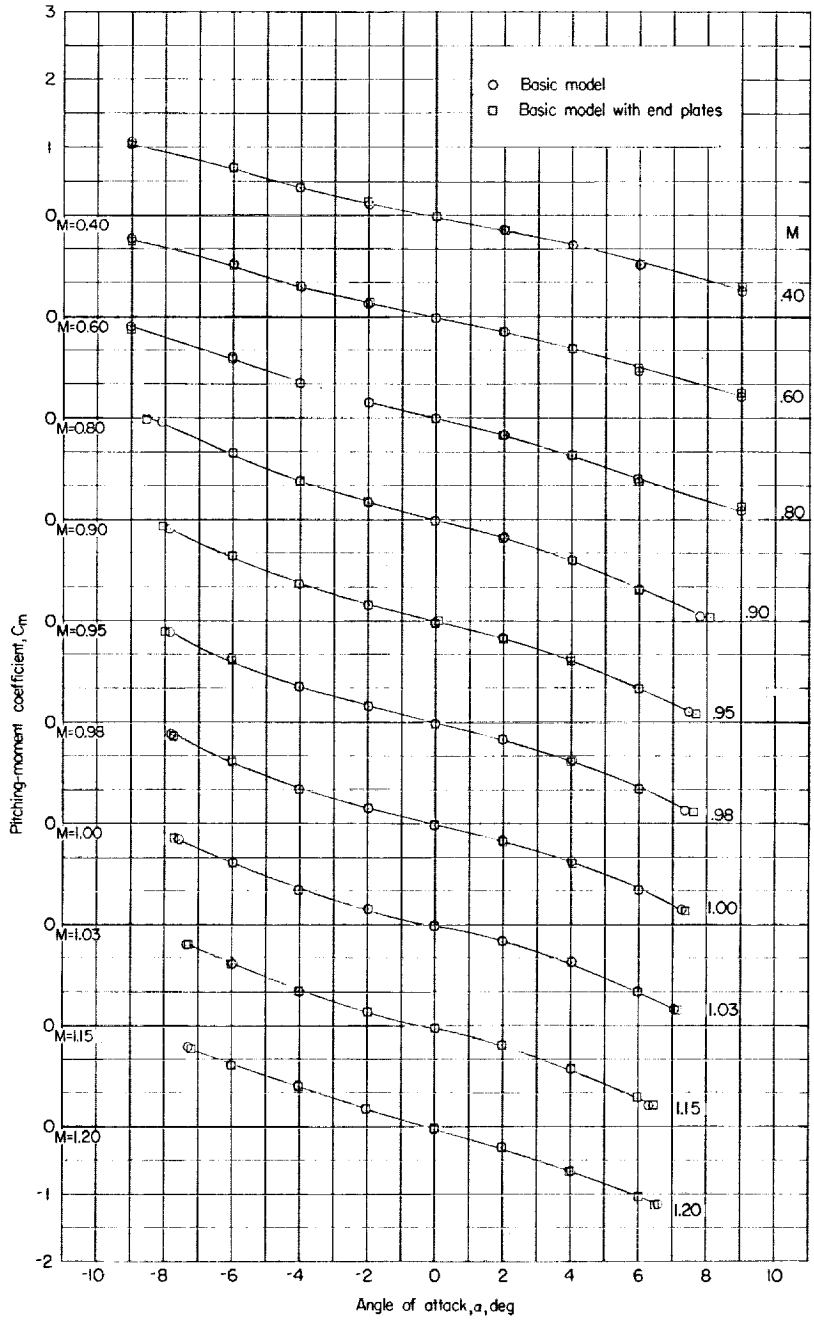

(a) Variation of C_m with α.

Figure 6.- Aerodynamic characteristics in pitch of basic model with and without end plates.

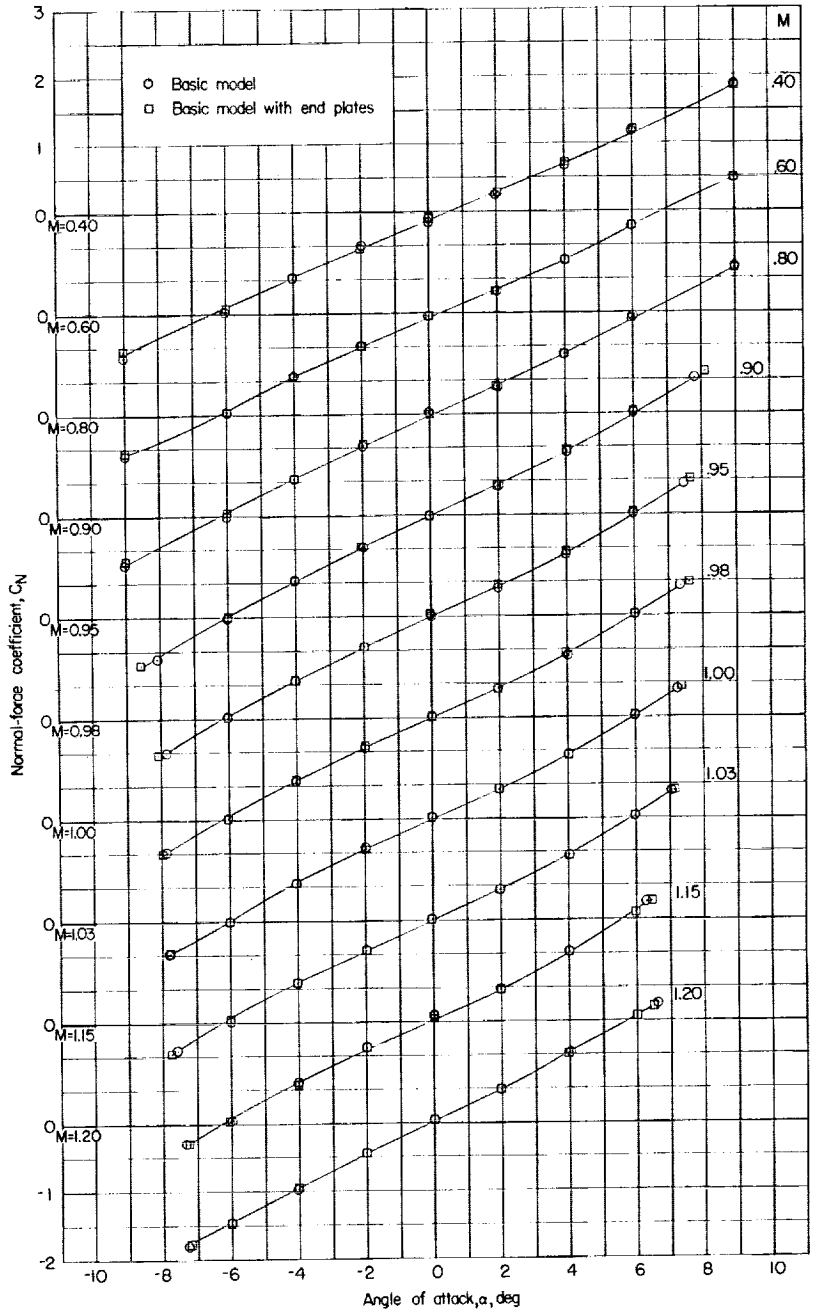

(b) Variation of C_N with α.

Figure 6.- Continued.

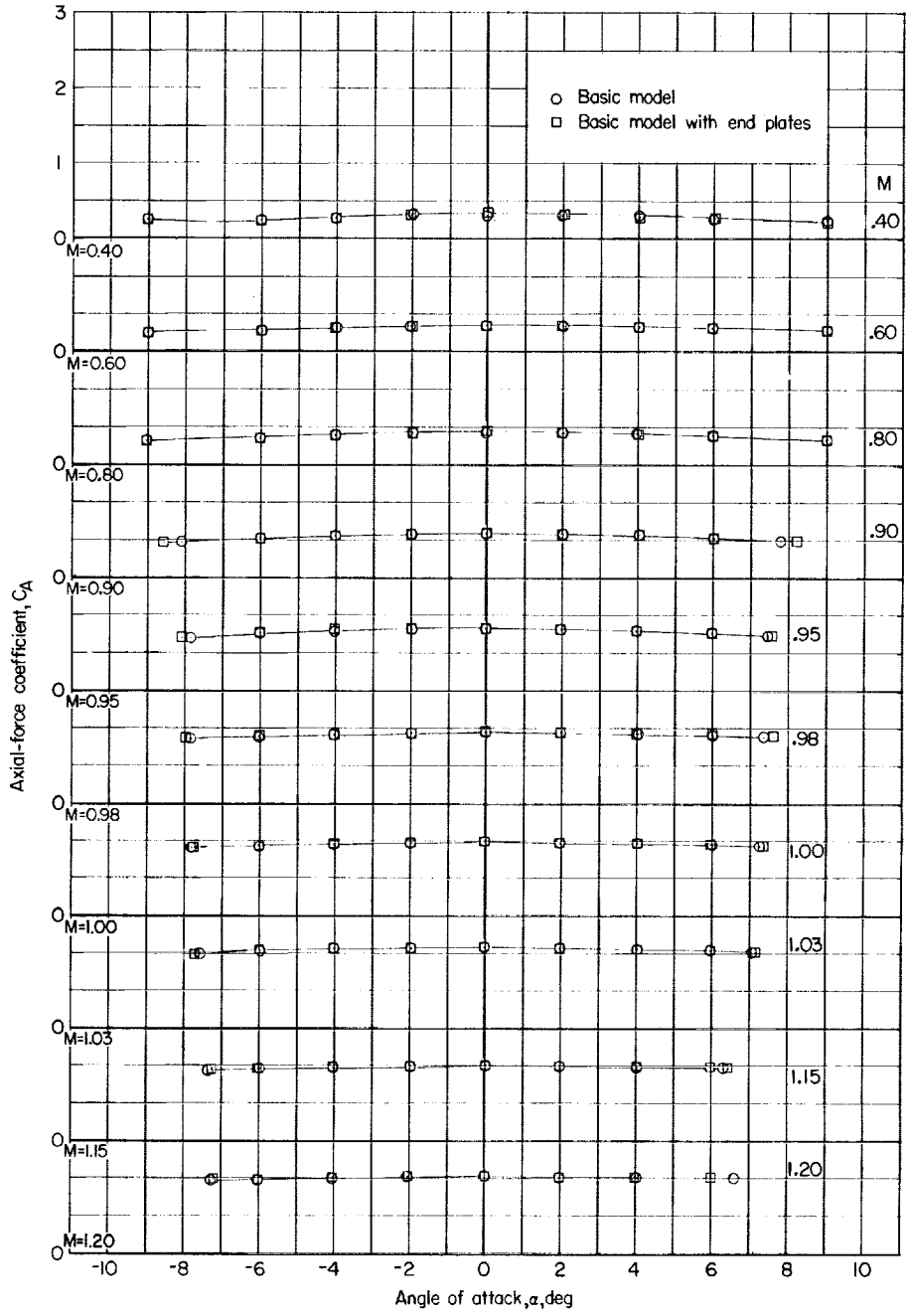

(c) Variation of C_A with α.

Figure 6.- Continued.

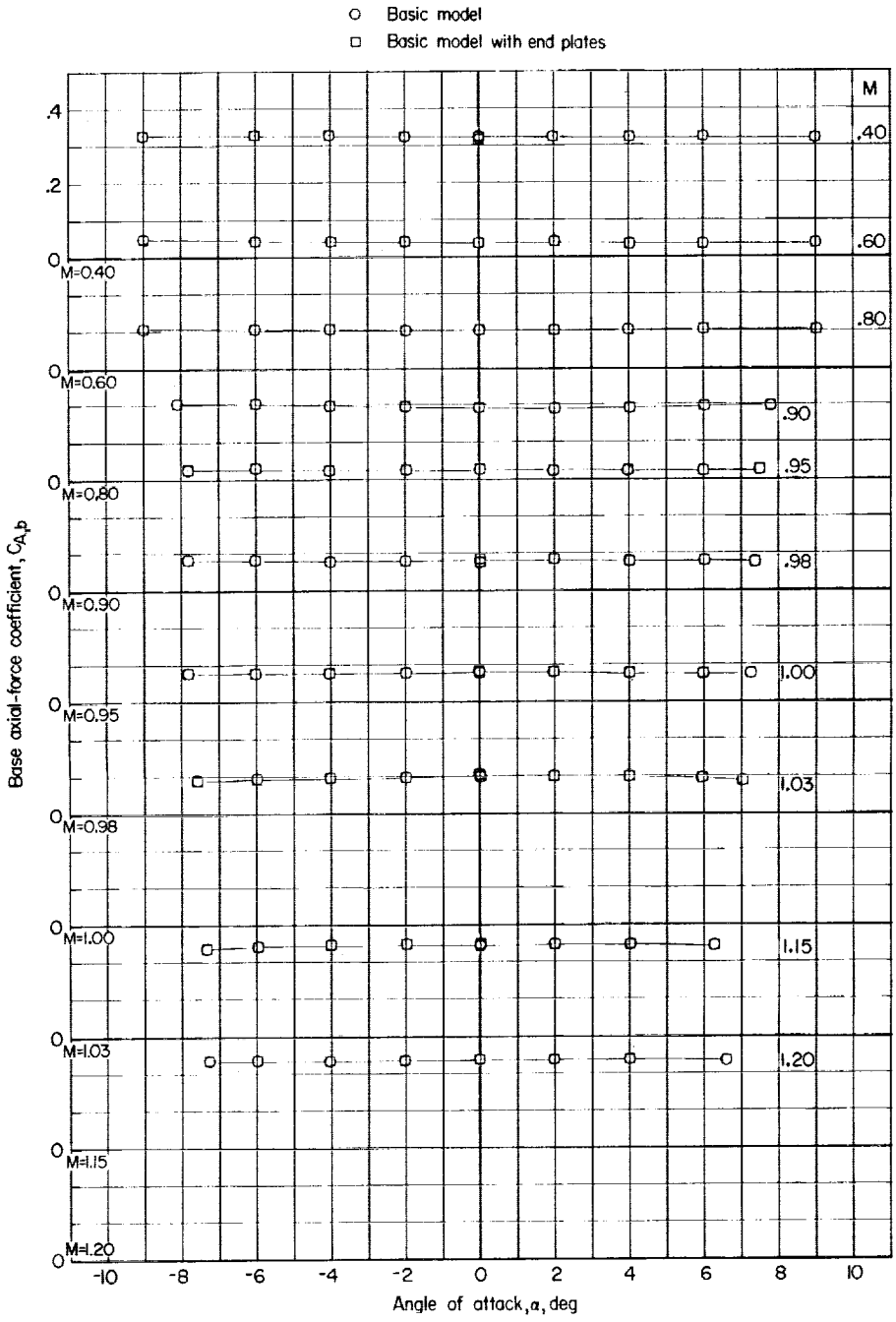

(d) Variation of $C_{A,b}$ with α.

Figure 6.- Concluded.

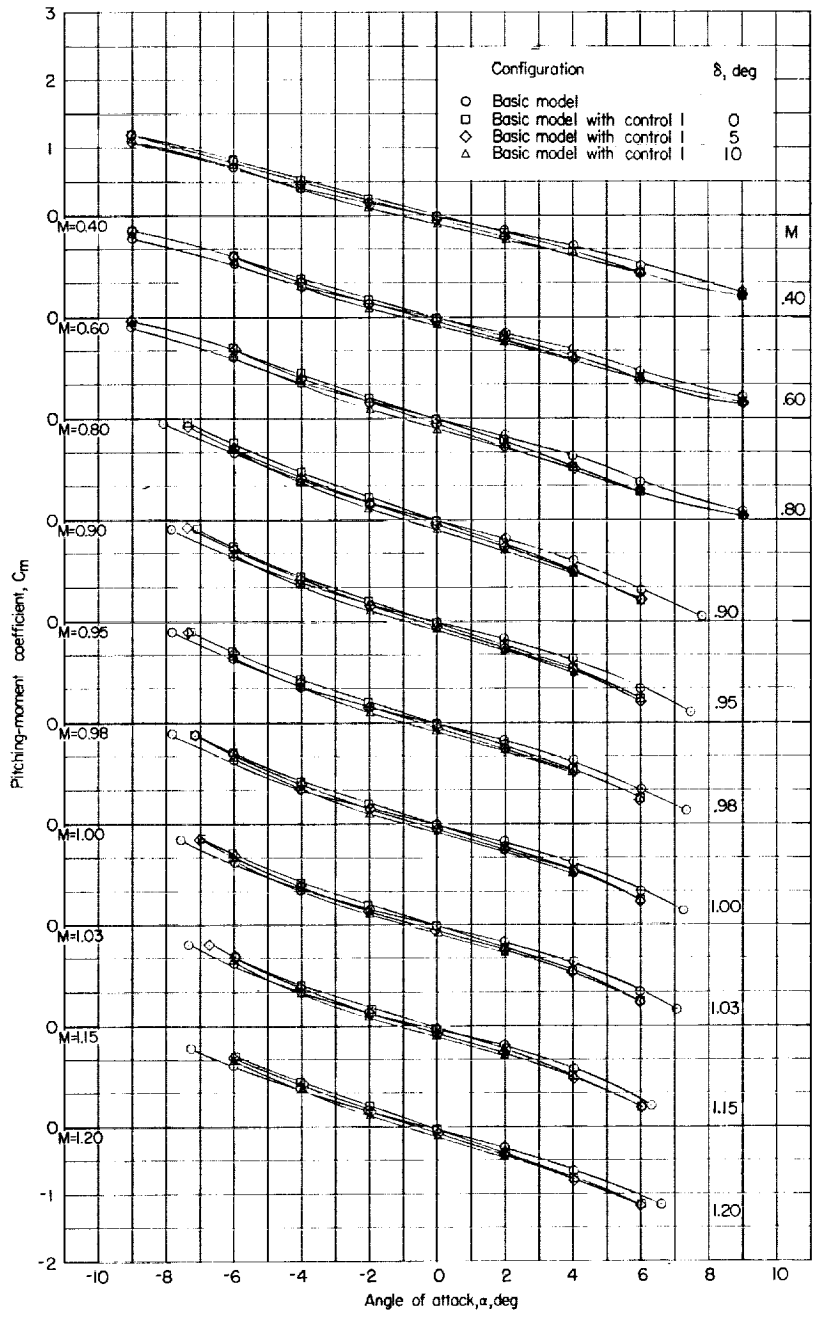

(a) Variation of C_m with α.

Figure 7.- Aerodynamic characteristics in pitch of basic model with and without control surface 1.

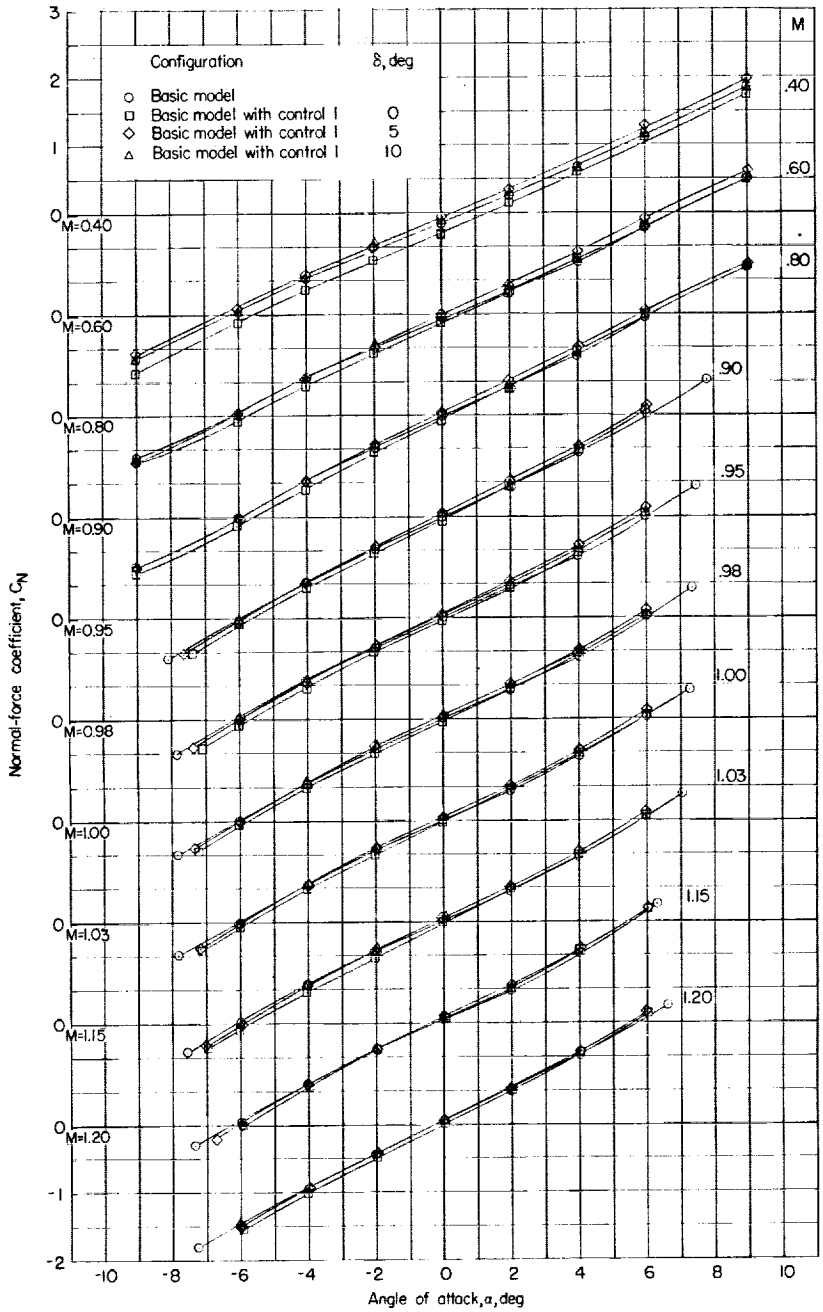

(b) Variation of C_N with α.

Figure 7.- Continued.

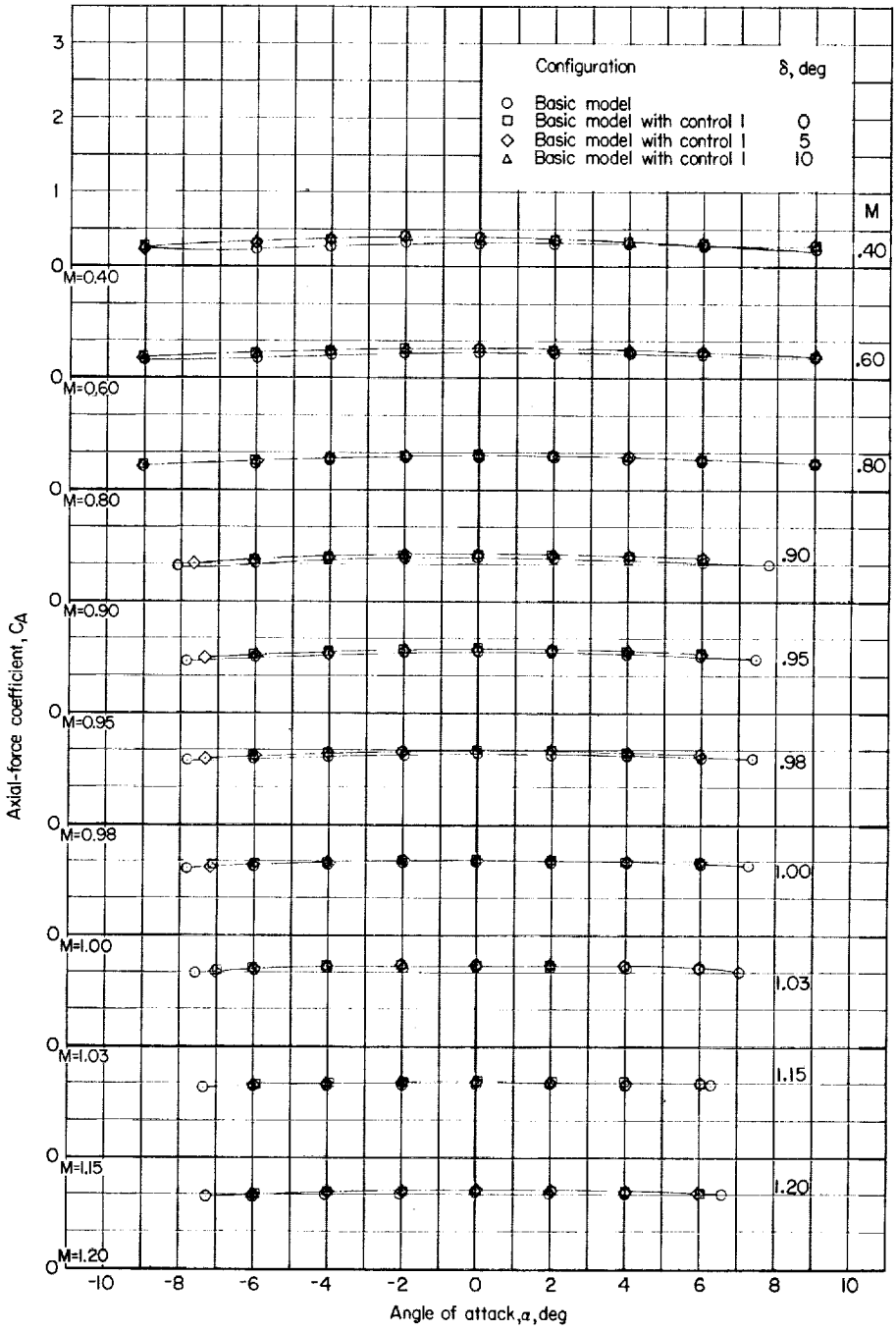

(c) Variation of C_A with α.

Figure 7.- Concluded.

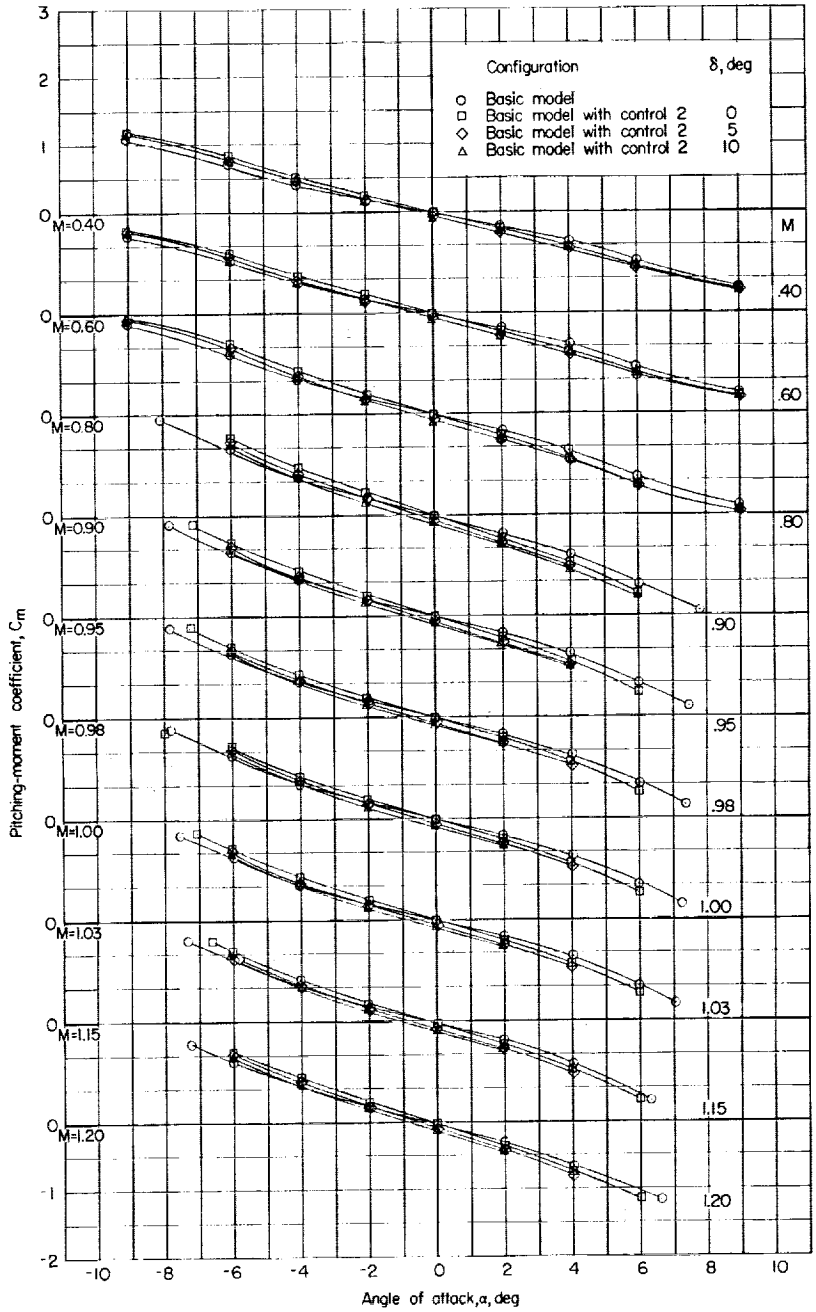

(a) Variation of C_m with α.

Figure 8.- Aerodynamic characteristics in pitch of basic model with and without control surface 2.

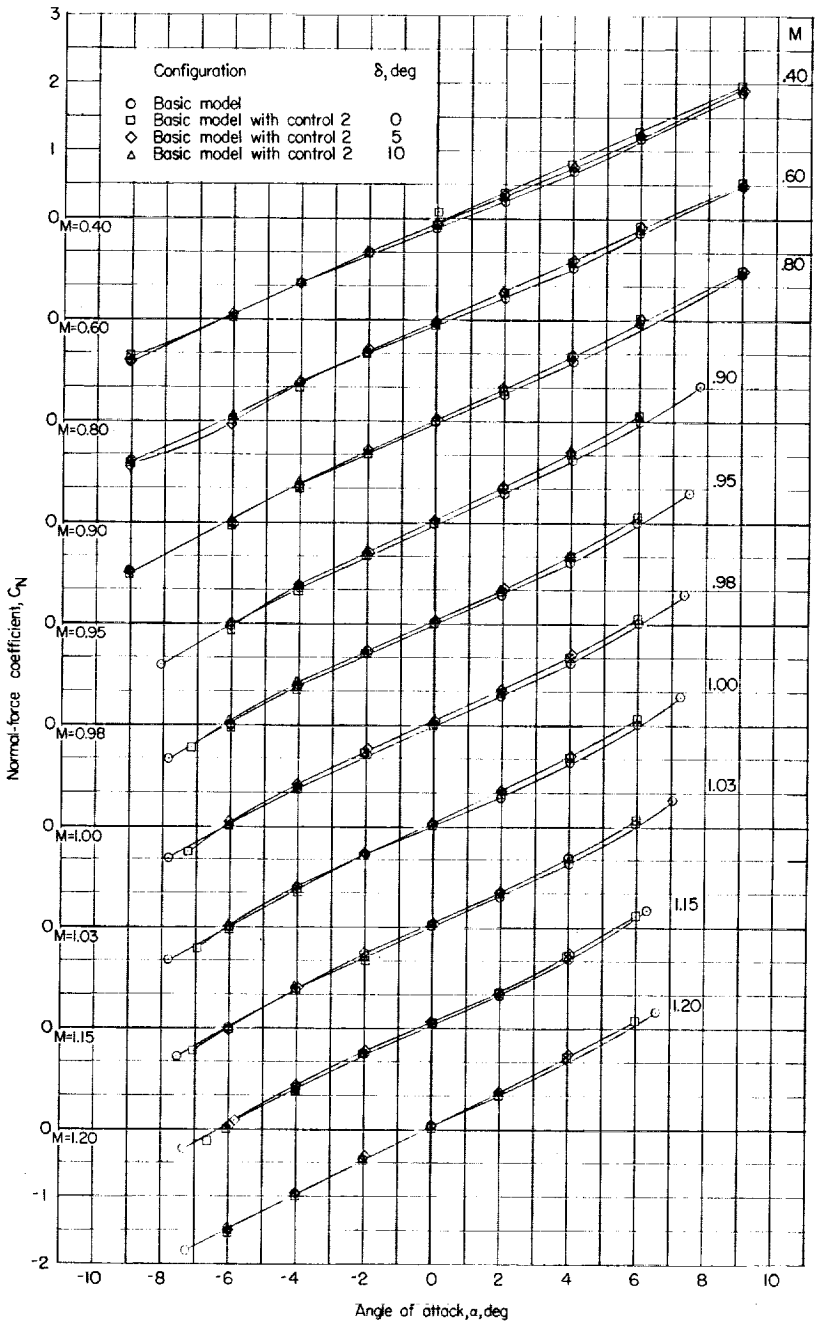

(b) Variation of C_N with α.

Figure 8.- Continued.

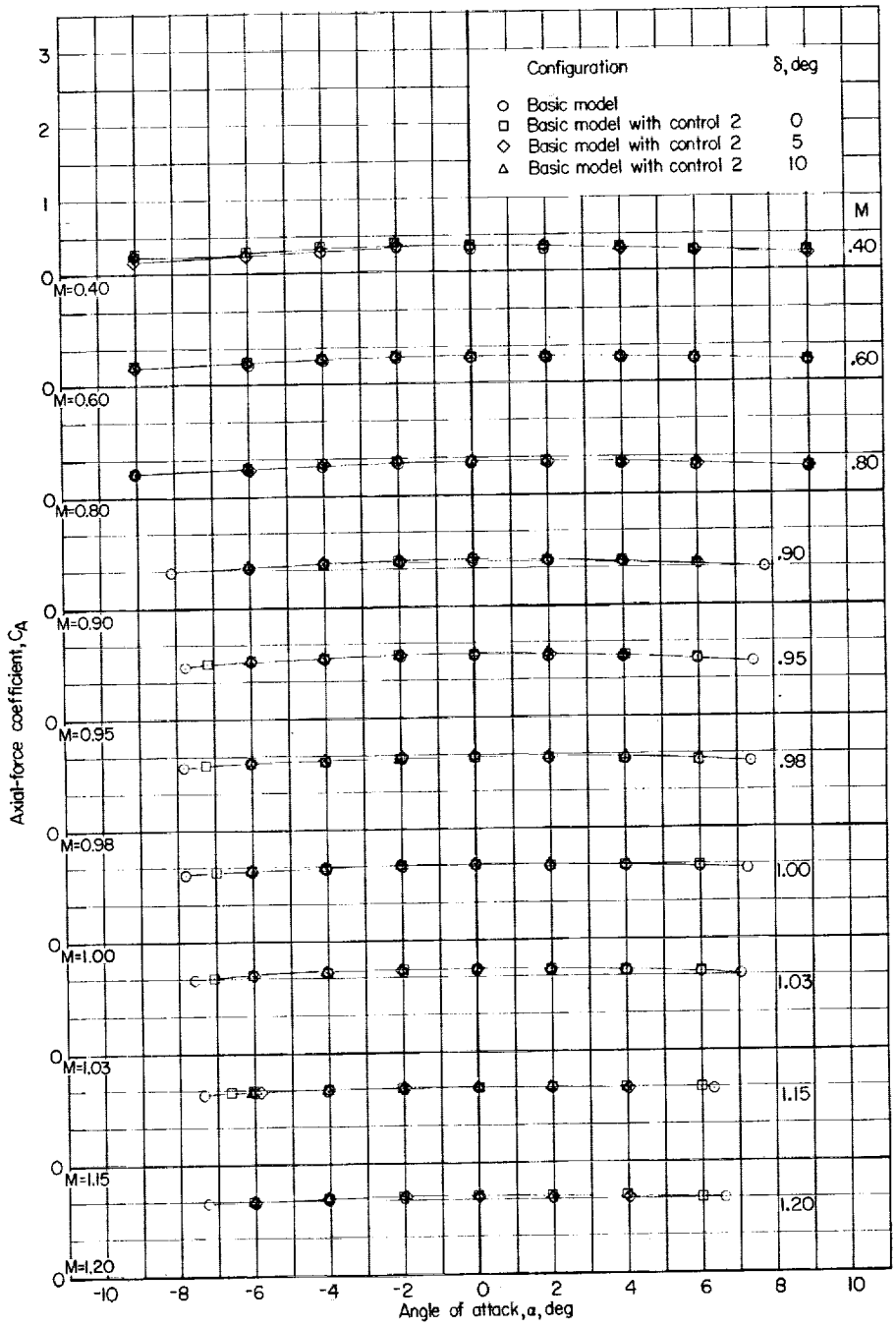

(c) Variation of C_A with α.

Figure 8.- Concluded.

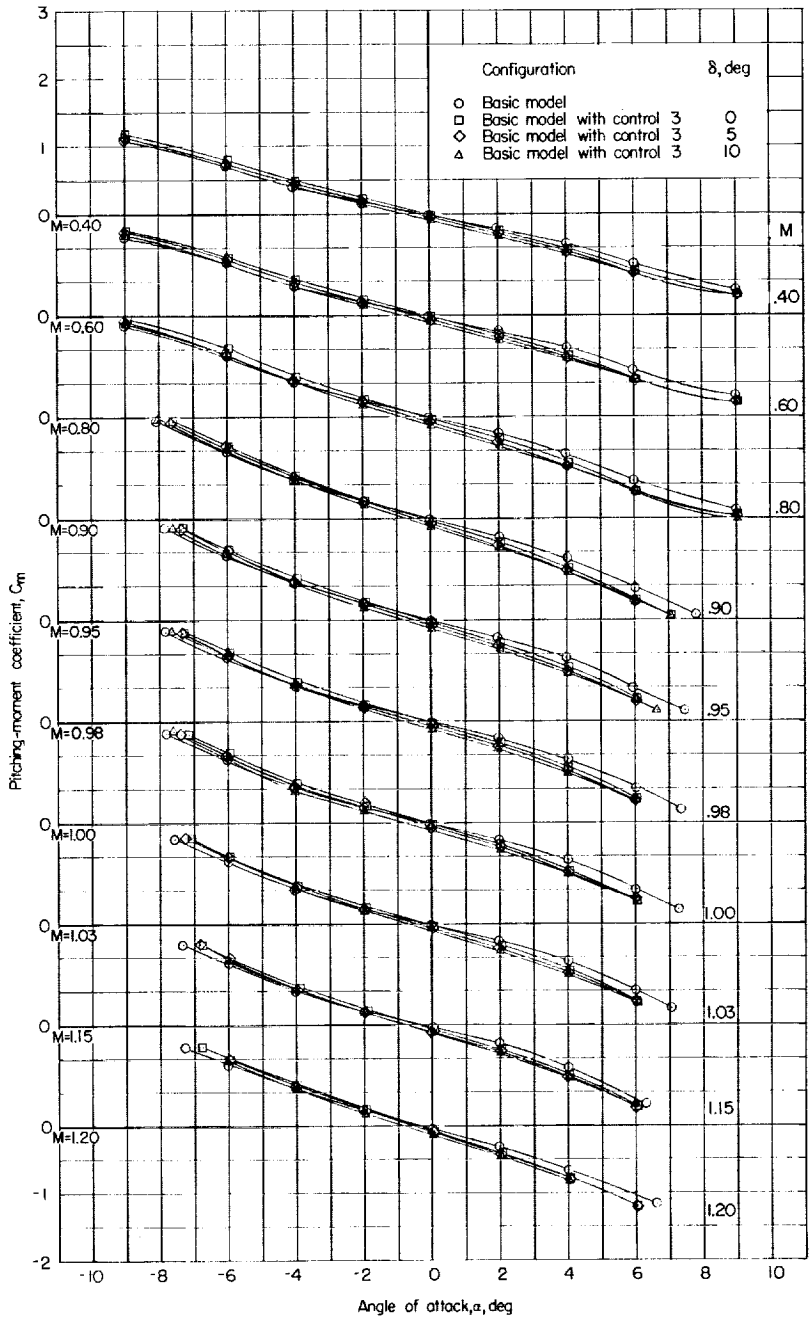

(a) Variation of C_m with α.

Figure 9.- Aerodynamic characteristics in pitch of basic model with and without control surface 3.

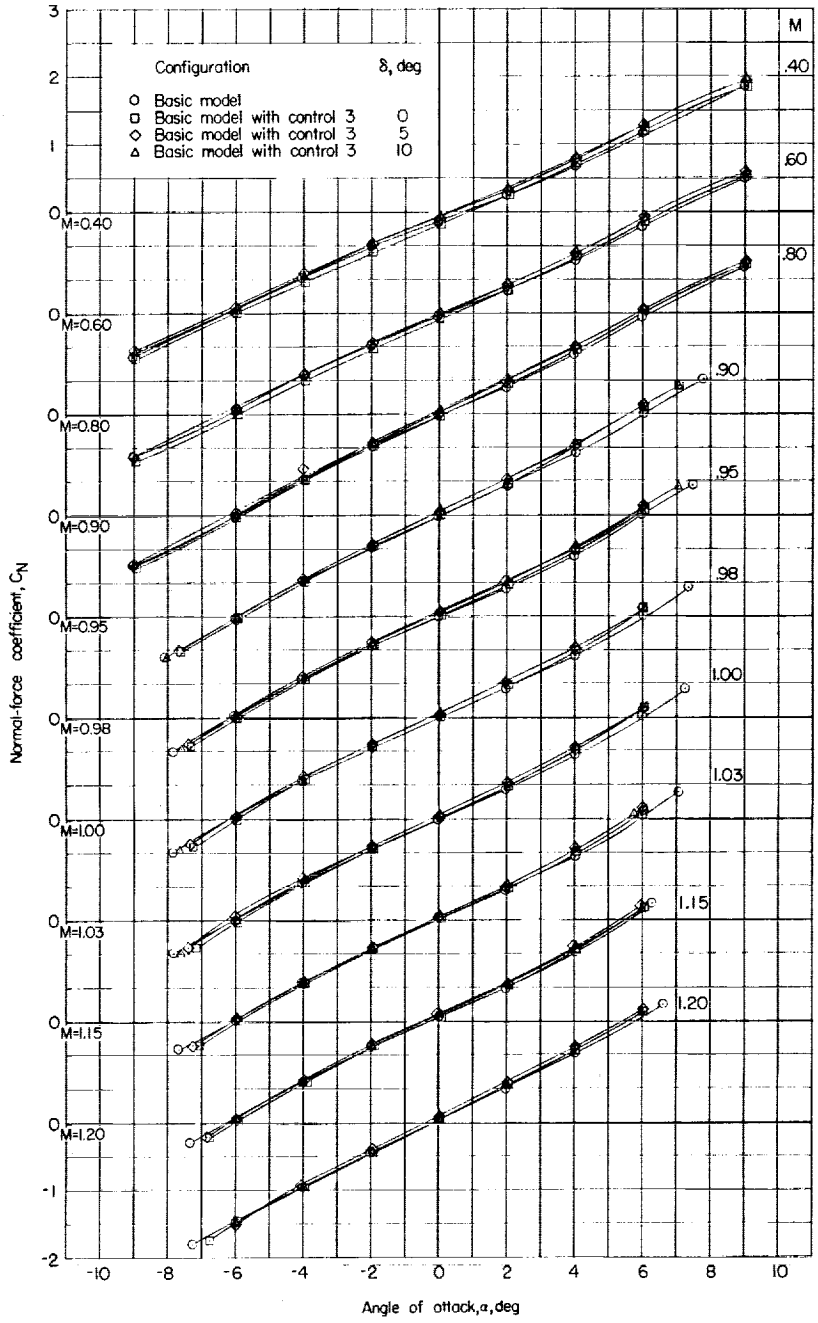

(b) Variation of C_N with α.

Figure 9.- Continued.

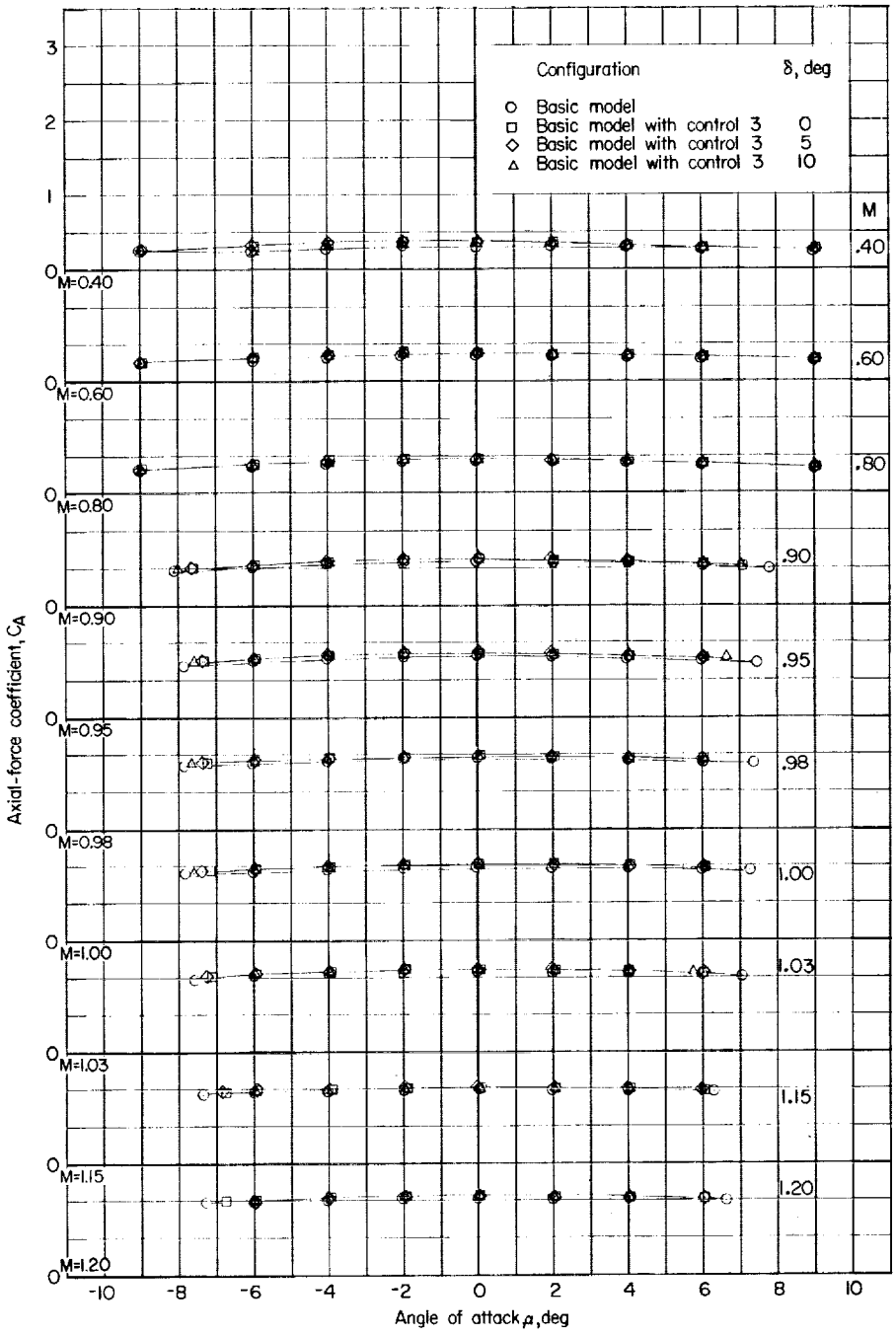

(c) Variation of C_A with α.

Figure 9.- Concluded.

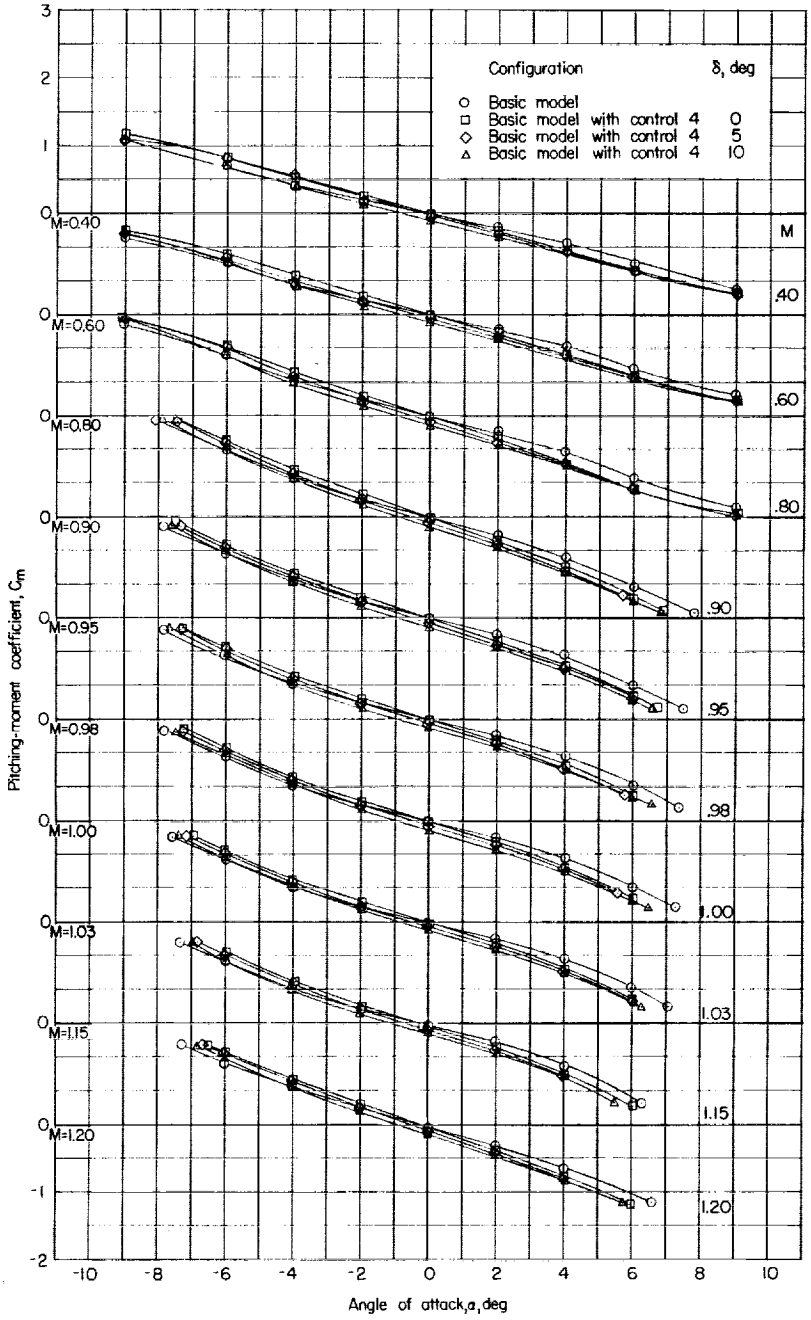

(a) Variation of C_m with α.

Figure 10.- Aerodynamic characteristics in pitch of basic model with and without control surface 4.

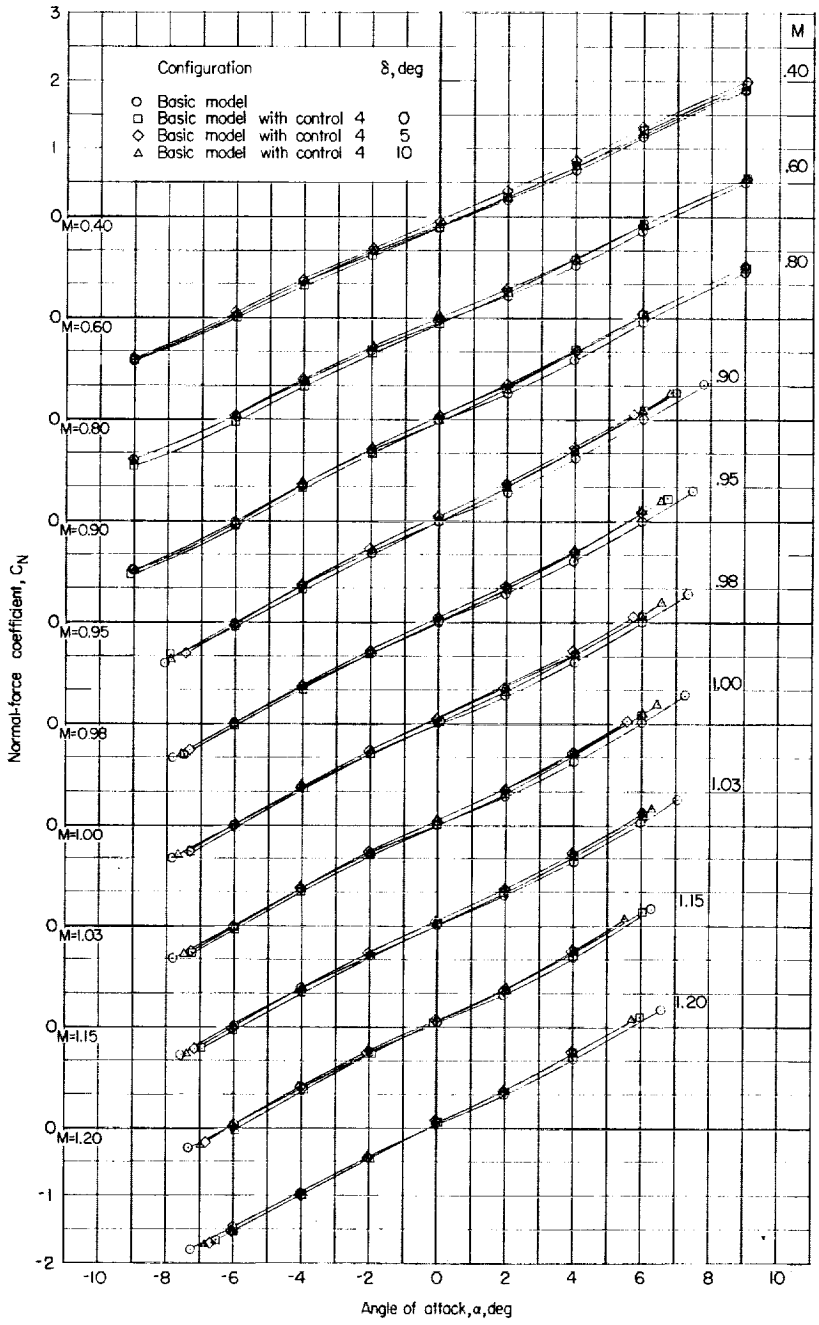

(b) Variation of C_N with α.

Figure 10.- Continued.

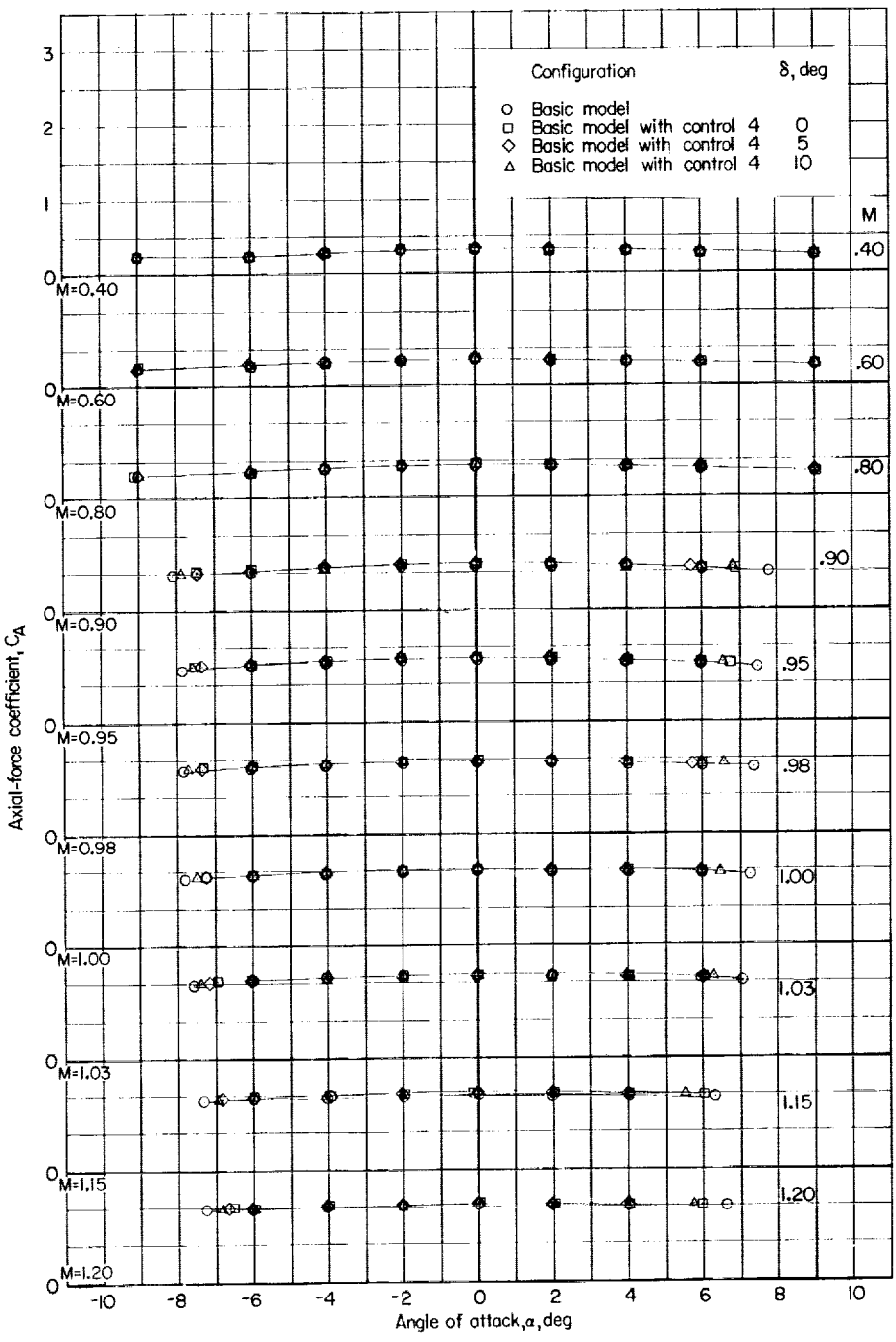

(c) Variation of C_A with α.

Figure 10.- Concluded.

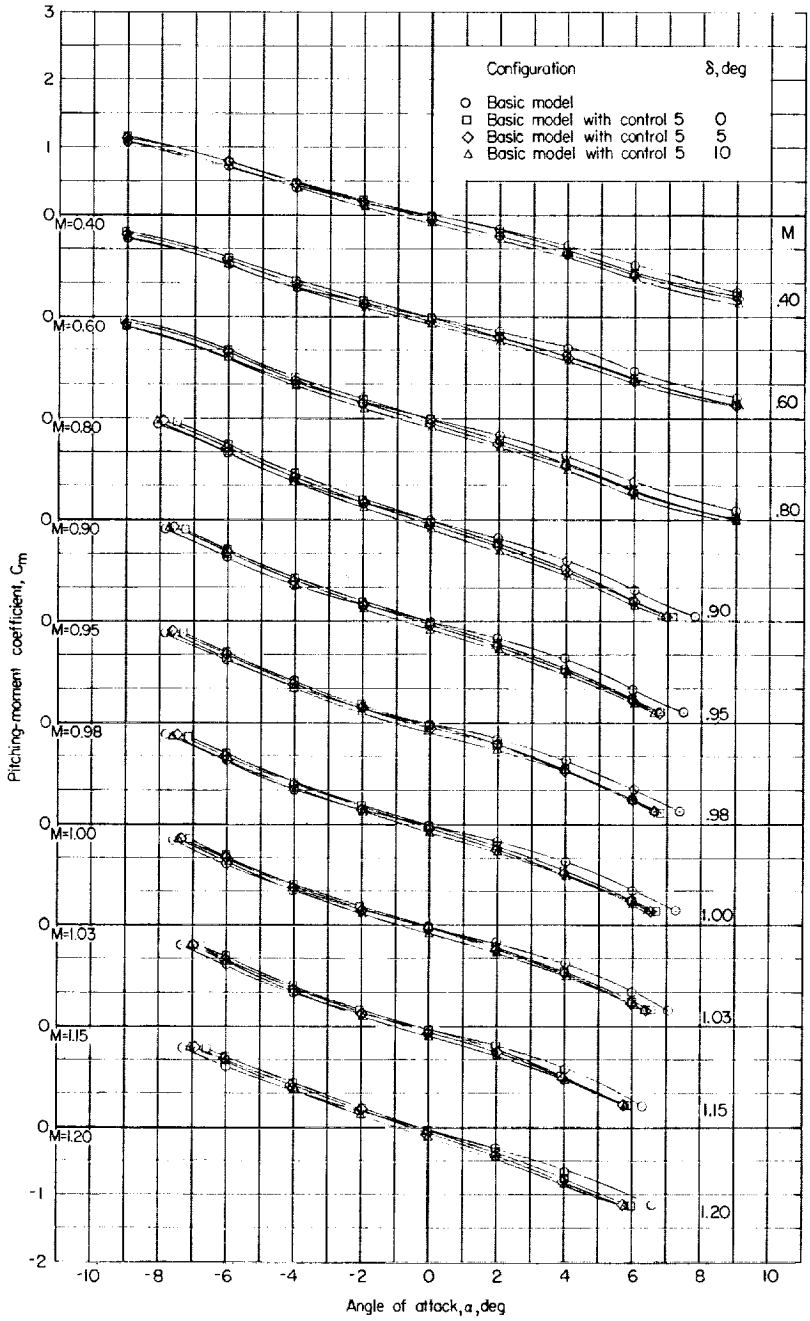

(a) Variation of C_m with α.

Figure 11.- Aerodynamic characteristics in pitch of basic model with and without control surface 5.

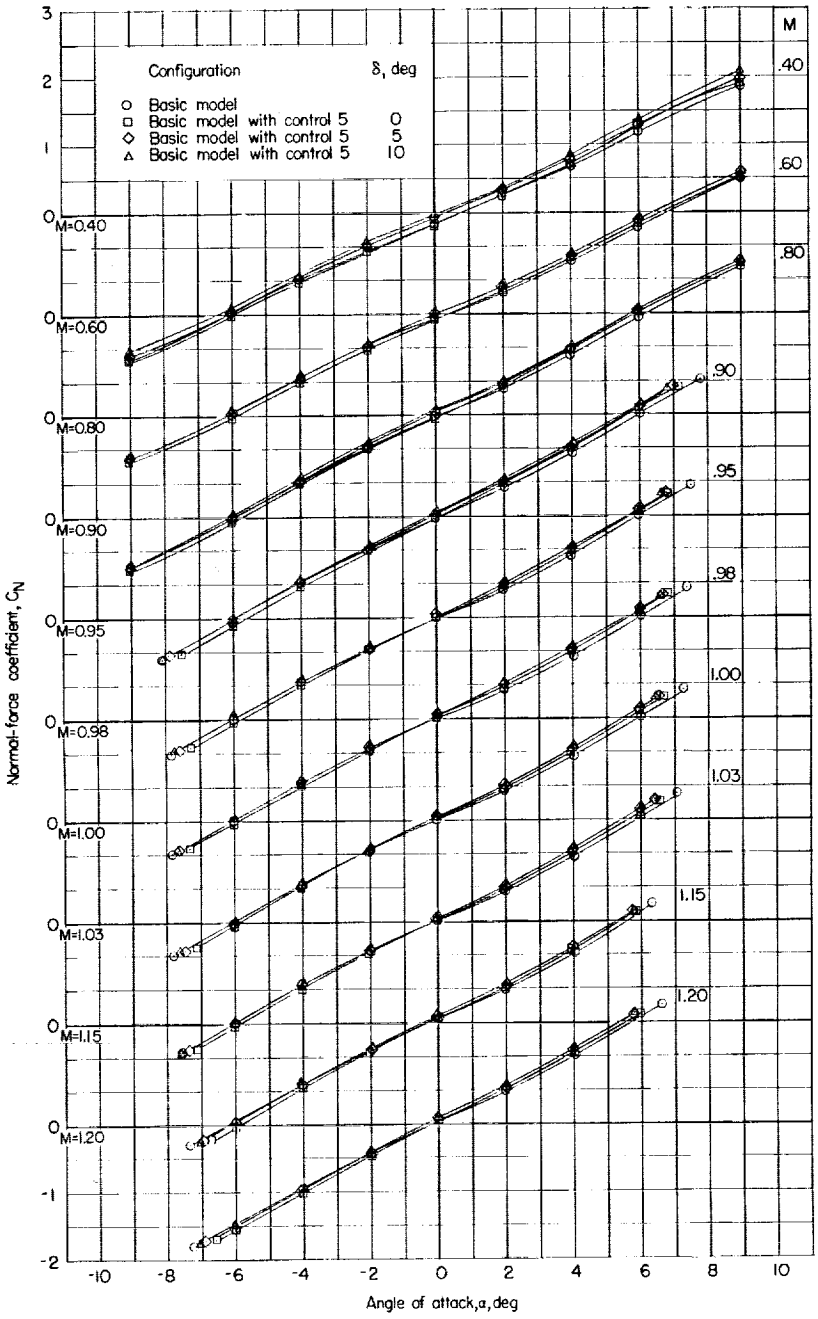

(b) Variation of C_N with α.

Figure 11.- Continued.

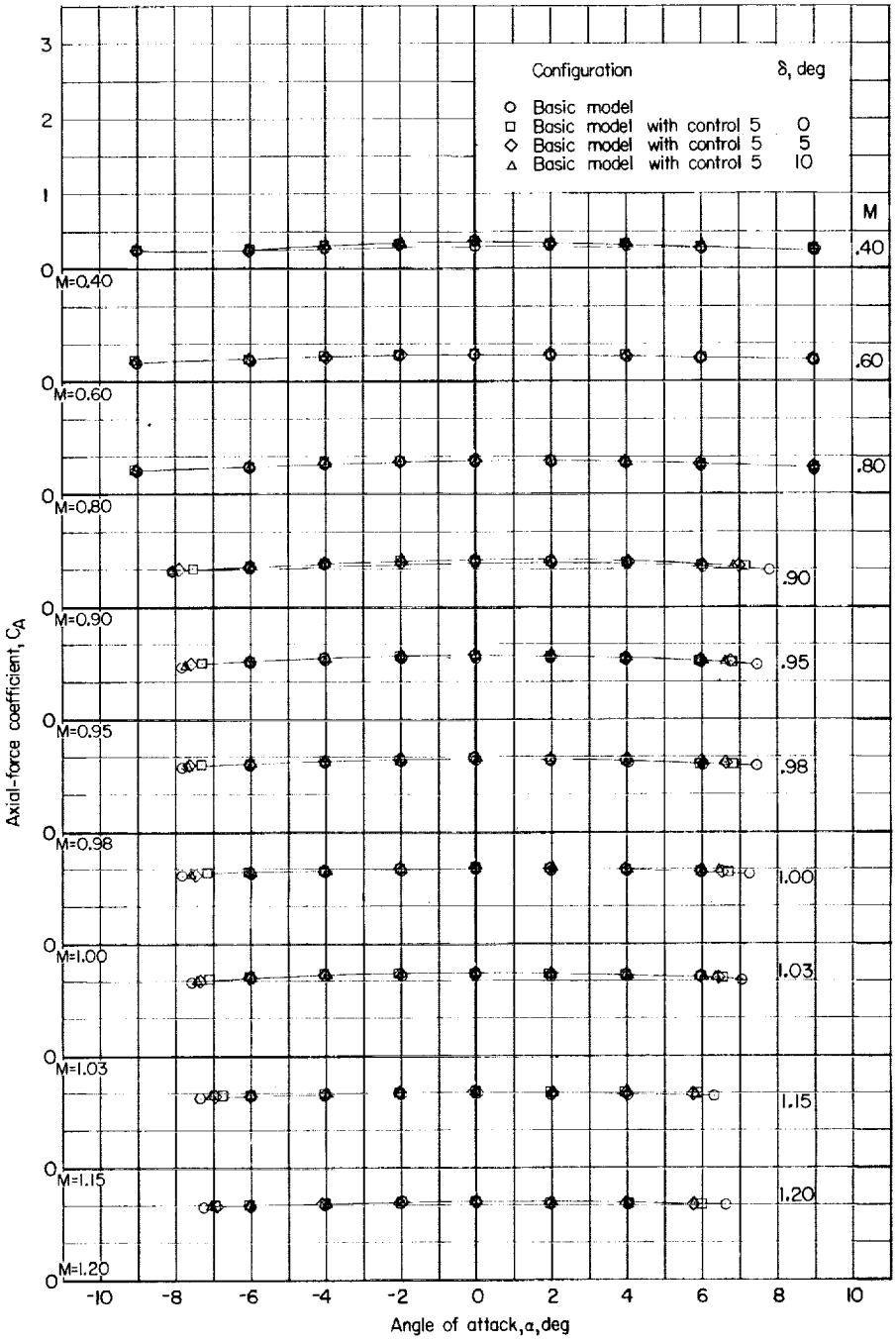

(c) Variation of C_A with α.

Figure 11.- Concluded.

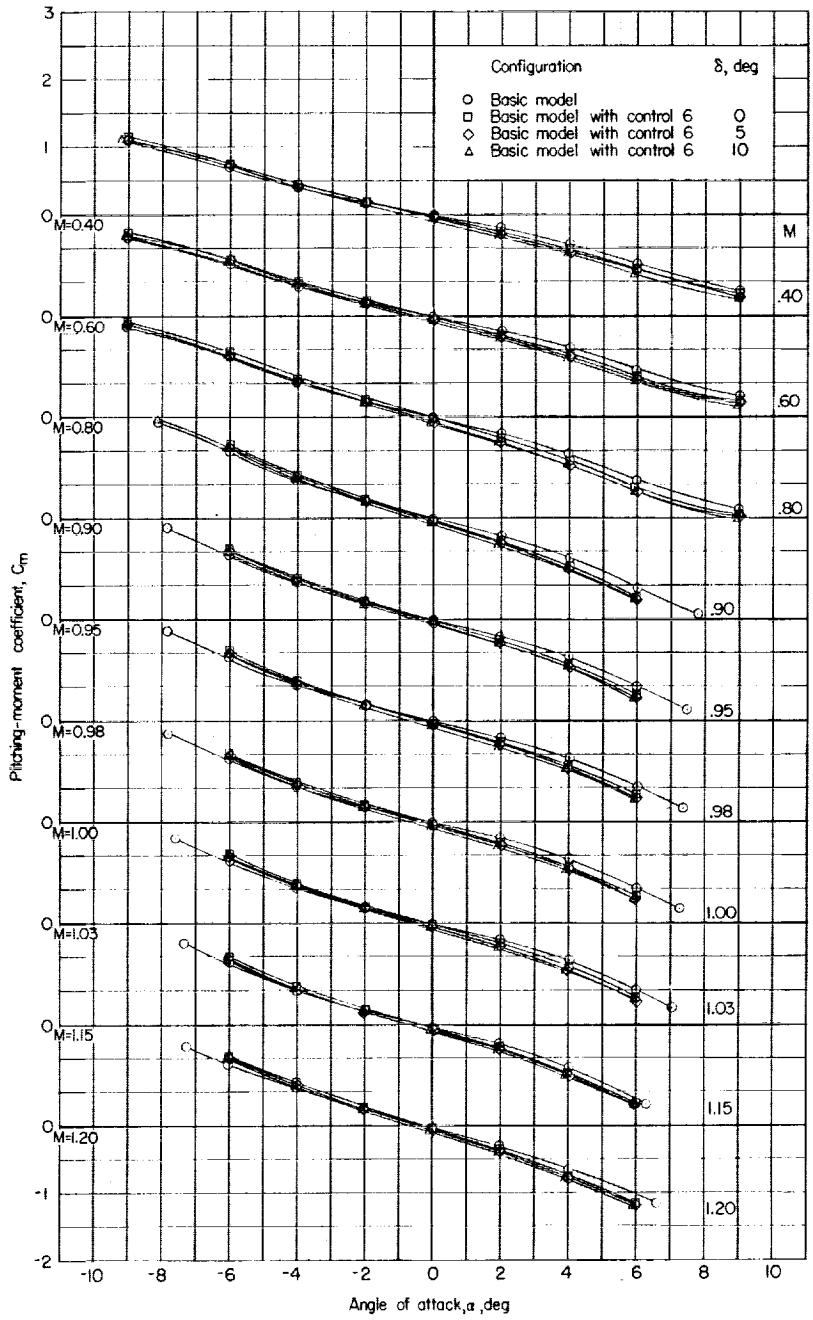

(a) Variation of C_m with α.

Figure 12.- Aerodynamic characteristics in pitch of basic model with and without control surface 6.

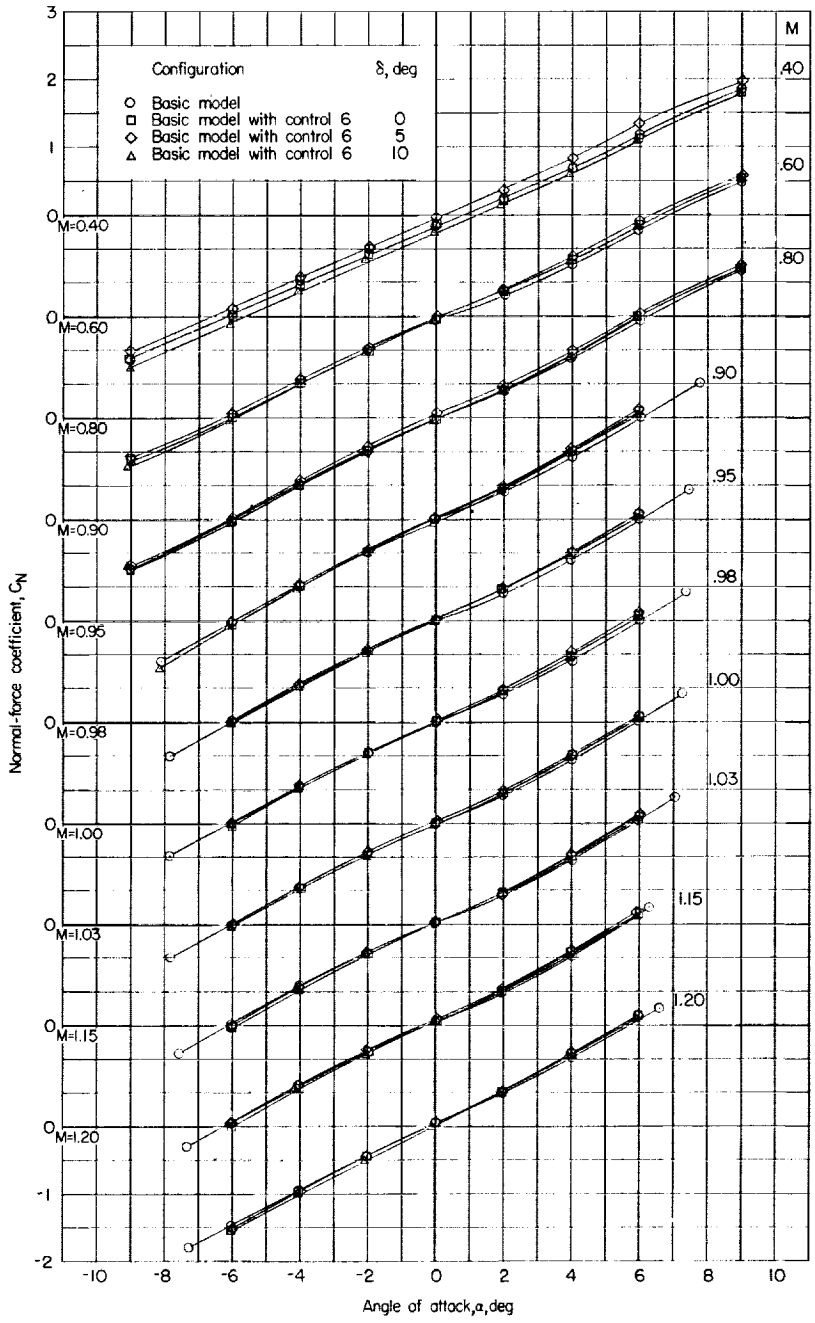

(b) Variation of C_N with α.

Figure 12.- Continued.

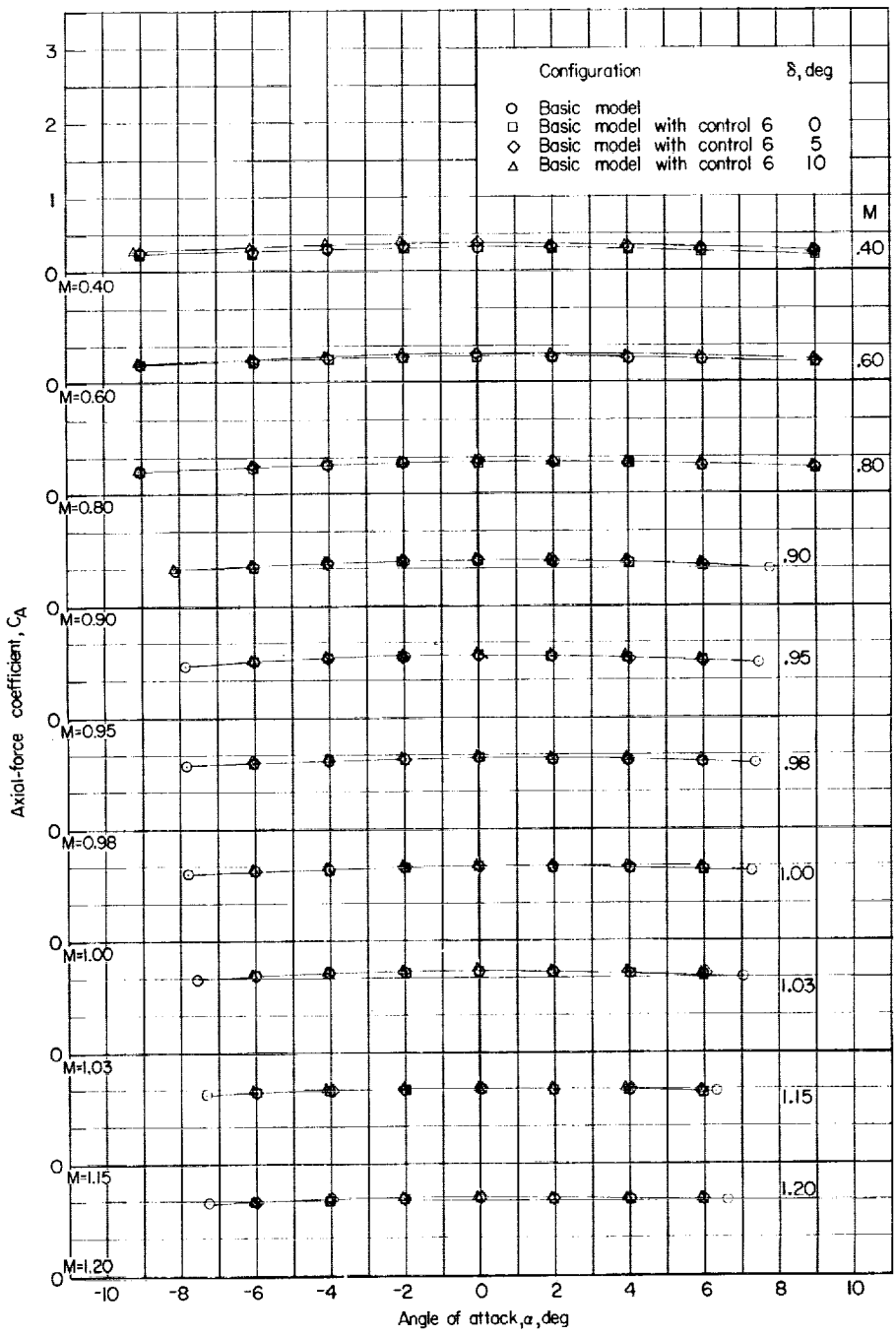

(c) Variation of C_A with α.

Figure 12.- Concluded.

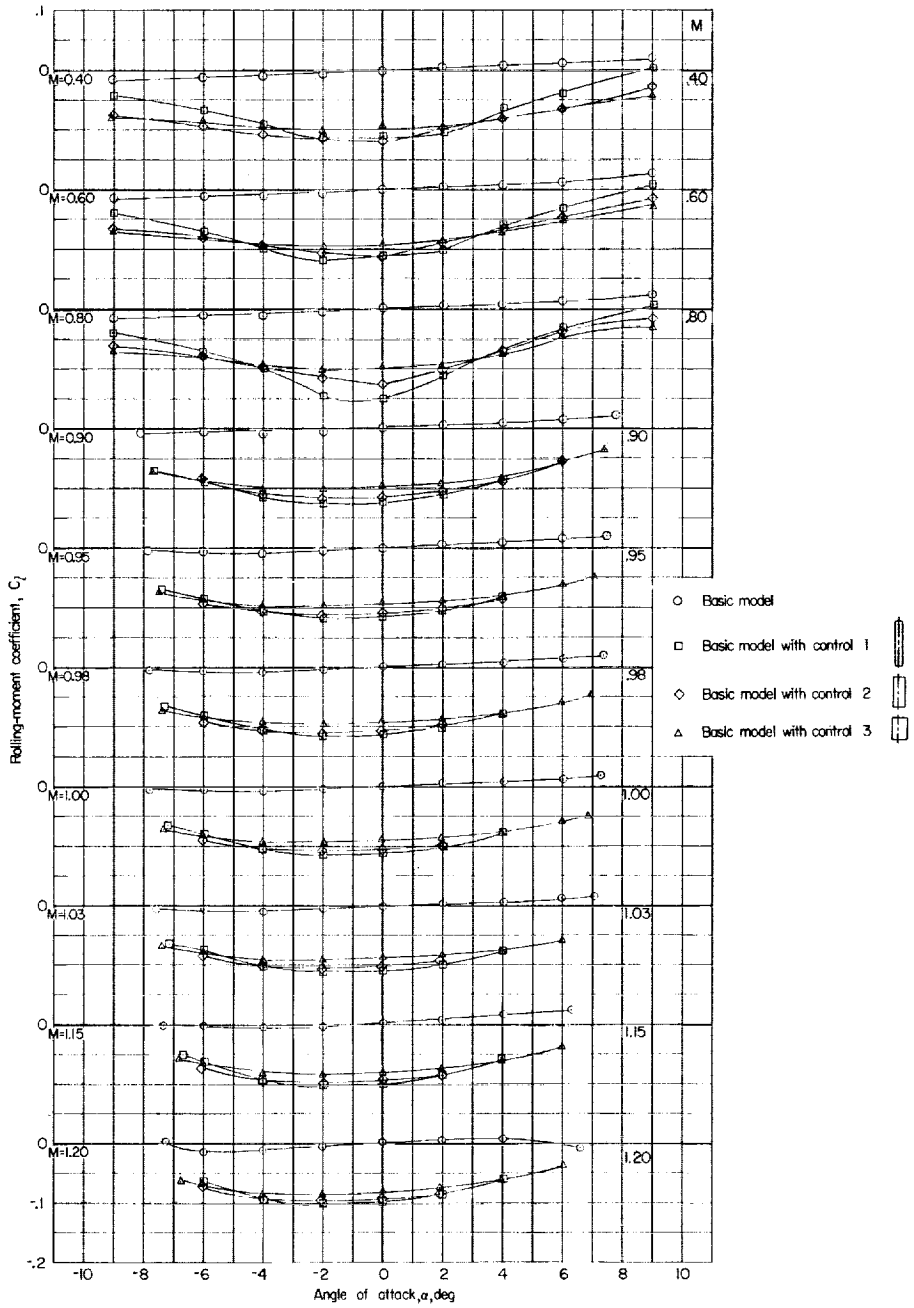

(a) Rectangular control surfaces.

Figure 13.- Variation of rolling-moment coefficient with angle of attack for model with and without control surfaces. Controls set differentially; $\delta_{left} = -10^{\circ}$; $\delta_{right} = 10^{\circ}$.

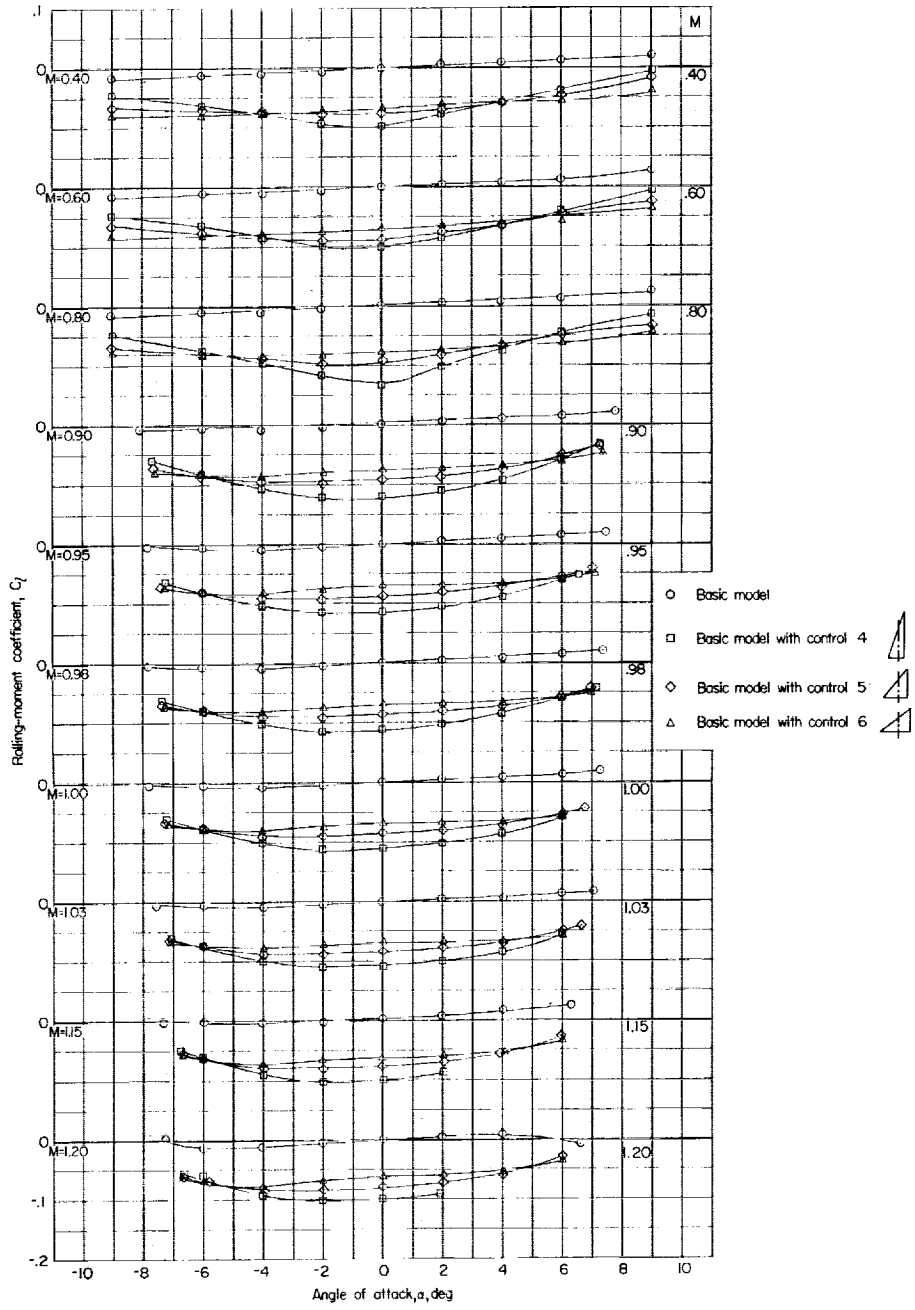

(b) Triangular control surfaces.

Figure 13.- Concluded.

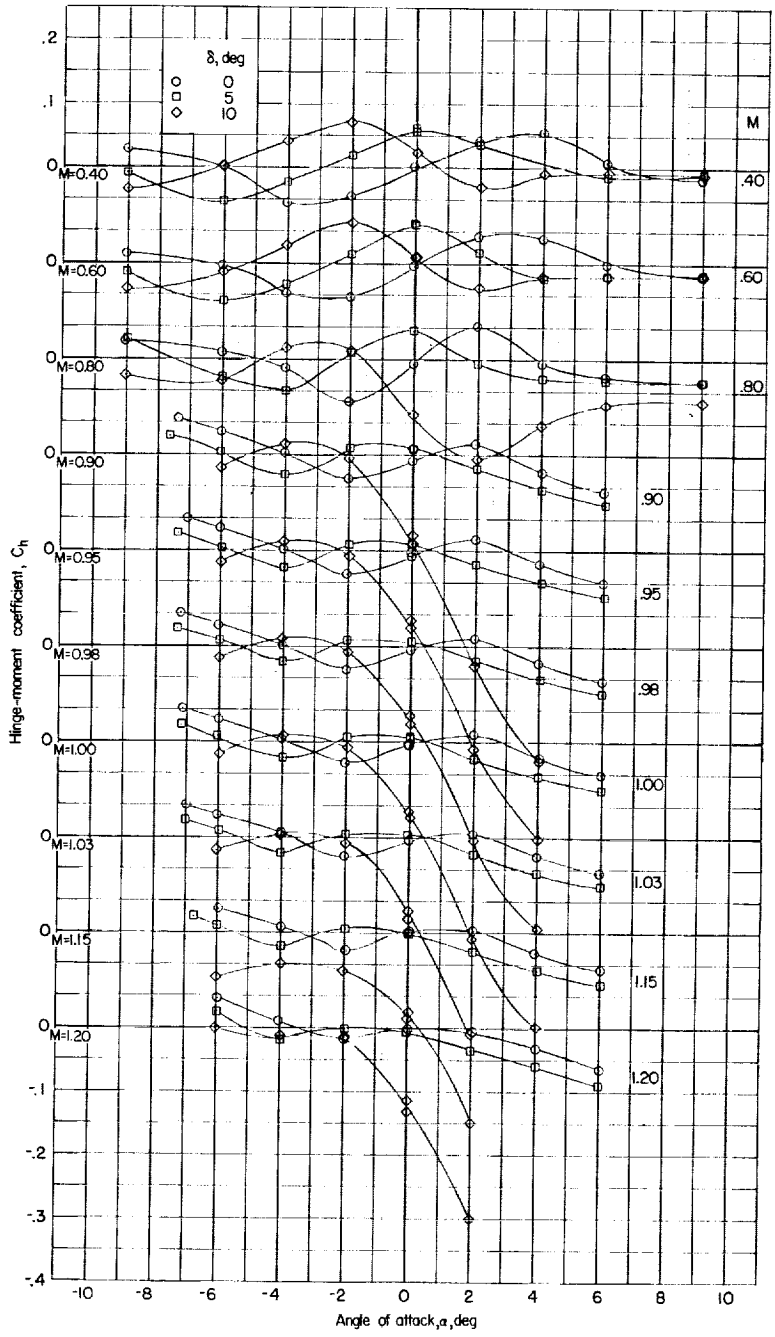

(a) Control surface 1.

Figure 14.- Variation with angle of attack of the hinge-moment characteristics of the six control surfaces for several nominal control-surface deflection angles and Mach numbers.

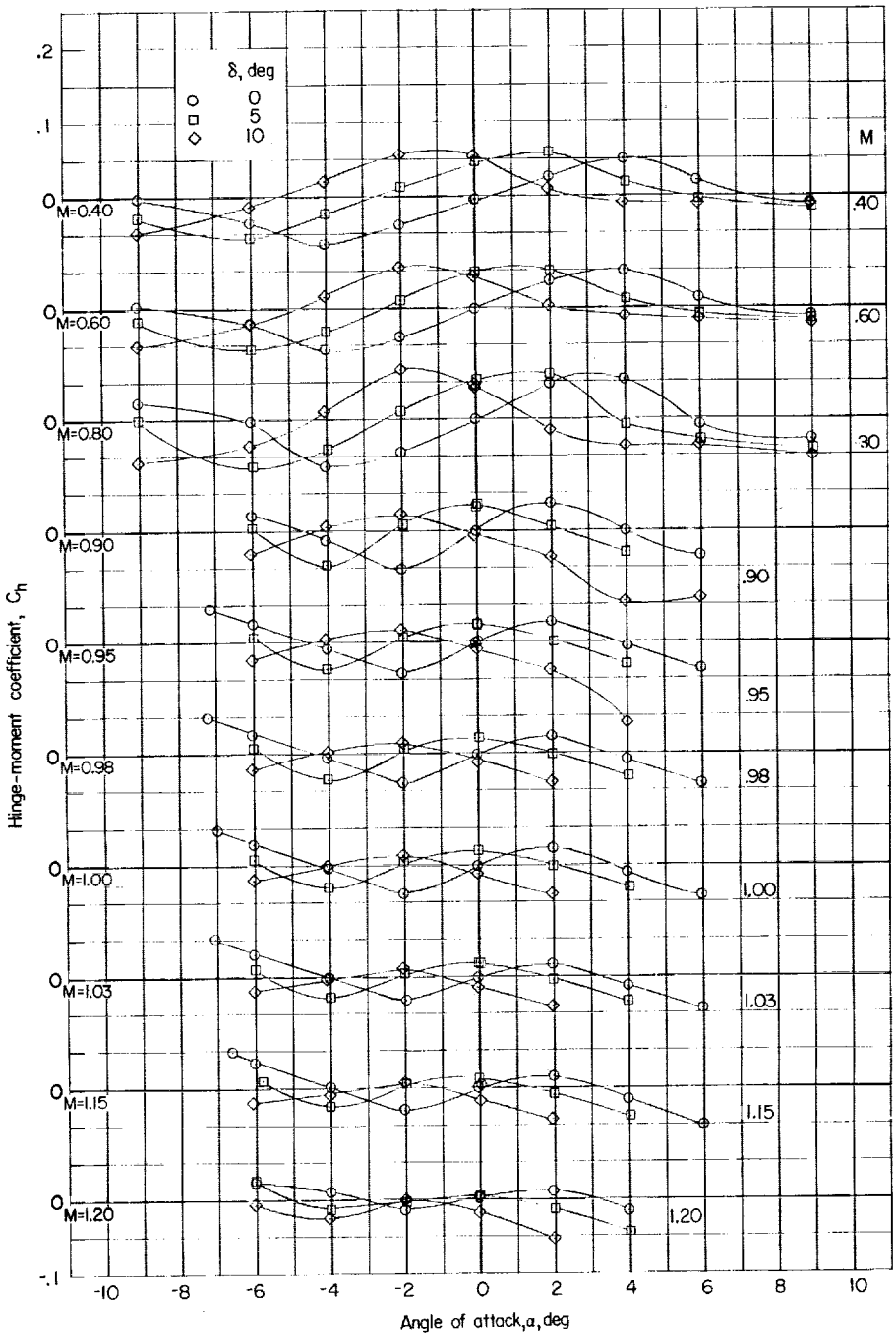

(b) Control surface 2.

Figure 14.- Continued.

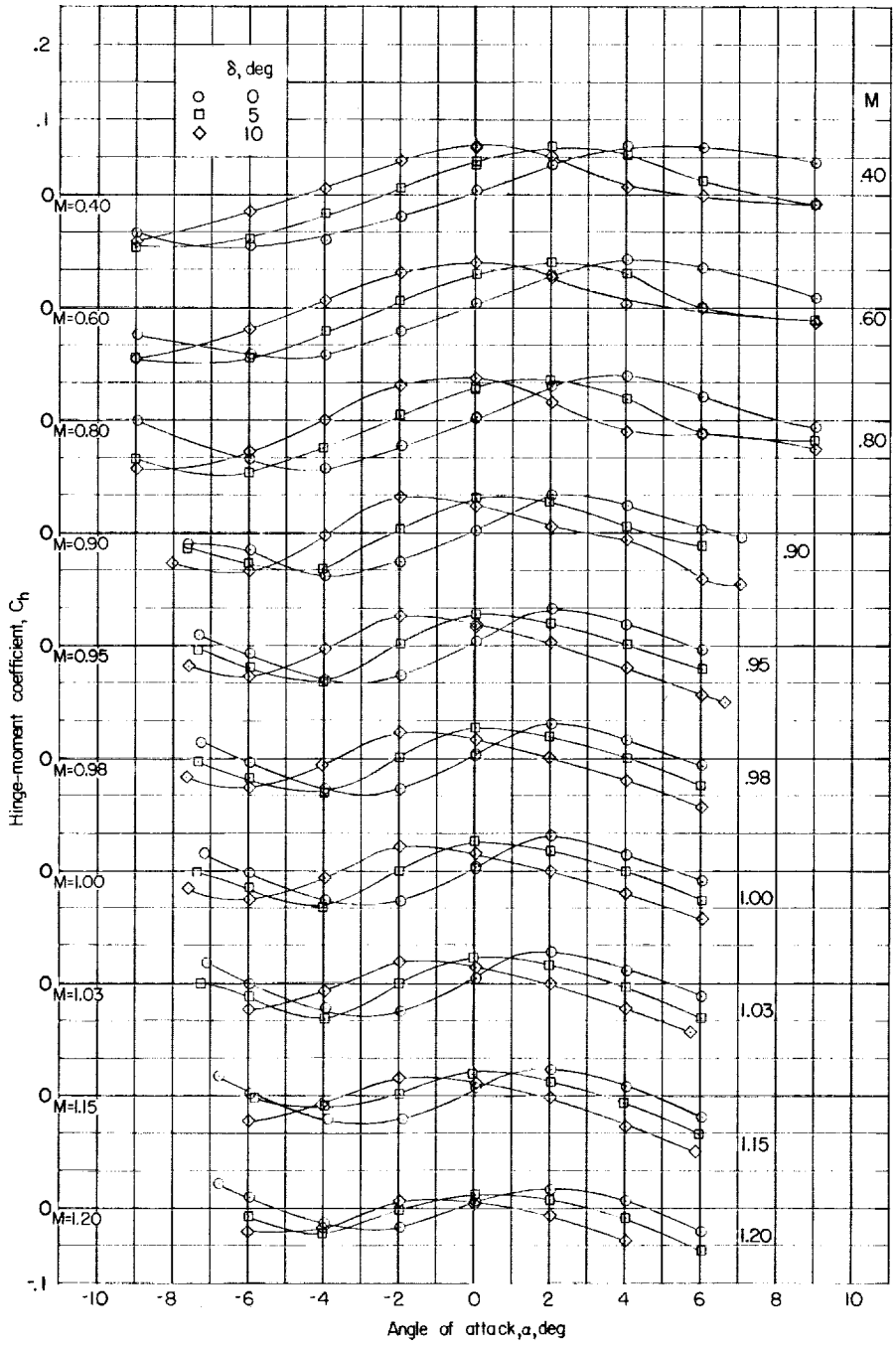

(c) Control surface 3.

Figure 14.- Continued.

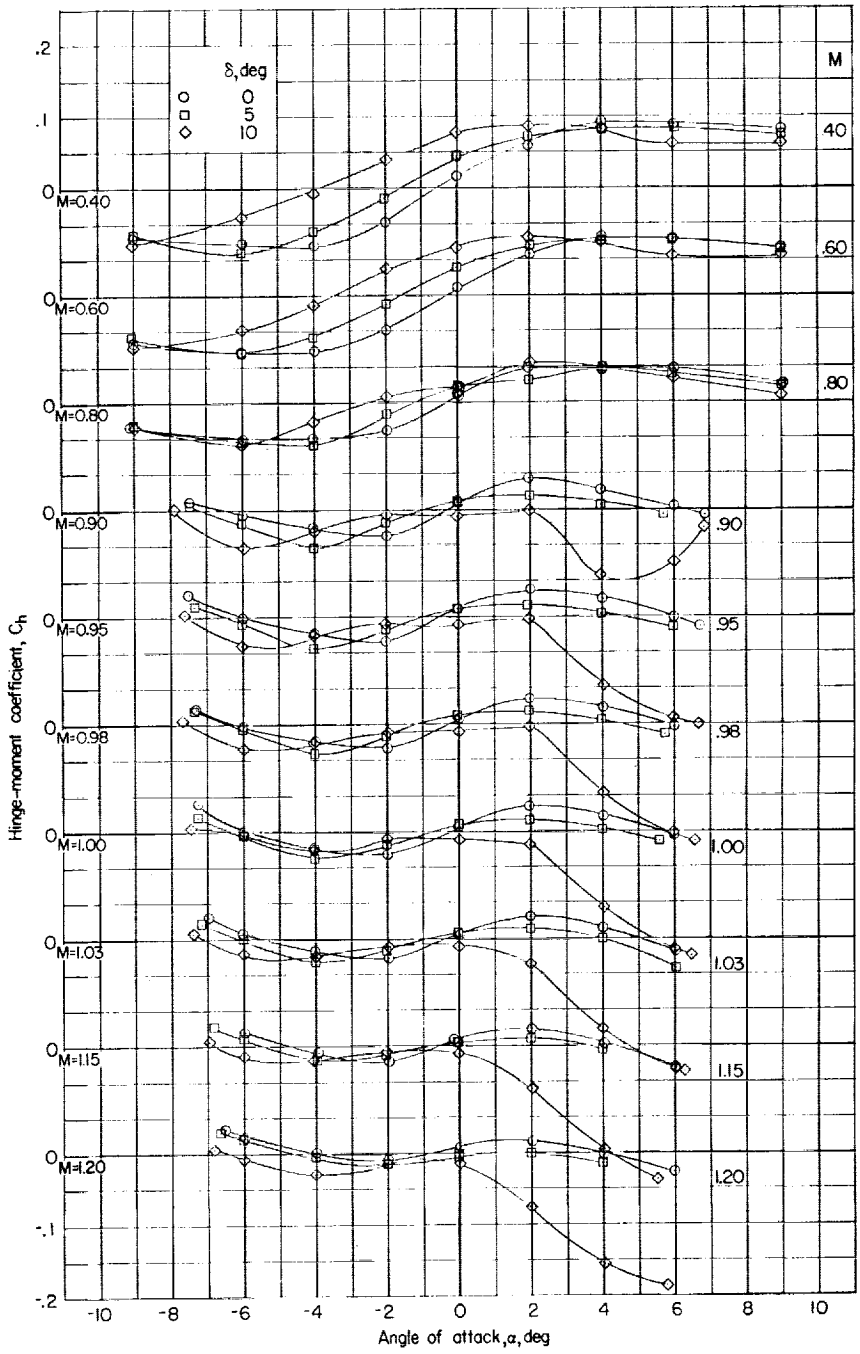

(d) Control surface 4.

Figure 14.- Continued.

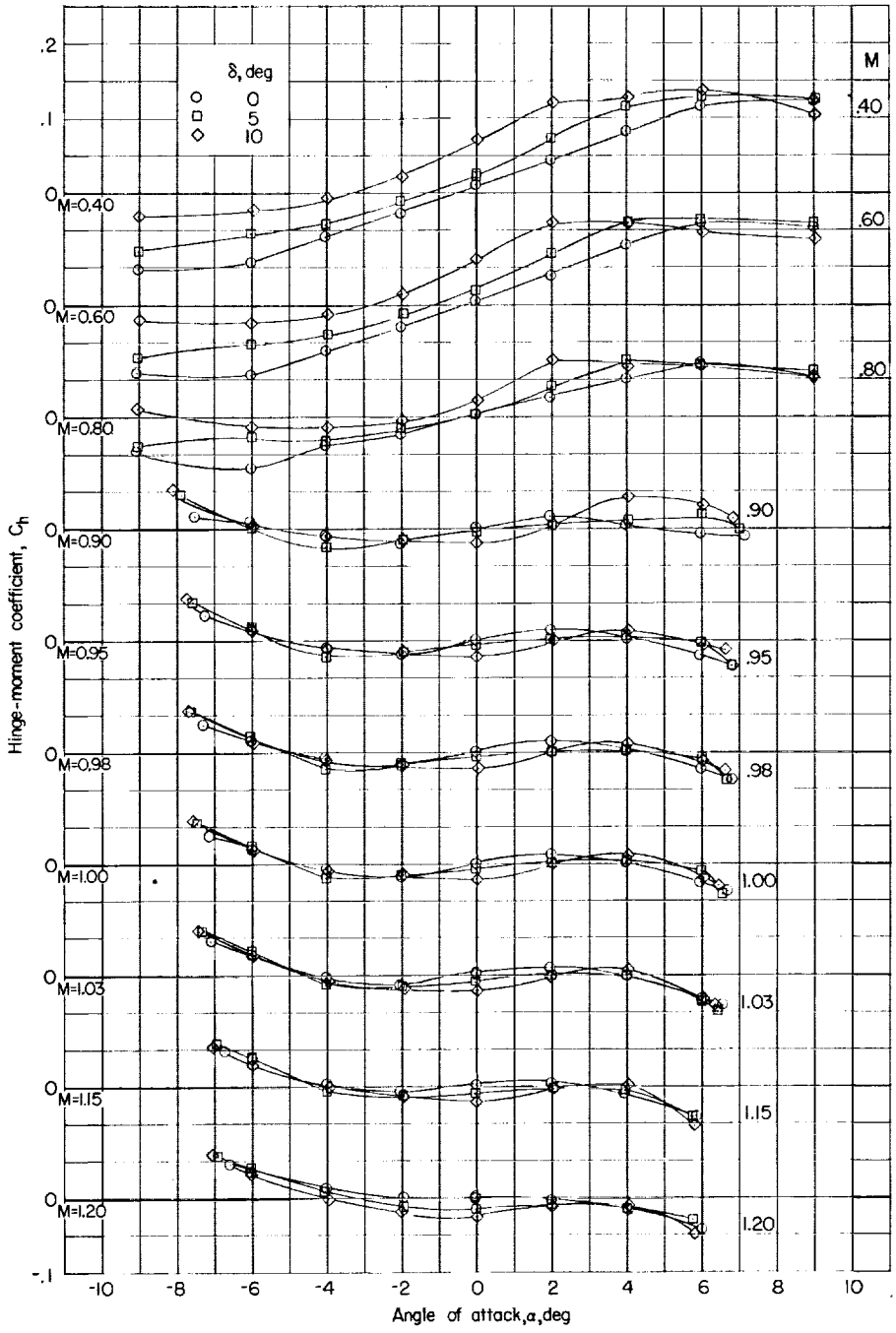

(e) Control surface 5.

Figure 14.- Continued.

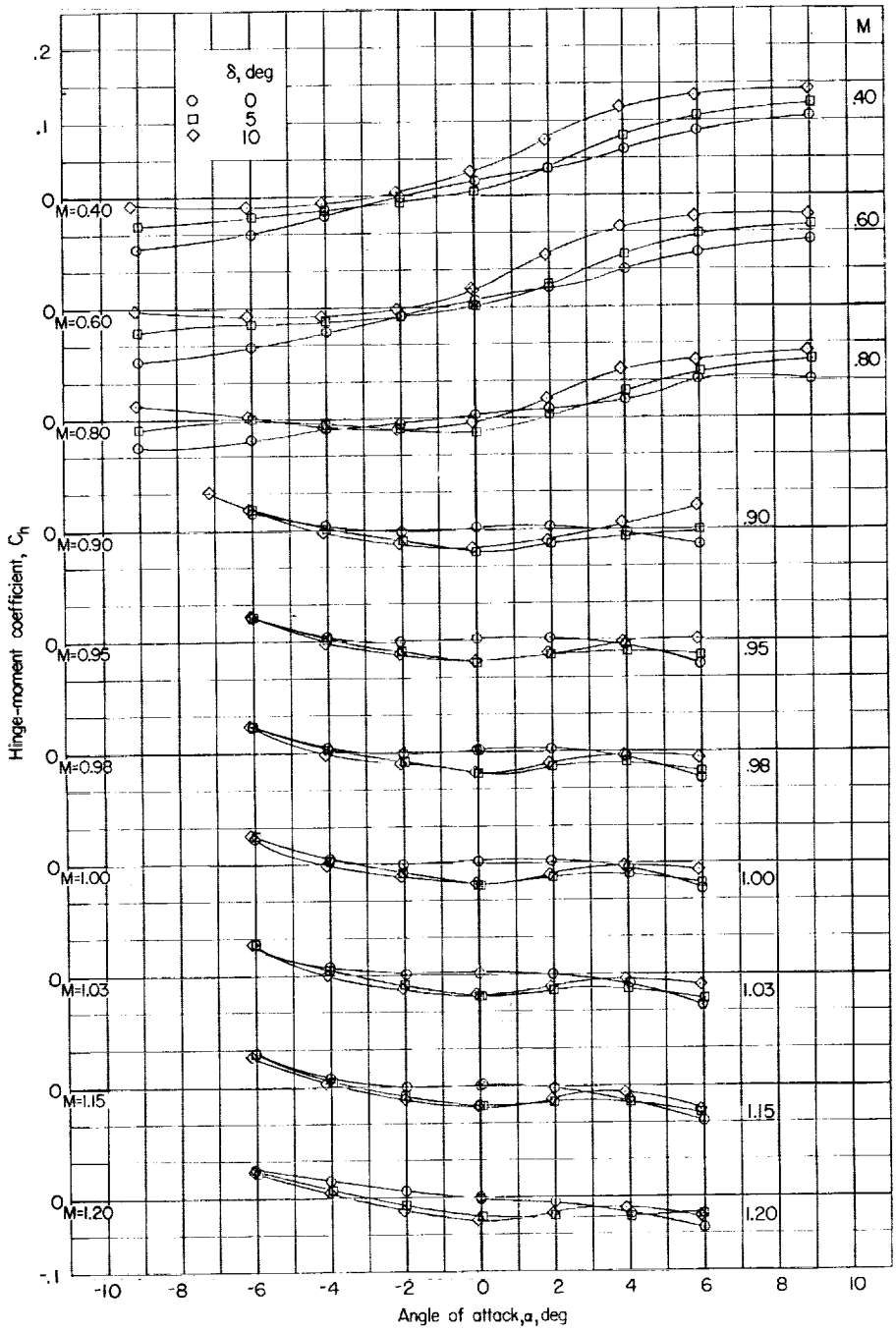

(f) Control surface 6.

Figure 14.- Concluded.

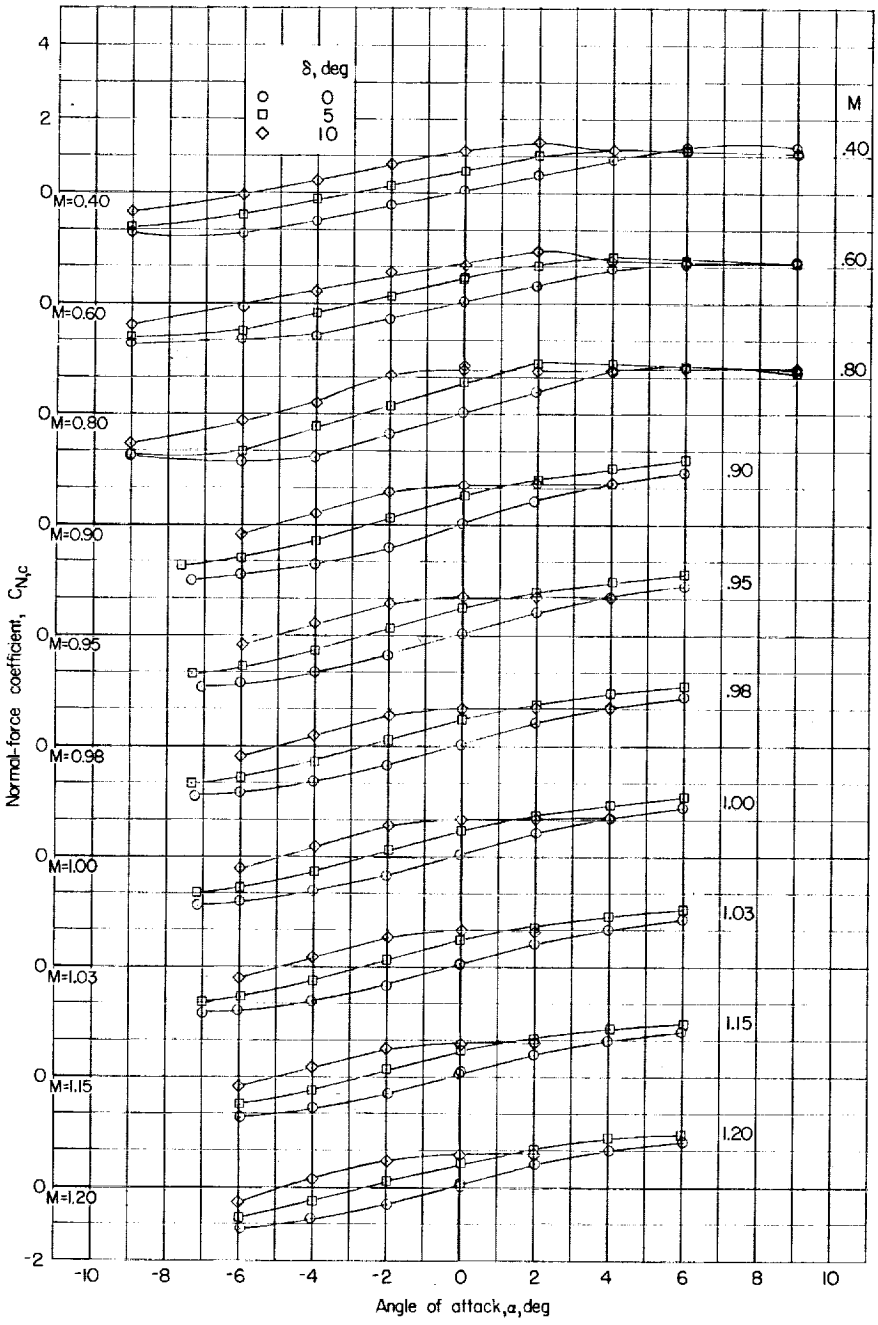

(a) Control surface 1.

Figure 15.- Variation with angle of attack of the normal-force characteristics of the six control surfaces for several nominal control-surface deflection angles and Mach numbers.

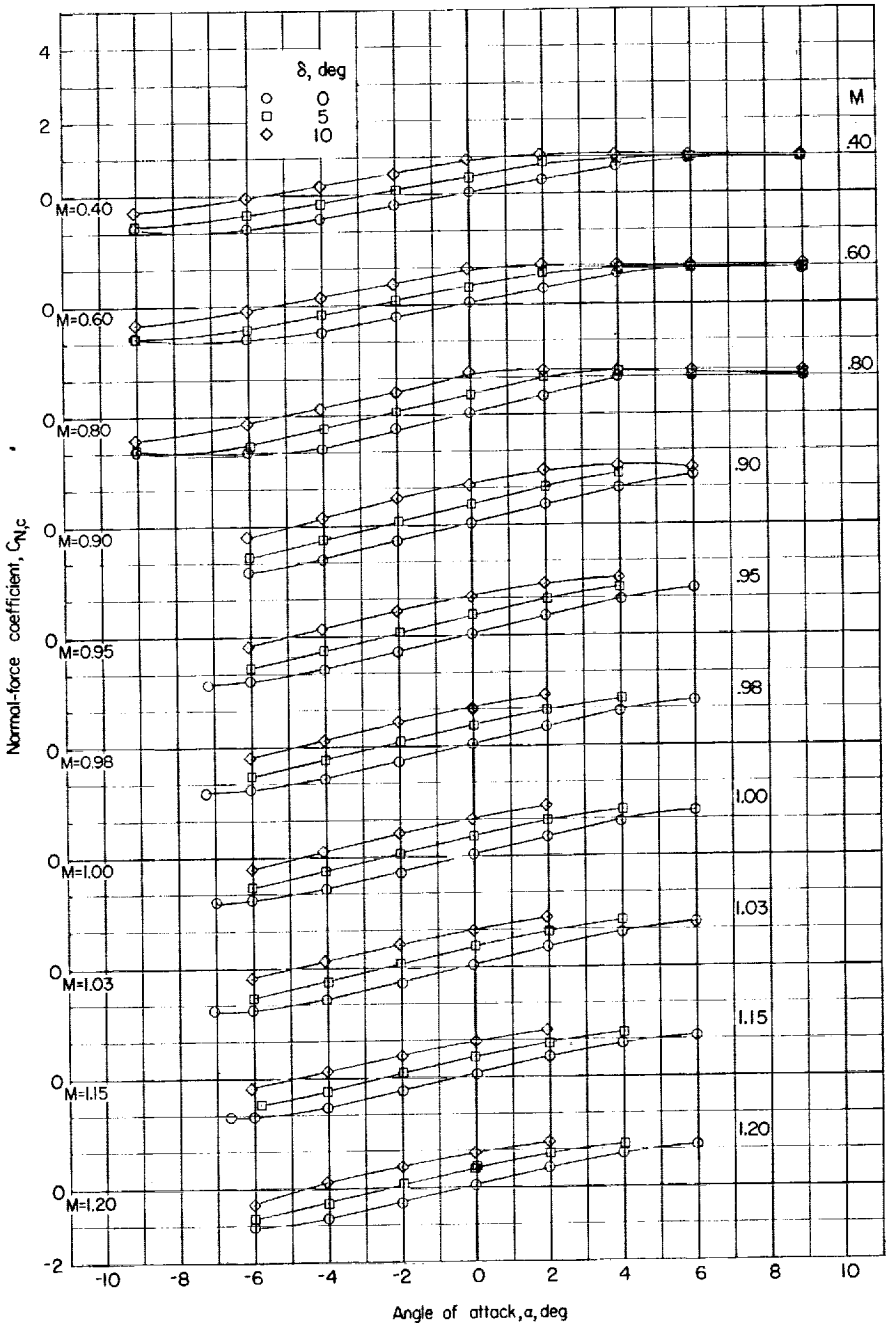

(b) Control surface 2.

Figure 15.- Continued.

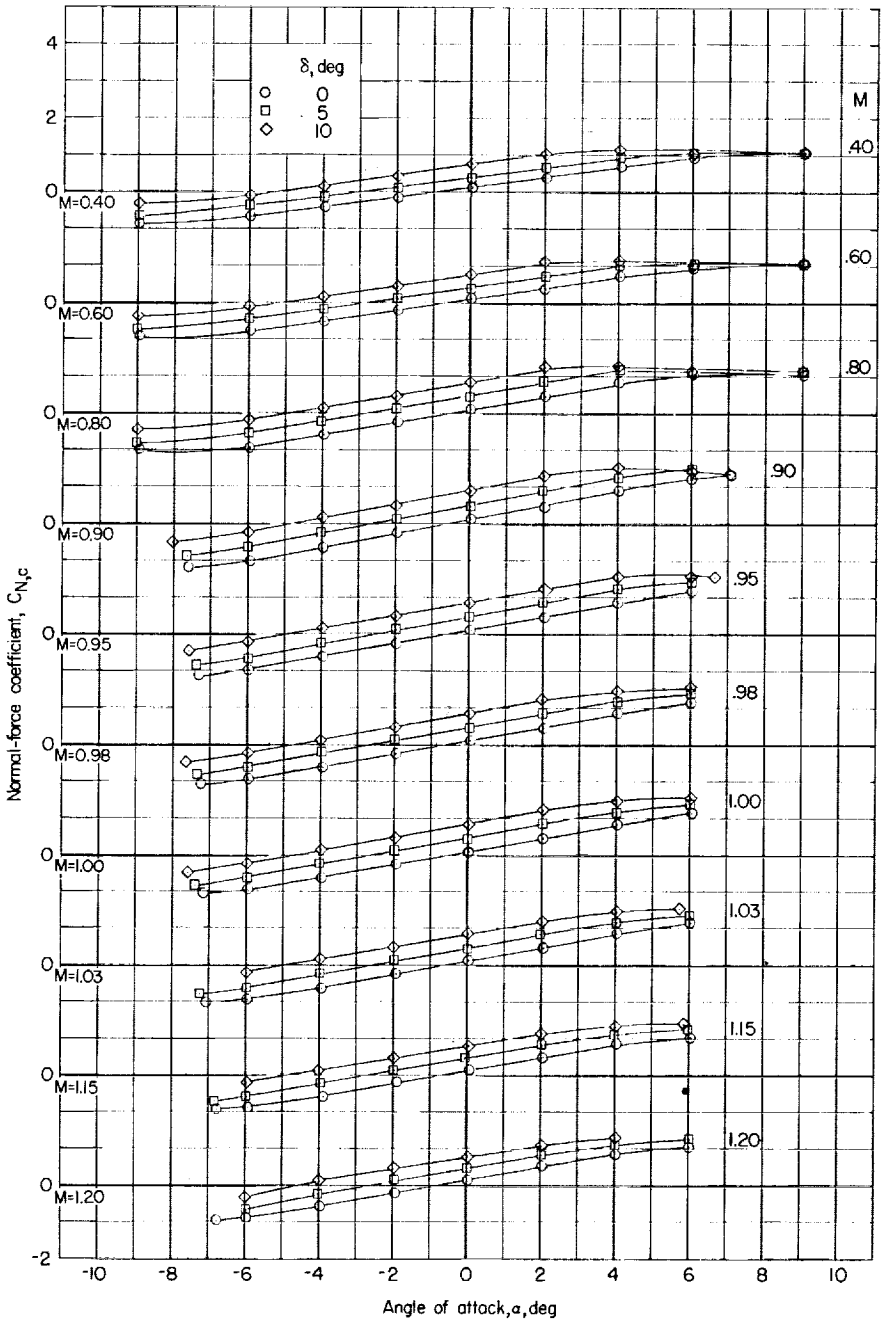

(c) Control surface 3.

Figure 15.- Continued.

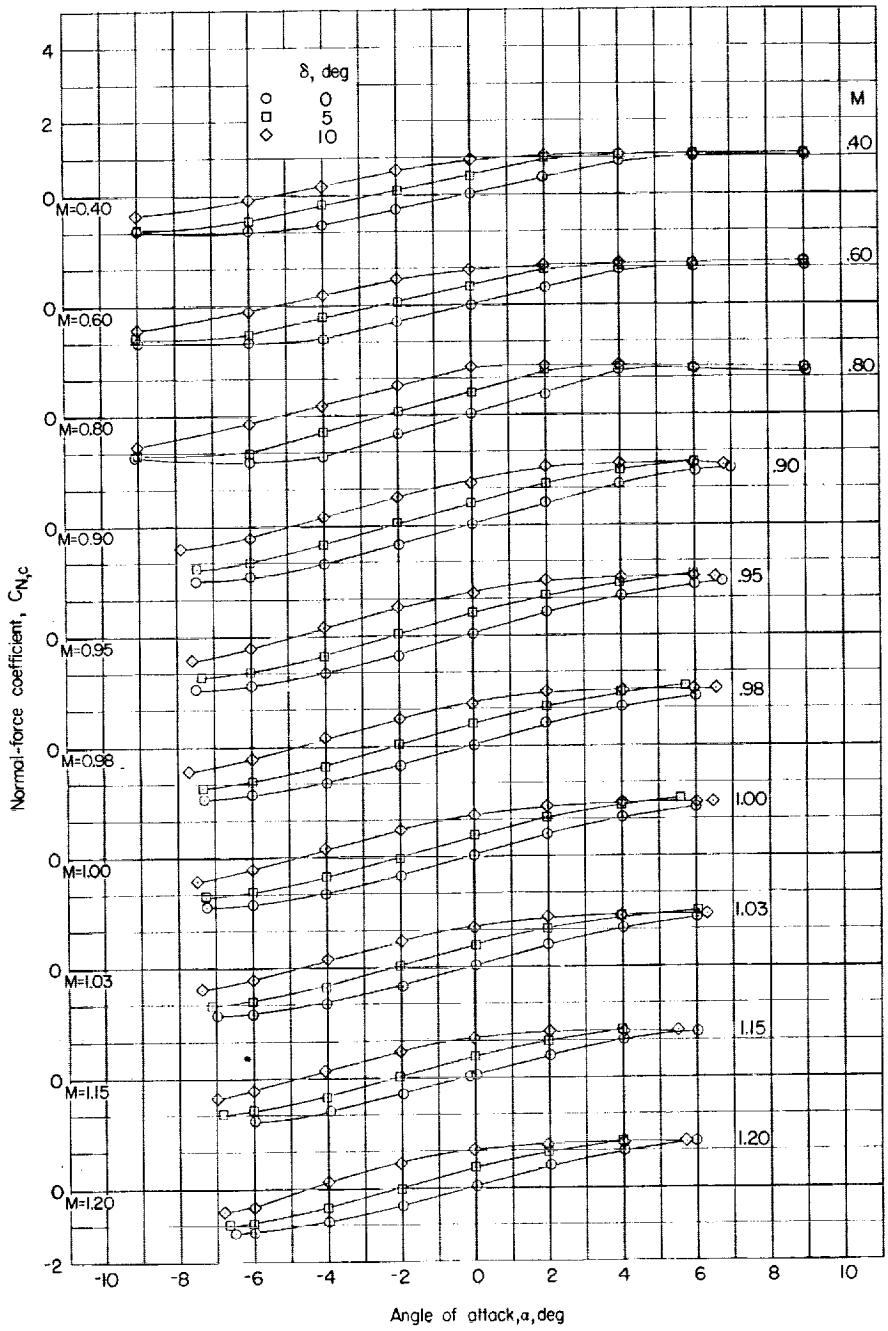

(d) Control surface 4.

Figure 15.- Continued.

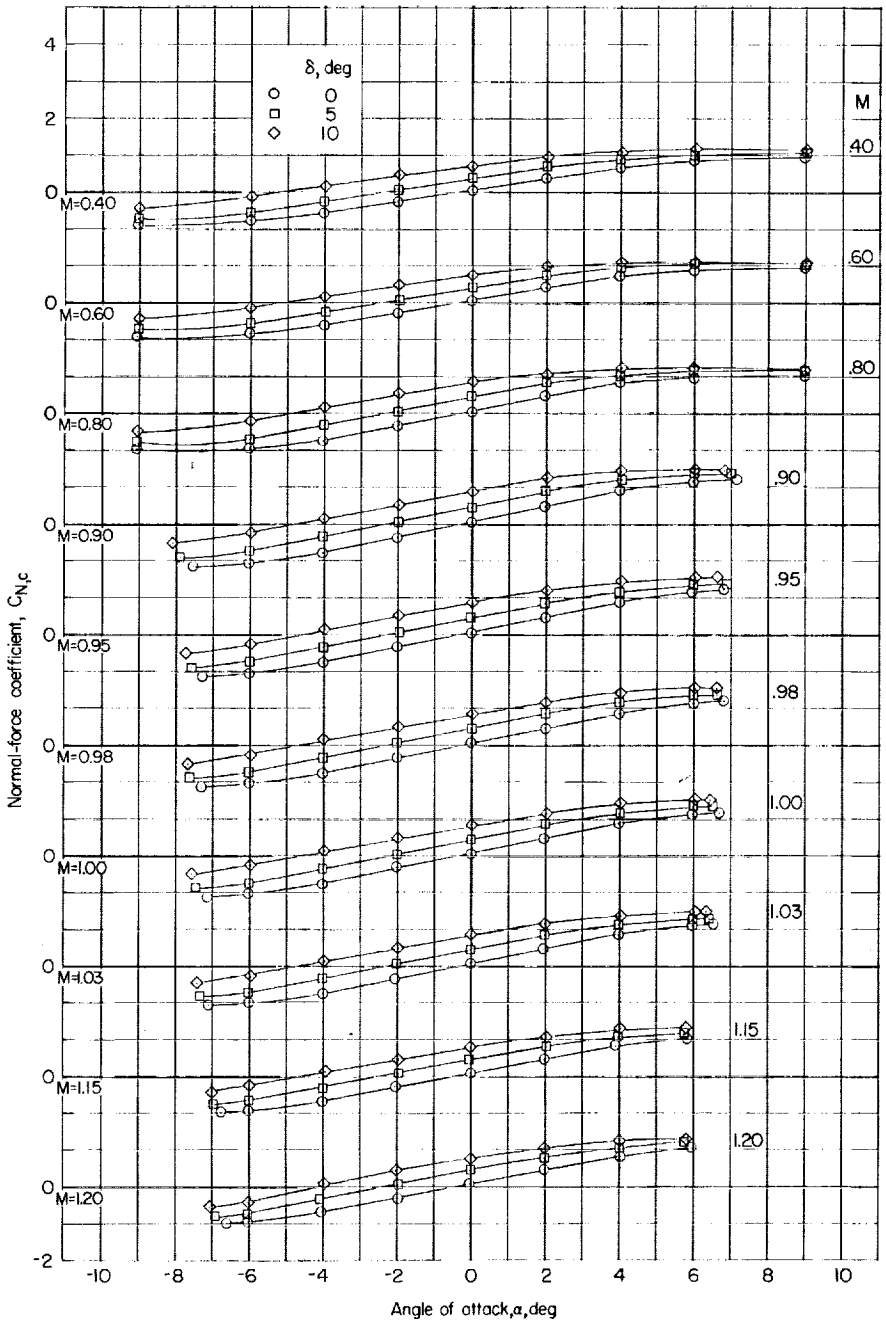

(e) Control surface 5.

Figure 15.- Continued.

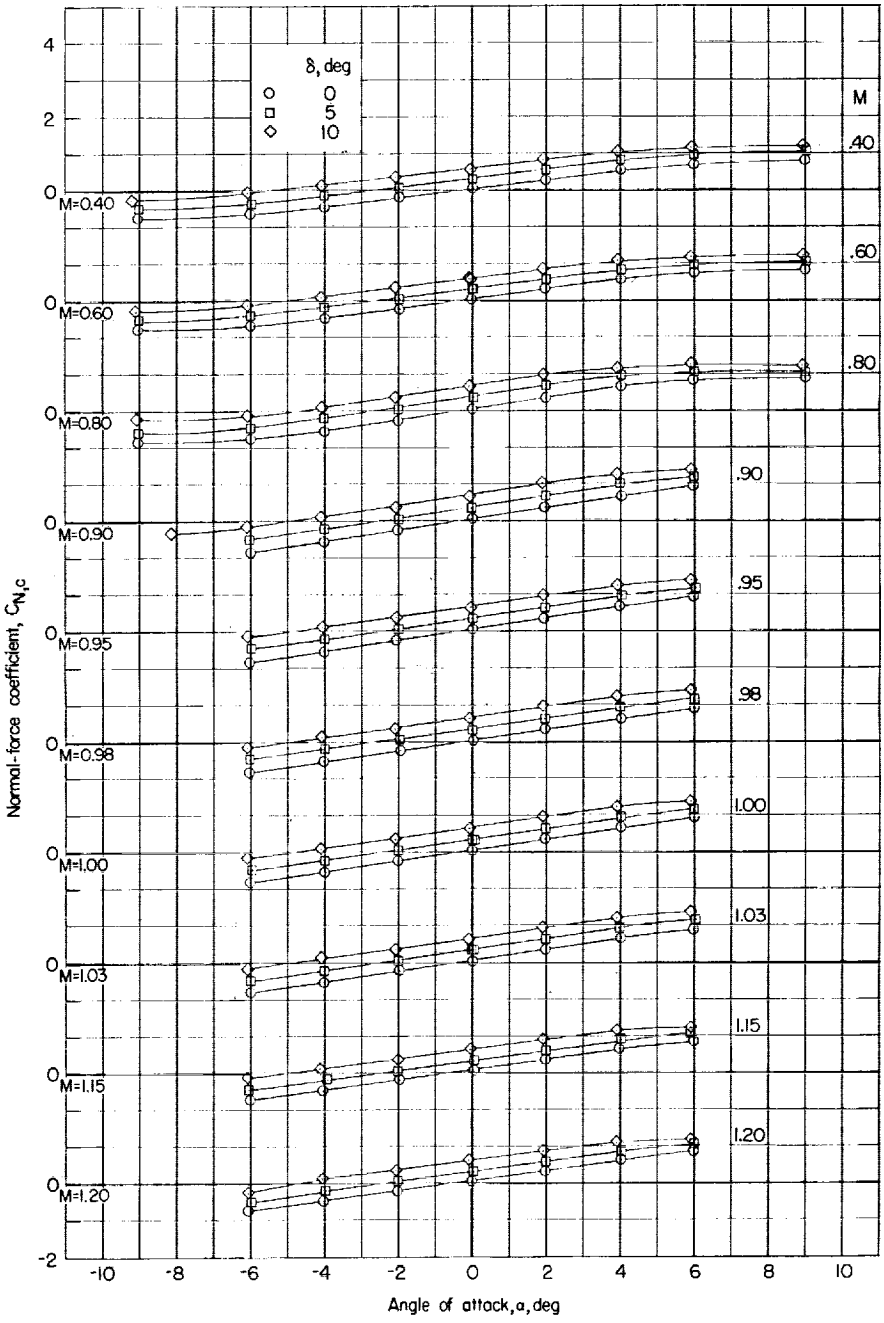

(f) Control surface 6.

Figure 15.- Concluded.

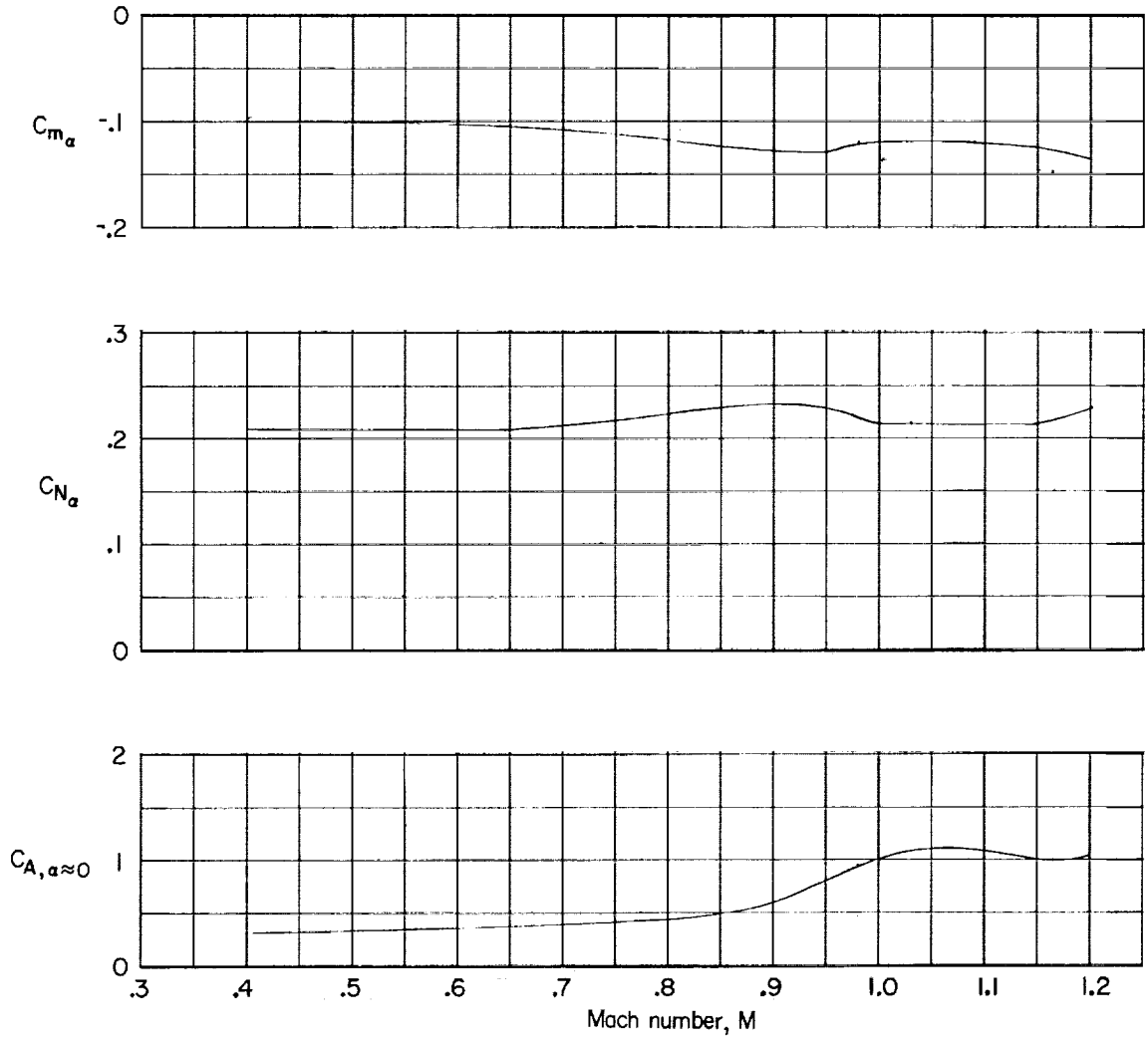

Figure 16.- Summary of static longitudinal characteristics of basic model with and without end plates.

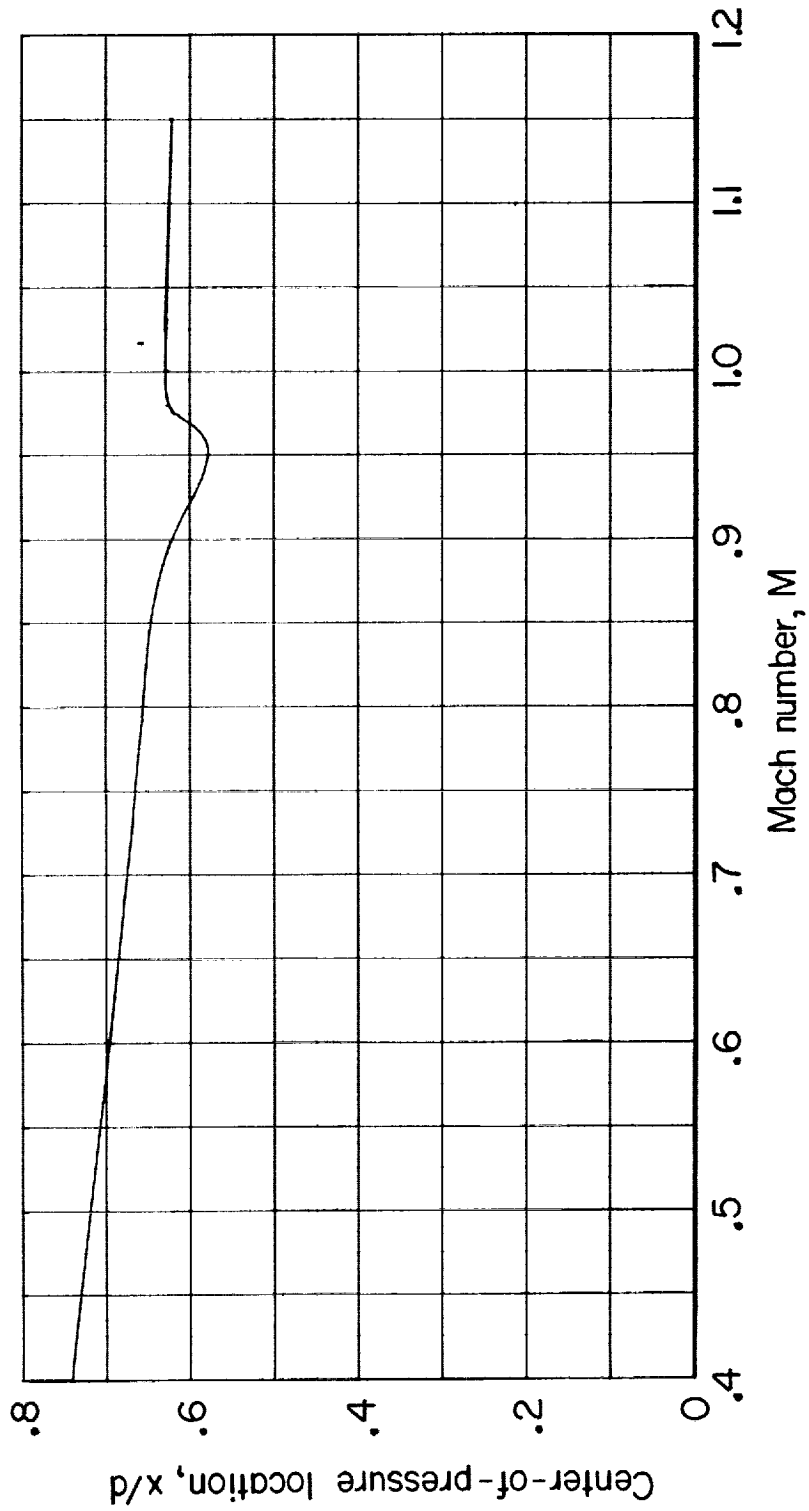

Figure 17.- Variation with Mach number of the center-of-pressure location of the basic model with and without end plates.

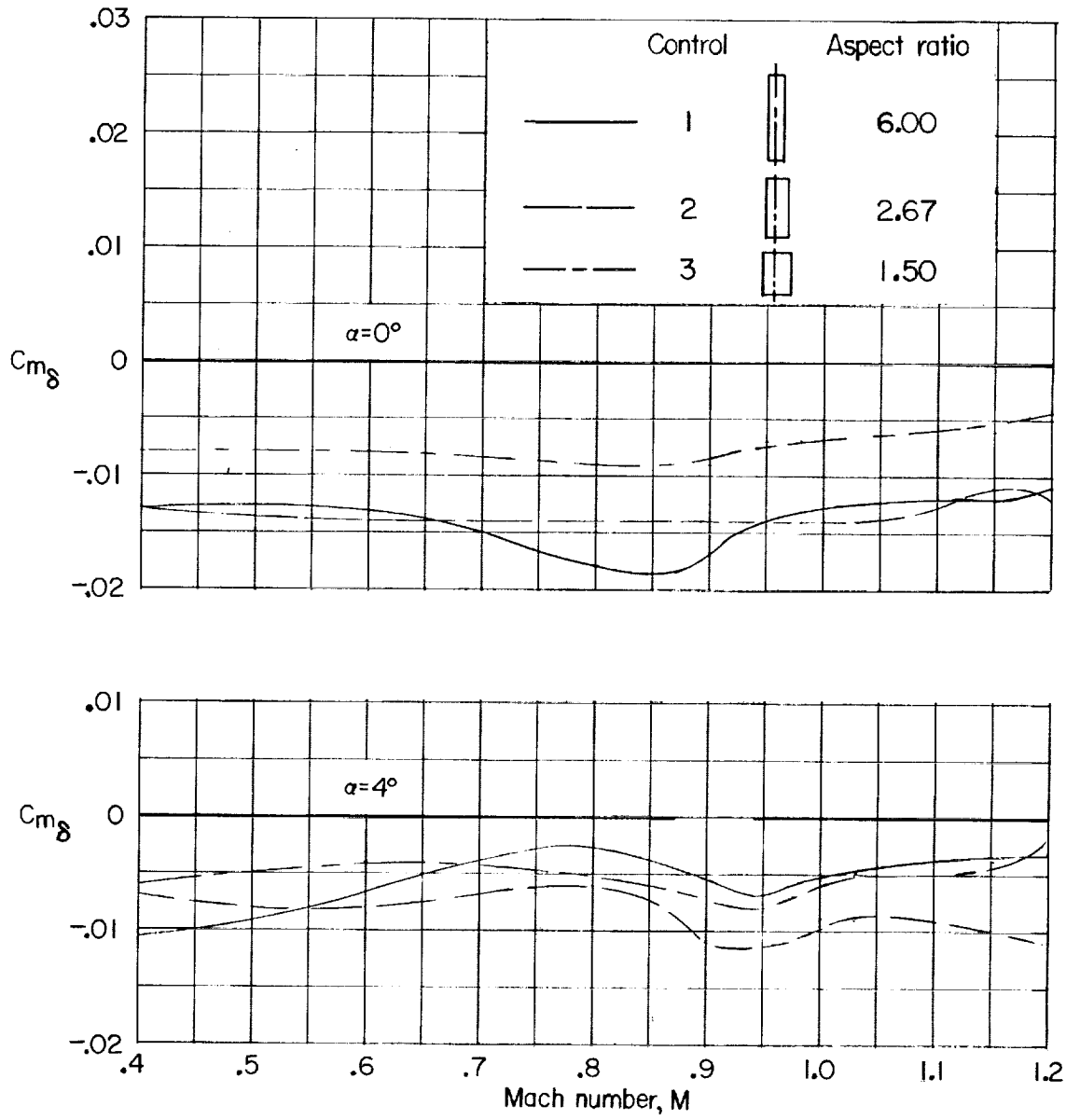

(a) Rectangular control surfaces.

Figure 18.- Variation with Mach number of control-effectiveness parameter C_{m_δ} of the six control surfaces.

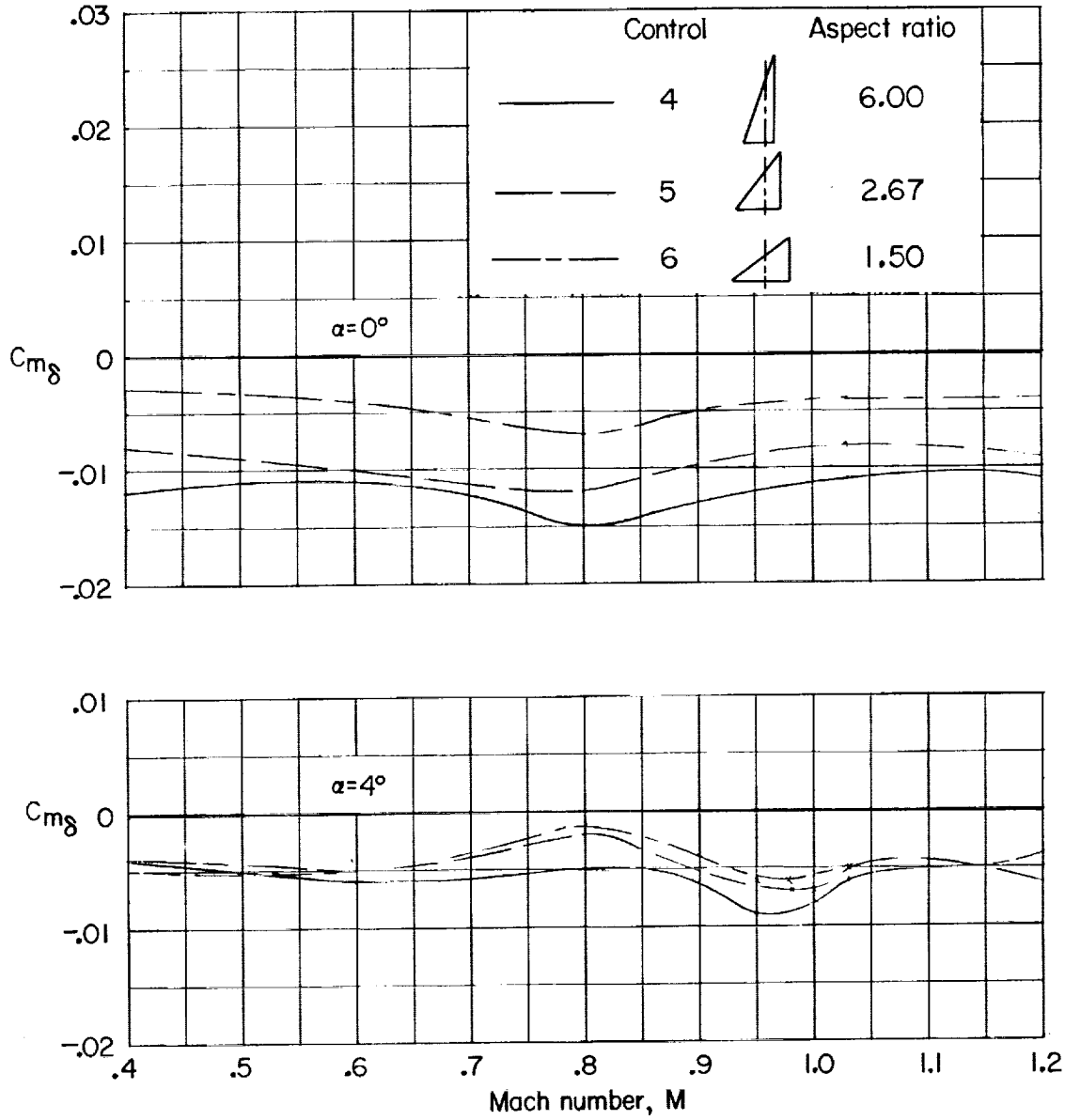

(b) Triangular control surfaces.

Figure 18.- Concluded.

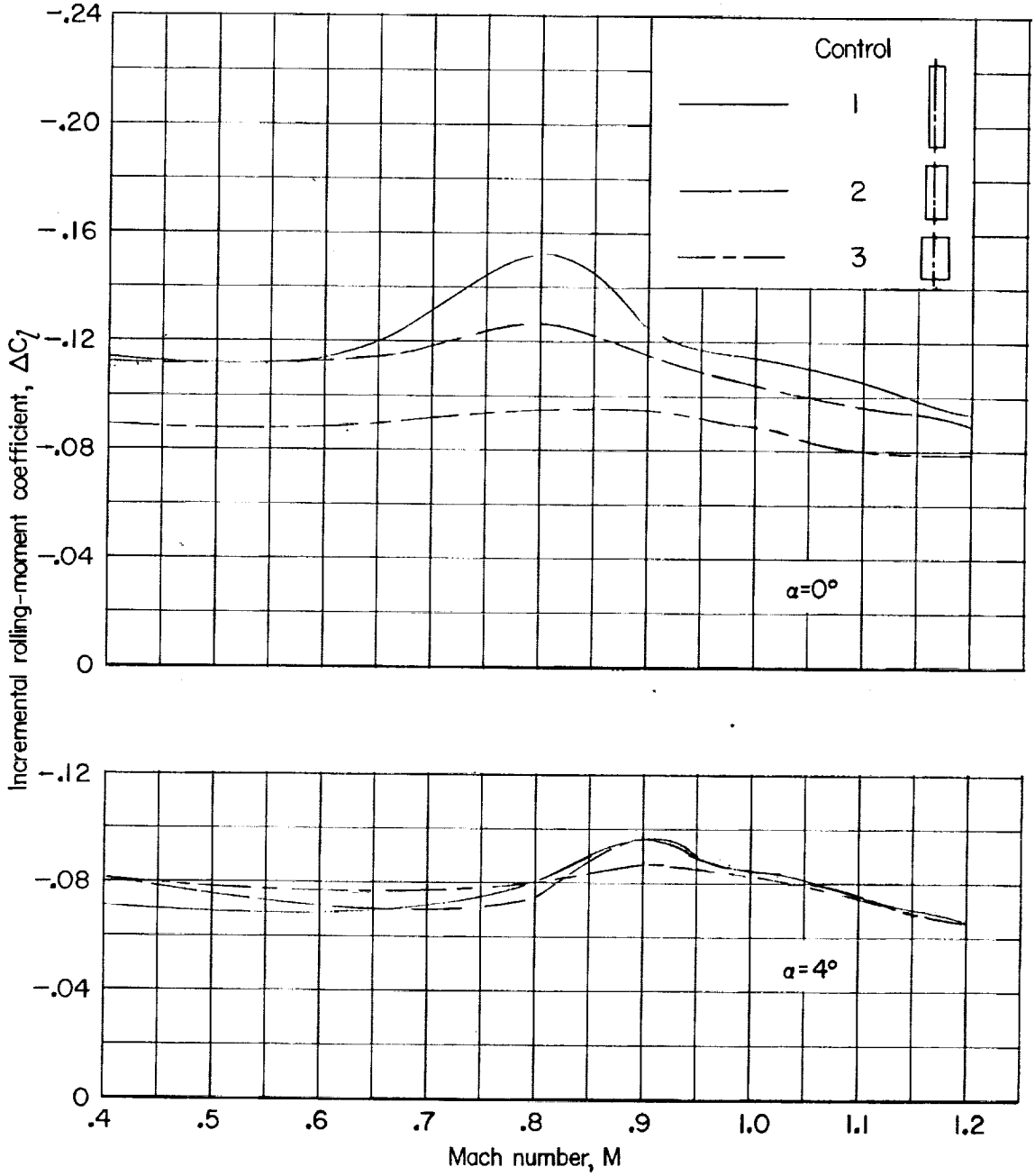

(a) Rectangular control surfaces.

Figure 19.- Variation with Mach number of incremental rolling-moment coefficient for constant angles of attack of 0° and 4°. Control surfaces set differentially; $\delta_{left} = -10°$; $\delta_{right} = 10°$.

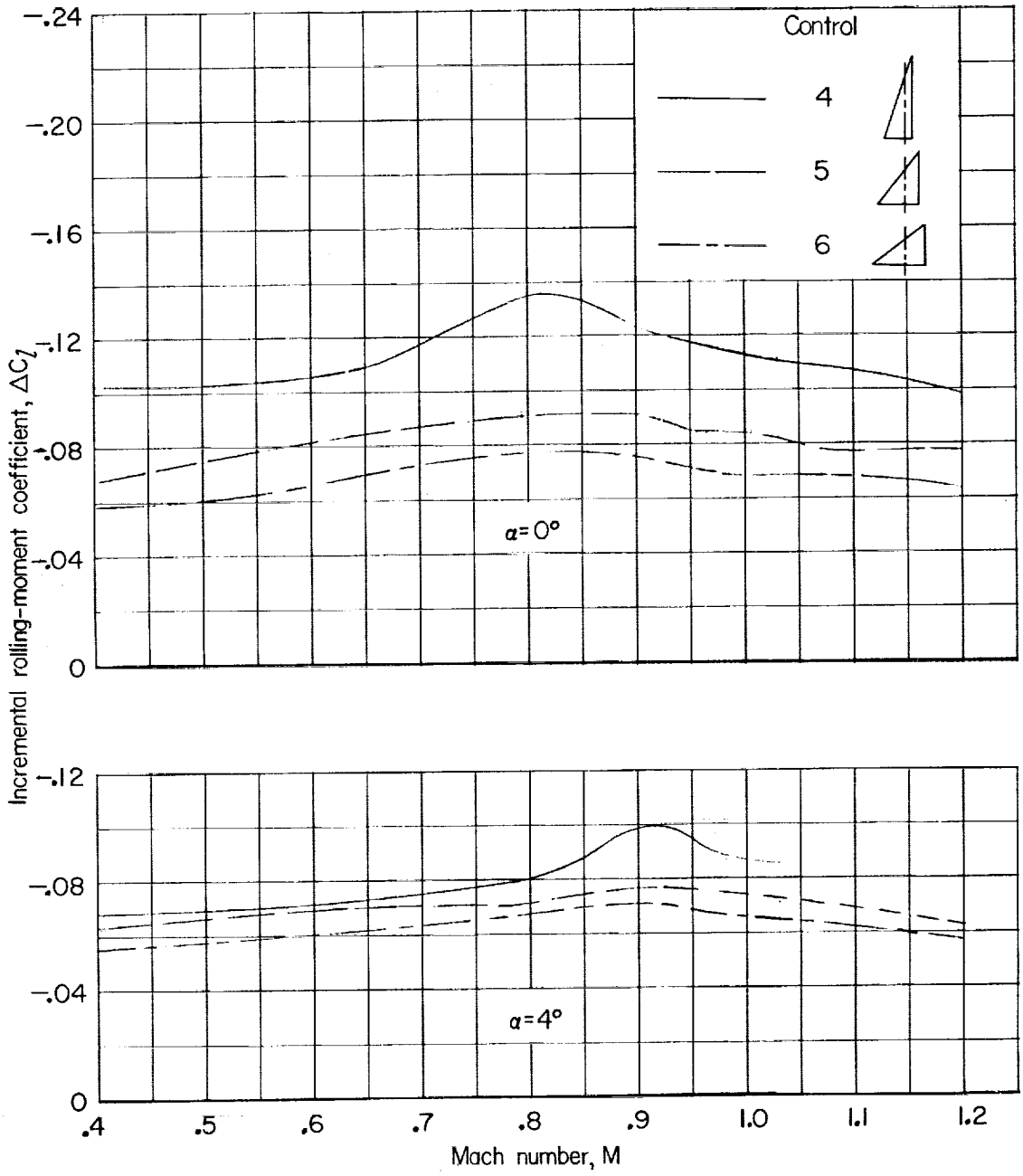

(b) Triangular control surfaces.

Figure 19.- Concluded.

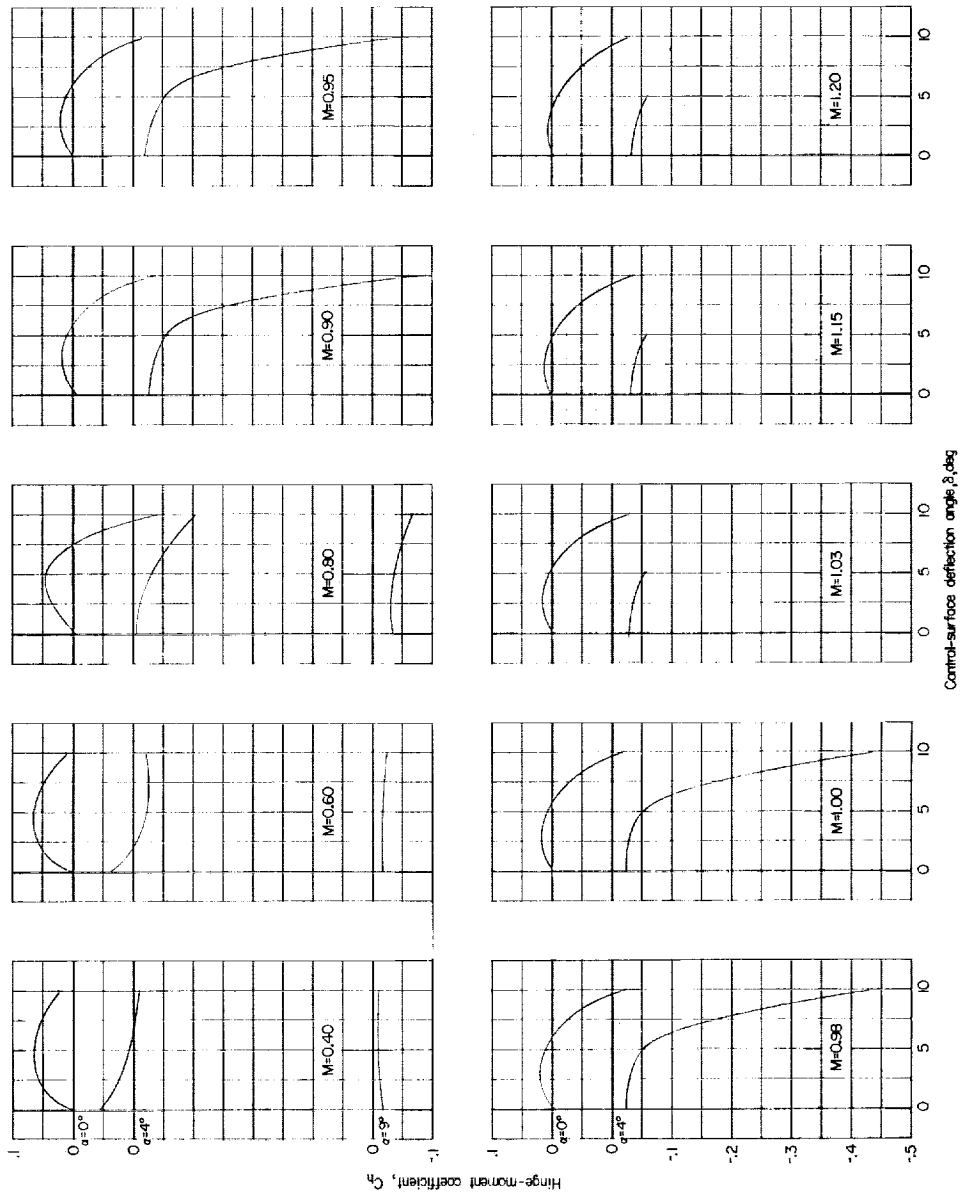

(a) Control surface 1.

Figure 20.- Variation with control-surface deflection angle of the hinge-moment coefficient for the six control surfaces at various Mach numbers.

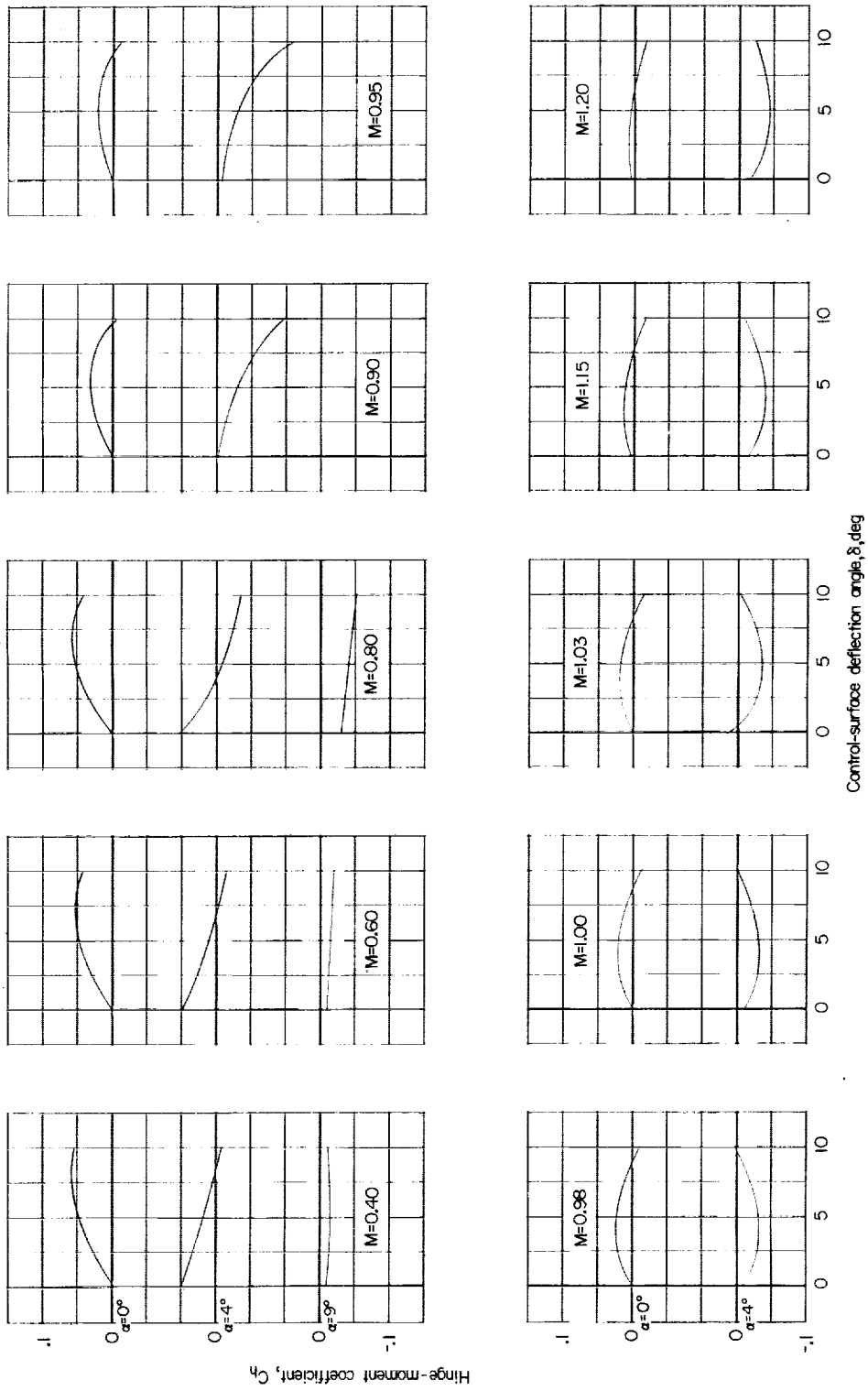

(b) Control surface 2.

Figure 20.- Continued.

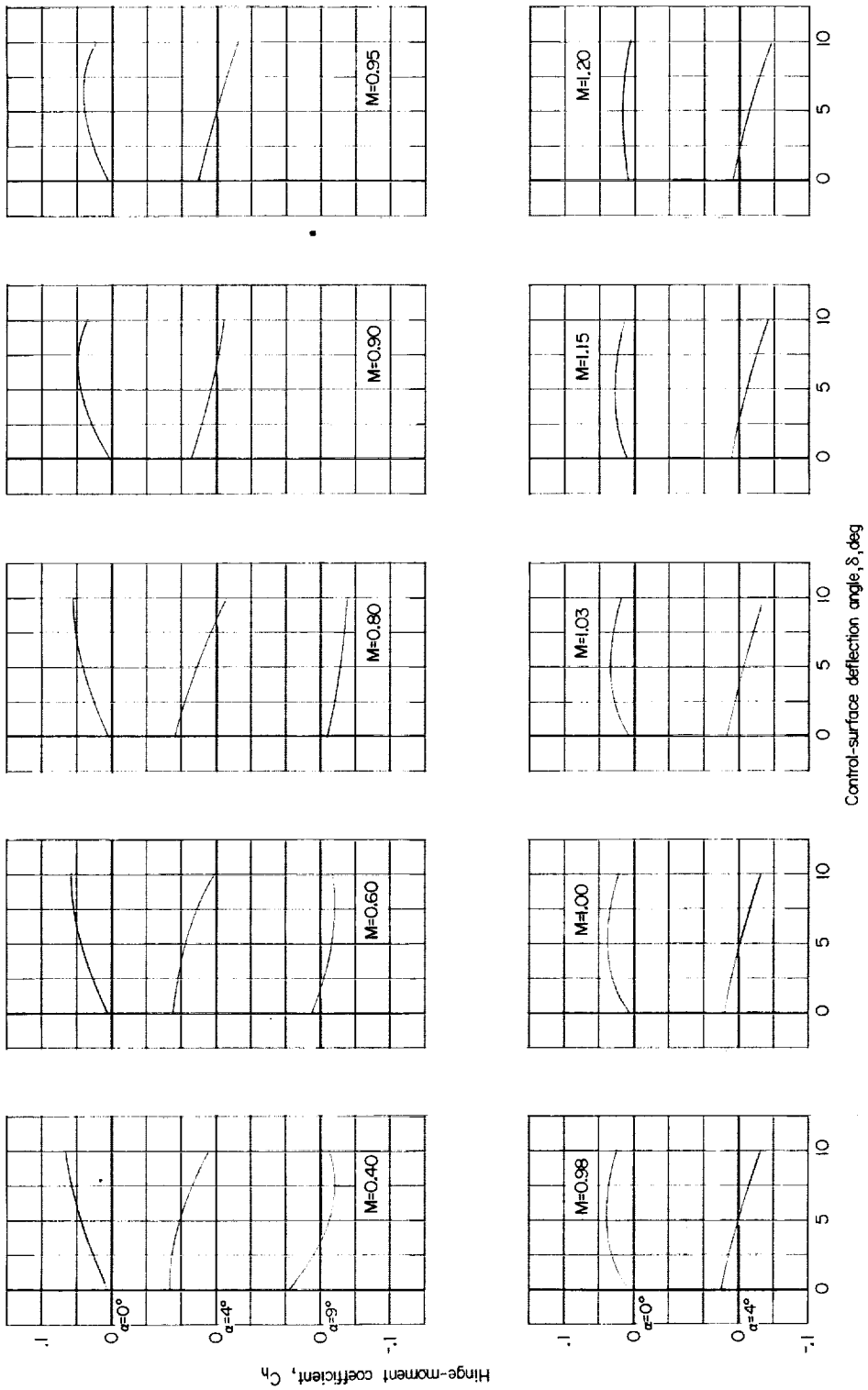

(c) Control surface 3.

Figure 20.- Continued.

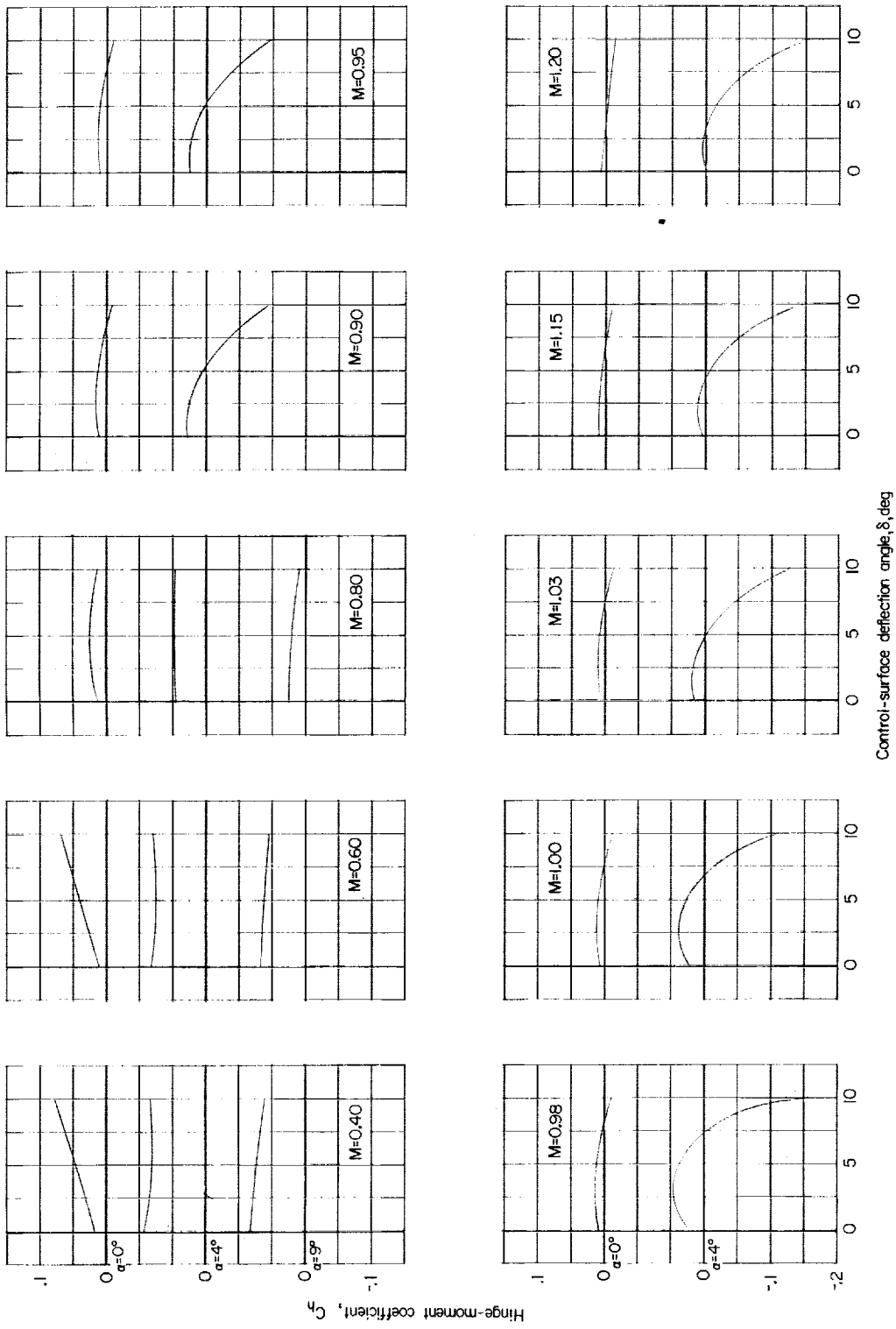

(d) Control surface 4.

Figure 20.- Continued.

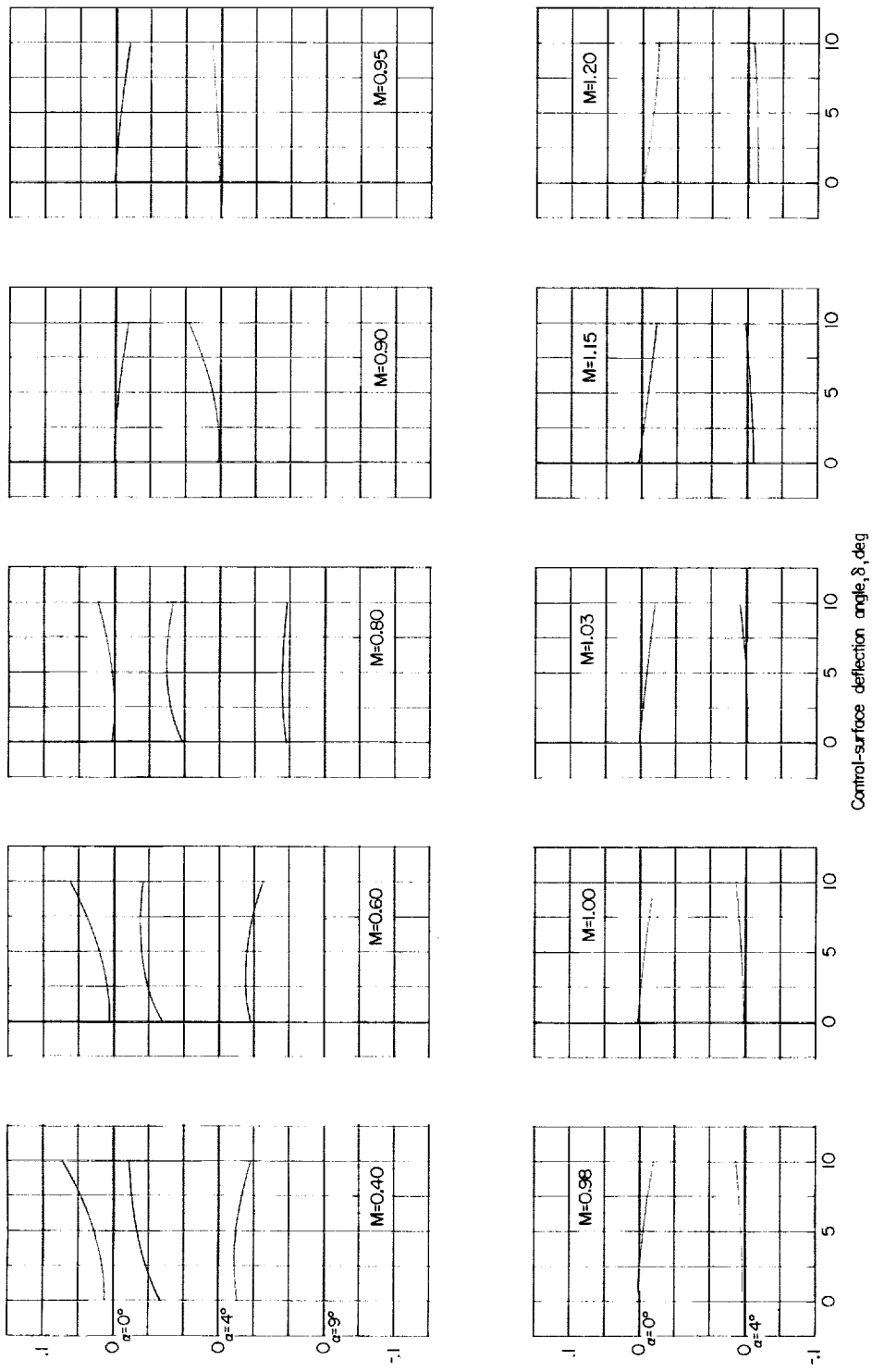

(e) Control surface 5.

Figure 20.- Continued.

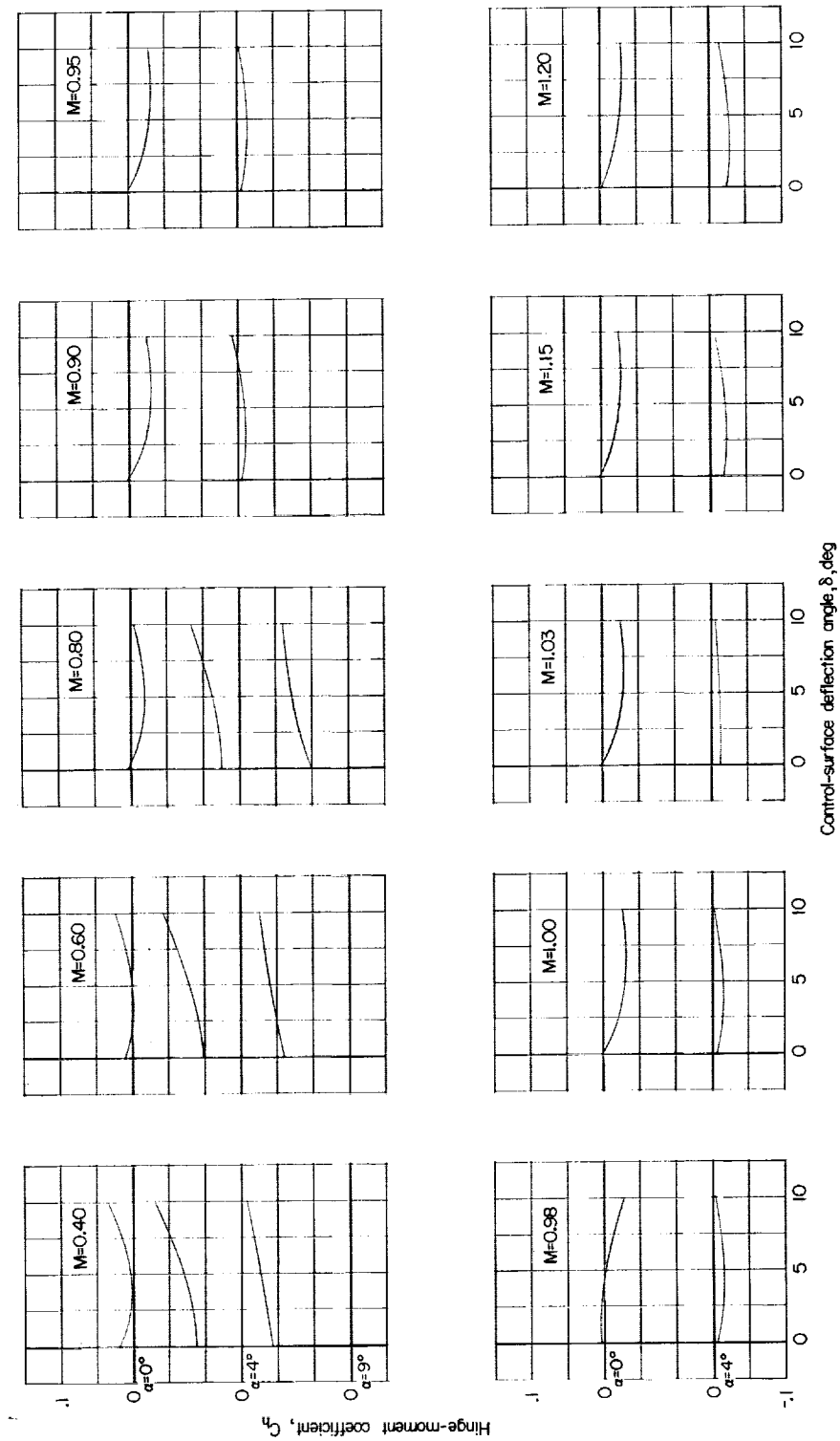

(f) Control surface 6.

Figure 20.- Concluded.

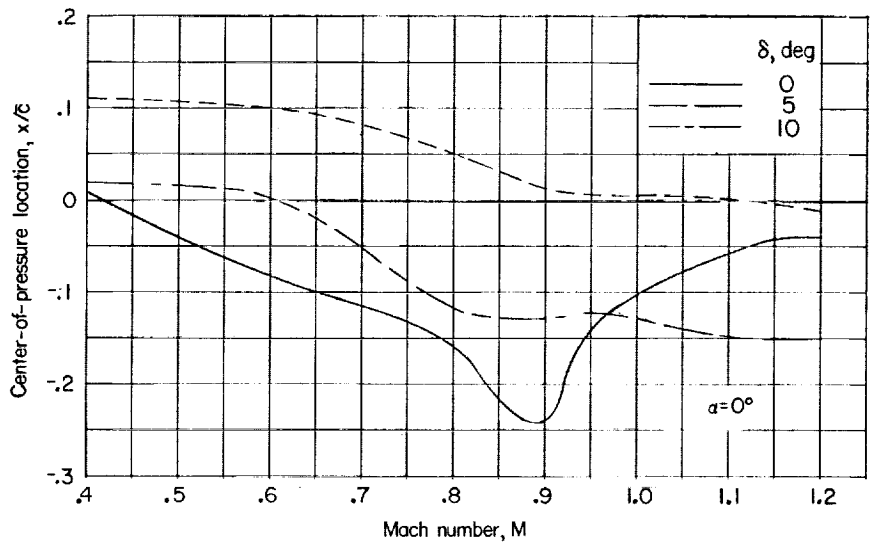

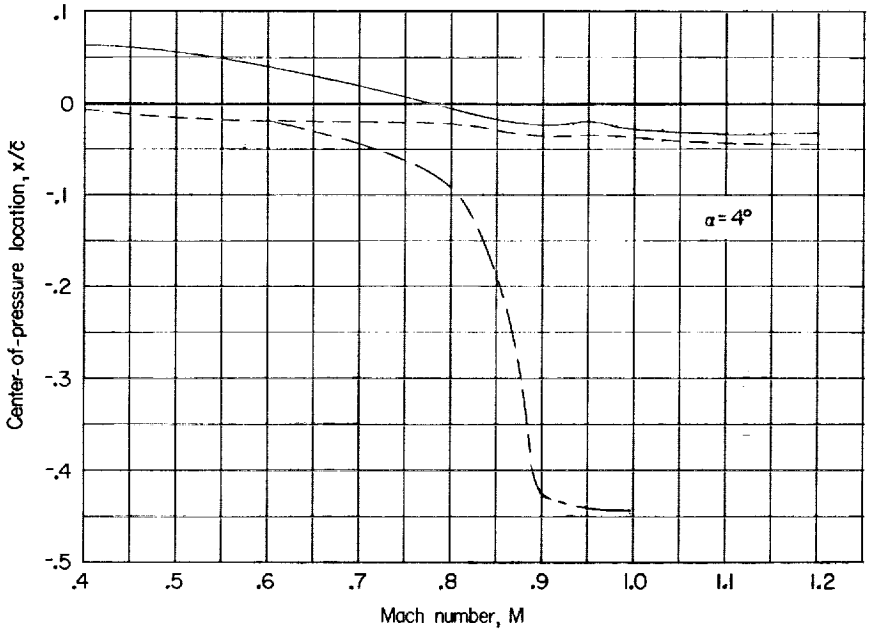

(a) Control surface 1.

Figure 21.- Variation with Mach number of the center-of-pressure locations for the six control surfaces.

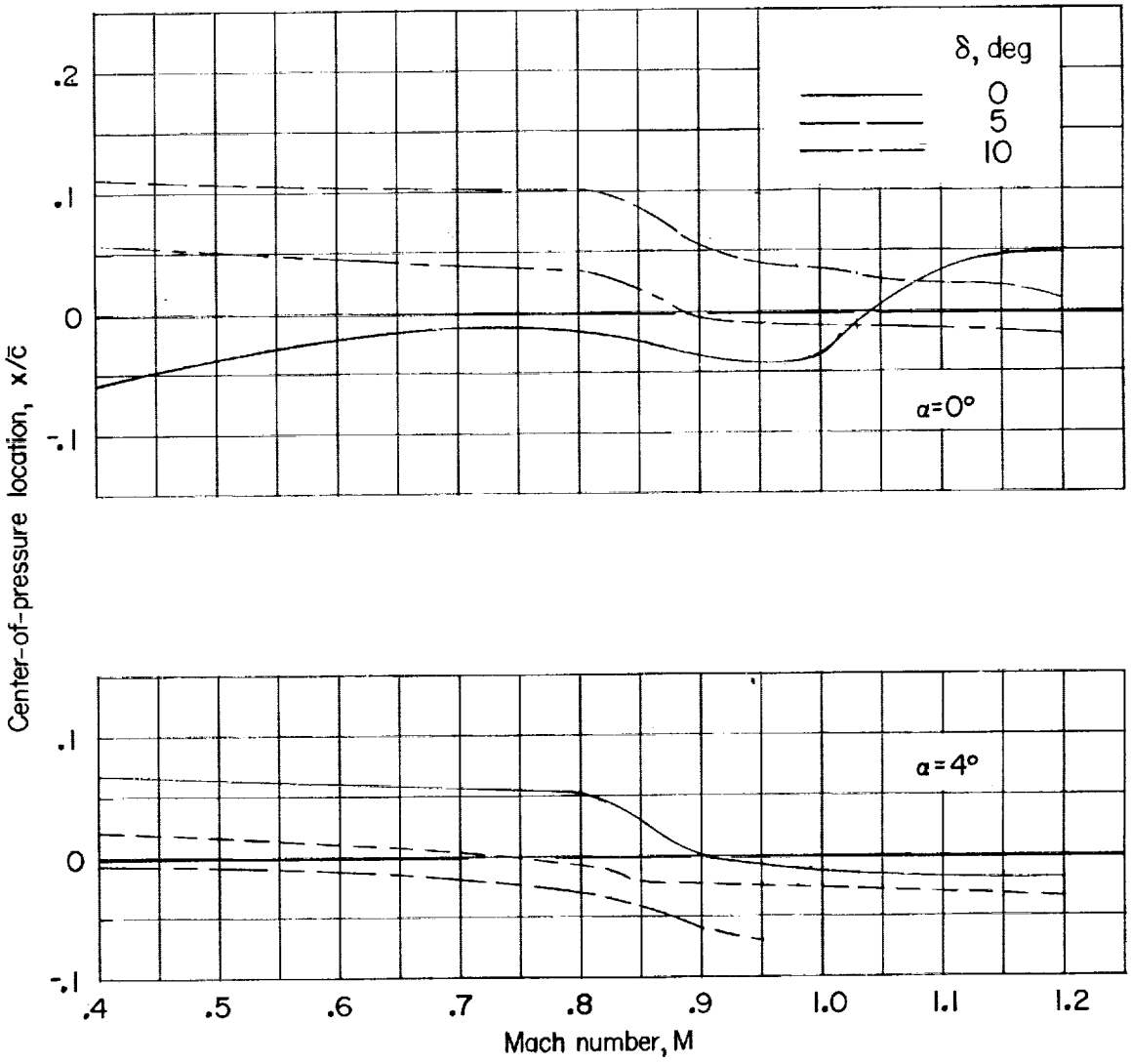

(b) Control surface 2.

Figure 21.- Continued.

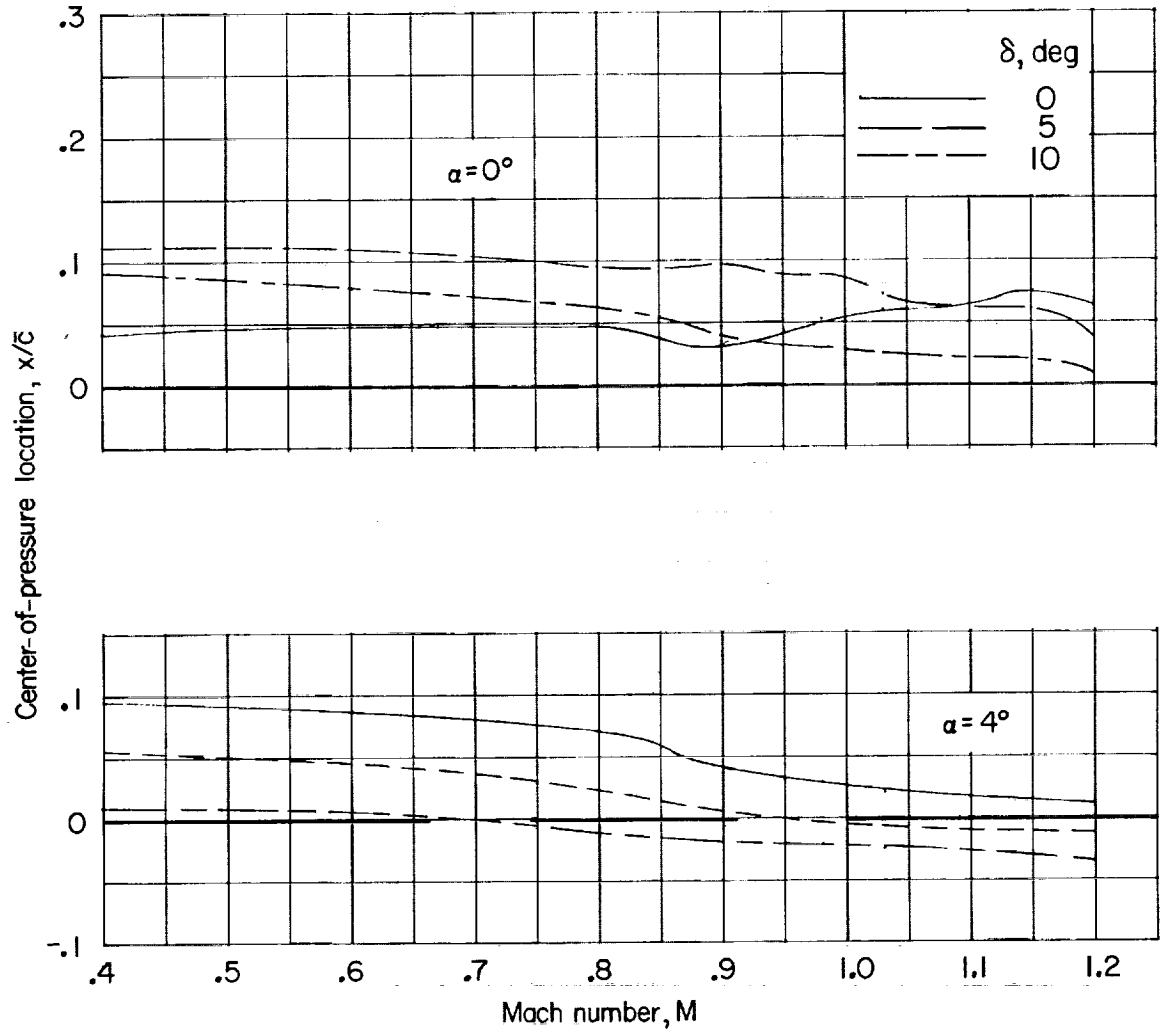

(c) Control surface 3.

Figure 21.- Continued.

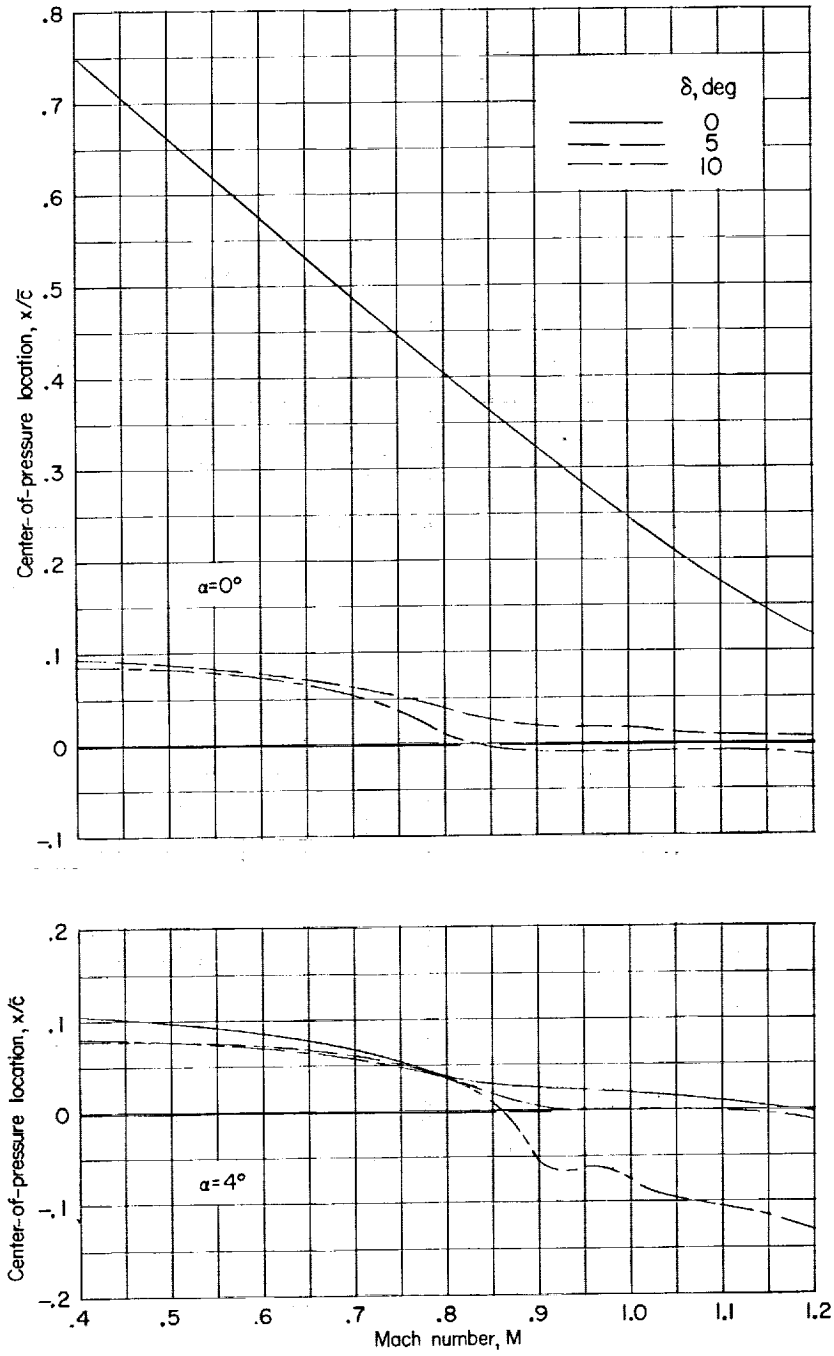

(d) Control surface 4.

Figure 21.- Continued.

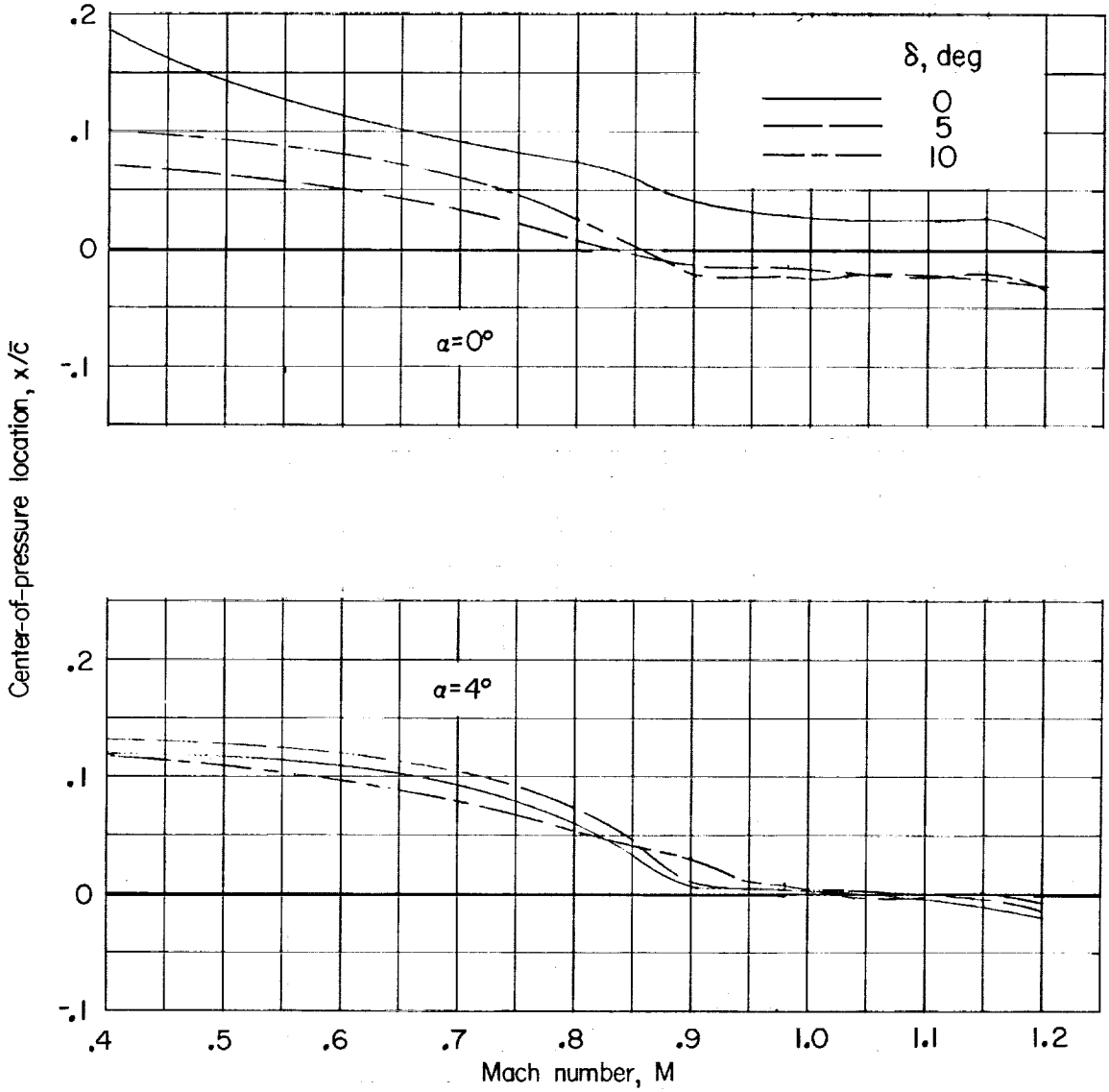

(e) Control surface 5.

Figure 21.- Continued.

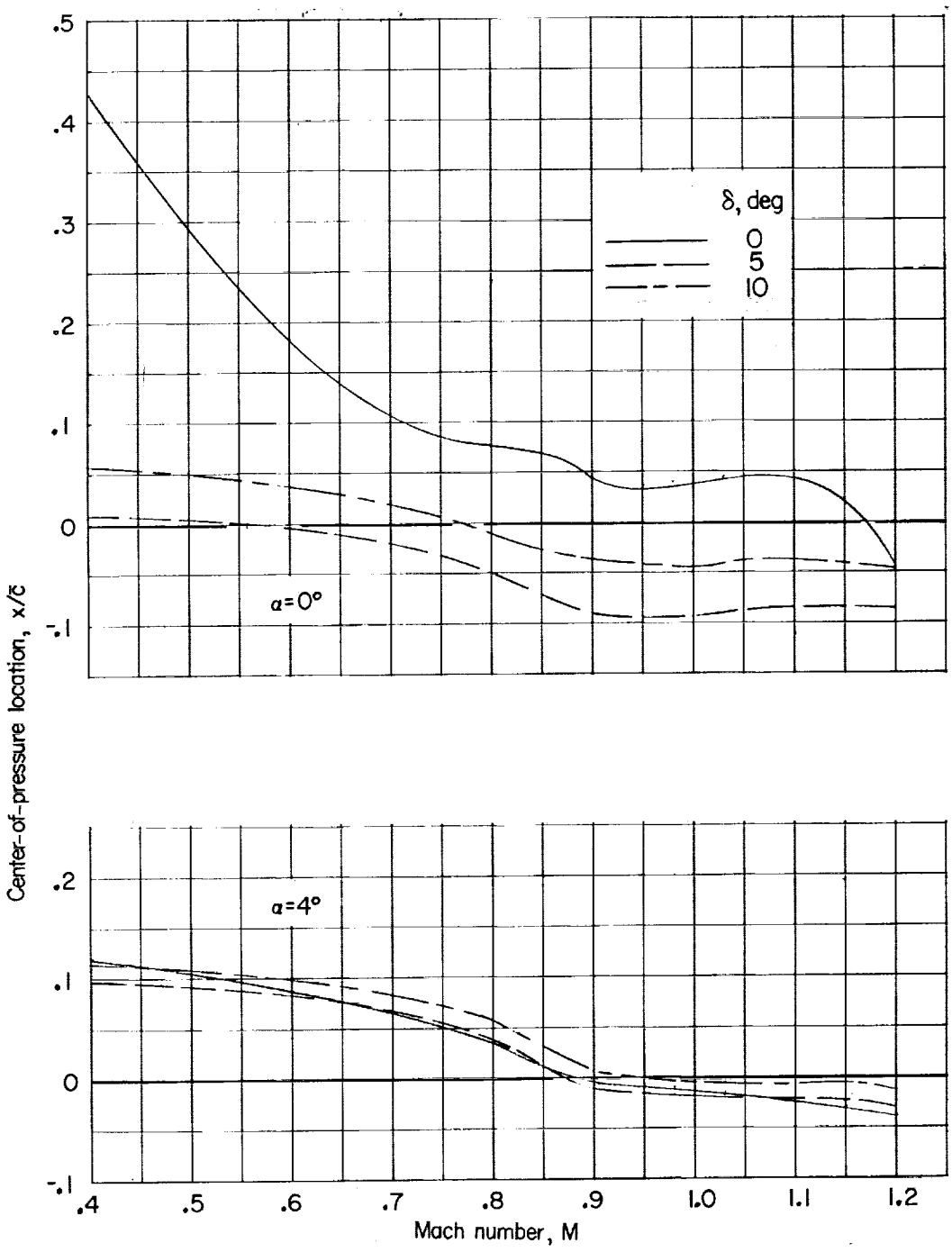

(f) Control surface 6.

Figure 21.- Concluded.

NASA - Langley Field, Va. L-1181